COMPRESSION CREEP OF A PULTRUDED E-GLASS/POLYESTER COMPOSITE AT ELEVATED SERVICE TEMPERATURES

A Thesis
Presented to
The Academic Faculty

By

Kevin Jackson Smith

In Partial Fulfillment
Of the Requirements for the Degree
Master of Science in Civil Engineering

Georgia Institute of Technology
August 2005

COMPRESSION CREEP OF A PULTRUDED E-GLASS/POLYESTER COMPOSITE AT ELEVATED SERVICE TEMPERATURES

Approved by:

Dr. David W. Scott , Chair
School of Civil and Environmental Engineering
Georgia Institute of Technology

Dr. Stanley Lindsey
School of Civil and Environmental Engineering
Georgia Institute of Technology

Dr. Rami Haj-Ali
School of Civil and Environmental Engineering
Georgia Institute of Technology

Date Approved: July 18, 2005

ACKNOWLEDGEMENTS

First, I would like to thank my thesis advisor, Dr. David Scott, for his immeasurable guidance, wisdom, and patience throughout the duration of this research program. Without his knowledge and ever-present motivation the work herein would not have been possible. I would also like to express my gratitude to Dr. Stanley Lindsey and Dr. Rami Haj-Ali for serving on my thesis committee.

I would also like to sincerely thank my good friend and colleague, Evan Bennett, for his assistance, insight, and friendship during the course of this work. Without his aid, many aspects of this study would have been overwhelming. I wish him the best of luck in the future. I would also like to extend deep gratitude to Melanie Parker for her assistance and friendship during the course of this work.

In addition, I would like to thank all of my friends who have helped me through all the hard times along the way. Thanks for reminding me to have a little fun.

Finally, my heartfelt thanks go to my family for their continuous encouragement. To my sister I would like to express my deepest appreciation for her understanding and patience. I would like to thank my parents for their guidance and unconditional support in all of my life's endeavors.

TABLE OF CONTENTS

ACKNOWLEDGEMENTS iii

LIST OF TABLES vi

LIST OF FIGURES vii

NOMENCLATURE ix

SUMMARY xii

CHAPTER I INTRODUCTION 1

1.1 Scope and Objectives 2

CHAPTER II PREVIOUS WORK 3

2.1 Ambient Temperature Studies 3

2.2 Elevated Temperature Studies 11

CHAPTER III SHORT-TERM TESTING

3.1 Tested Specimens 22

3.2 Characterization of Material Properties 22

3.2.1 Determination of Longitudinal Tensile Properties 23

3.2.2 Determination of Longitudinal Compressive Properties 29

3.2.3 Coupon Test Results 34

3.3 Short-Term Elevated Temperature Tests 38

CHAPTER IV LONG-TERM EXPERIMENTAL PROGRAM

4.1 Introduction 43

4.2 Specimen Details 43

4.3 Long-Term Experimental Setup 46

4.4 Development of a Semi-Empirical Viscoelastic Model 57

4.5 Time-Temperature Superposition Principle 72

4.6 Prediction of Time and Temperature Dependent Modulus 84

CHAPTER V CONCLUSIONS AND PROPOSED DESIGN EQUATION

5.1 Conclusions 91

5.2 Proposed Design Equation for the Time and Temperature-Dependent Modulus 93

5.3 Suggestions for Further Research 97

APPENDIX A DESIGN EXAMPLE – LONG-TERM BEAM DEFLECTION 98

APPENDIX B STRESS VS. STRAIN CURVES FROM SHORT-TERM TESTING 102

REFERENCES 128

LIST OF TABLES

Table 2.1 – Test Matrix of Creep Experiments (Yen & Williamson, 1990) 14

Table 3.1 – Nominal Coupon Dimensions 25

Table 3.2 – Measured Coupon Dimensions 35

Table 3.3 – Results of Short-Term Tensile Tests 36

Table 3.4 – Results of Short-Term Compression Tests 37

Table 3.5 – Average Values from Short-Term Testing 38

Table 3.6 – Results of Short-Term Elevated Temperature Tests 42

Table 3.7 – Reduction of Mechanical Properties Due to Temperature 42

Table 4.1 – Nominal Coupon Dimensions for Creep Studies 44

Table 4.2 – Creep Constants m and n from Equation (6) at 0.33 $F_L{}^c$ 60

Table 4.3 – Average values for the Material Constant n from Previous Work 60

Table 4.4 – Values for Constants m_T and n_T 63

Table 4.5 – Initial Elastic Strains 66

Table 4.6 – Increase in Longitudinal Strain over a 50 Year Service Life 71

Table 4.7 – Comparison of Short-Term Strain Values with Creep Values 71

Table 4.8 – Predicted Strains for Material Using Two Methods 79

Table 4.9 – Predicted Strains Utilizing 120 Hour TTSP Curves and Semi-Empirical Model 83

Table 4.10 – Predicted Modulus Reduction for Material at Room Temperature 88

Table 4.11 – Predicted Modulus Reduction for Material at 37.7°C 88

Table 4.12 – Predicted Modulus Reduction for Material at 54.4°C 89

Table 4.l3 – Predicted 50 Year Reduction in Modulus 89

LIST OF FIGURES

Figure 3.1 – Short-Term Coupons 24

Figure 3.2 – Nominal Tensile Coupon Dimensions 26

Figure 3.3 – Short-term Tensile Testing Setup 27

Figure 3.4 – Typical Tensile Coupon Stress-Strain Curve 28

Figure 3.5 – Nominal Compression Coupon Dimensions 31

Figure 3.6 – Nominal Compression Coupon Tested with Extensometer 32

Figure 3.7 – Short-term Compression Test Setup 32

Figure 3.8 – Typical Compression Coupon Stress-Strain Curve 33

Figure 3.9 – Test Setup for Short-Term Elevated Temperature Tests 40

Figure 3.10 – Typical Stress-Strain Curves at Elevated Temperatures 41

Figure 4.1 – Typical Room Temperature Creep Coupon 45

Figure 4.2 – Typical Elevated Temperature Creep Coupon 45

Figure 4.3 – Schematic of Creep Fixture (from Scott and Zureick (1998)) 47

Figure 4.4 – Typical Compression Cage (from Scott and Zureick (1998)) 48

Figure 4.5A – Creep Fixture with Environmental Chamber 49

Figure 4.5B – Room Temperature Creep Fixture 49

Figure 4.6 – Creep Fixture with Applied Dead Load 52

Figure 4.7 – Creep Strains for Coupons at Room Temp. 23.3°C (74°F) and 0.33 F_L^c 53

Figure 4.8 – Creep Strains for Coupons at 37.7°C (100°F) and 0.33 F_L^c 54

Figure 4.9 – Creep Strains for Coupons at 54.4°C (130°F) and 0.33 F_L^c 55

Figure 4.10 – Creep Strains for Coupons under Cyclic Heating at 37.7°C (100°F) and 0.33 F_L^c 56

Figure 4.11 – Logarithmic Plot for Evaluation of Constants m and n at 23.3°C 59

Figure 4.12 – Plot of Creep Strain at Elevated Temp., minus Creep Strain Measured at Room Temp**.** 62

Figure 4.13 – Logarithmic Plot of Creep Strain at Elevated Temp., minus Creep Strain Measured at Room Temp. 63

Figure 4.14 – Experimental Creep Strain with Time/Temperature-Dependent Model 65

Figure 4.15 – 37.7°C Cyclic Heat Creep Strains with Power Law Model 67

Figure 4.16 – Predicted Strains over a 50 Year Service Life 70

Figure 4.17 – Creep Strain for Temperature of 23.3°C, 37.7°C, and 54.4°C 73

Figure 4.18 –Master Curve Including Shift of 37.7°C Curve 75

Figure 4.19 –Master Curve for T_o (23.3°C) Including Shifts of Creep Data at 37.7°C and 54.4°C 76

Figure 4.20 – Shift Factors for TTSP 77

Figure 4.21 – Master Curve for T_o (37.7°C) Including Shift of Creep Data at 54.4°C 78

Figure 4.22 - Recorded Creep Strain for 120 hours 81

Figure 4.23 - TTSP Master Curve for Test Durations of 120 Hours, Allowing Prediction of Strain Response over a 50 Year Service Life 82

Figure 4.24 – Evaluation of Creep Parameter m' and T_o 85

Figure 4.25 – Predicted Reduction in Modulus of Elasticity Over a 50 Year Service Life 90

Figure 5.1 – Reduction in Modulus with Simplified Design Equation 96

Figure A1 – Beam Deflection Example 99

NOMENCLATURE

a_T	shift factor
$D(t)$	total time-dependent creep compliance
D_o	instantaneous creep compliance
D_t	transient creep compliance
E_L	longitudinal elastic modulus
E_L^c	longitudinal elastic compression modulus from coupon tests
E_L^t	longitudinal elastic tensile modulus from coupon tests
E_L^o	initial elastic longitudinal modulus independent of time
$E_L(t)$	time-dependent longitudinal elastic modulus
$E_L(T)$	temperature-dependent longitudinal elastic modulus
$E_L(T,t)$	time-dependent and temperature-dependent longitudinal elastic modulus
E_t	modulus which characterizes only the time-dependent behavior
E_T	modulus which characterizes only the temperature-dependent behavior
f	applied stress
F_L^c	longitudinal elastic ultimate compressive stress from coupon tests
F_L^t	longitudinal elastic ultimate tensile stress from coupon tests
g_2	non-linearizing material parameters in the Schapery equation
G_{LT}	elastic inplane shear modulus
I	moment of inertia
l_g	coupon gage length
L	length
m	stress-dependent and temperature-dependent coefficient

m'	stress-dependent and temperature-dependent coefficient
m_{RT}	stress-dependent coefficient from room temperature creep test
m_T	stress-dependent and temperature-dependent coefficient from elevated temperature tests
n	stress-independent material constant
n_{RT}	stress-independent material constant from room temperature creep test
n_T	stress-independent material constant from elevated temperature test
t	time after loading
T	temperature
T_o	creep material parameter used in the hyperbolic form of the coefficient of the temperature-dependent portion of strain in Findley's power law equation
V_f	the volume fraction of reinforcing fibers
β:	ratio of creep modulus to initial elastic modulus
Δ	beam deflection
Δ_o	initial beam deflection
$\Delta_{(T,t)}$	beam deflection due to time and temperature effects
$\Delta E(T)$	reduction in modulus due to temperature
$\Delta E(t)$	reduction in modulus due to time
ΔT	difference between given T and the material constant T_o
ε	total elastic strain

ε^T	strain due to temperature
ε^t	strain due to stress and time
$\varepsilon(t)$	total time-dependent creep strain
$\varepsilon(T)$	total temperature-dependent creep strain
$\varepsilon(T,t)$	total time-dependent and temperature dependent creep strain
ε_o	stress-dependent initial elastic strain
$\phi_{(t)}$	modulus reduction factor for time
$\phi_{(T,t)}$	modulus reduction factor for time and temperature
ζ	"reduced time"

SUMMARY

This thesis presents the results of an experimental investigation into the behavior of a pultruded E-glass/polyester fiber reinforced polymer (FRP) composite under sustained loads at elevated temperatures in the range of those that might be seen in service. This investigation involved compression creep tests of material coupons performed at a constant stress level of 33% of ultimate strength and three temperatures levels; 23.3°C (74°F), 37.7°F (100°F), and 54.4°C (130°F). The results of these experiments were used in conjunction with the Findley power law and the Time-Temperature Superposition Principle (TTSP) to formulate a predictive curve for the long-term creep behavior of these pultruded sections. Further experiments were performed to investigate the effects of thermal cycles in order to better simulate service conditions.

CHAPTER I

INTRODUCTION

Fiber reinforced polymeric (FRP) composite materials are rapidly becoming state of practice in many civil engineering construction applications. These materials often display many useful characteristics when compared with traditional building materials such as structural steel or reinforced concrete. Depending on the constitutive materials used, those characteristics can include corrosion resistance, high strength to weight ratio and non-conductivity. Another characteristic of FRP materials is a large degree of adaptability to a particular design situation. The mechanical properties of FRP materials can be altered by manipulating the type of fiber, the type of resin, the fiber volume fraction, and most importantly, the fiber orientation.

One of the more popular and cost efficient methods of producing FRP sections is the pultrusion process. The pultrusion process takes continuous fibers and pulls them through a resin bath and then through a heated die where the desired shape is formed and the polymerization of the resin occurs. The pultrusion process offers the ability to construct many of the same shapes that are typically found with other construction materials such as I-shapes, channels, bars, angles, tees, and tubular sections.

While FRP plates and sheets have been used for many years to strengthen existing structures (ACI 440 (1996)), the lack of reliable design criteria for FRP structural sections has slowed the acceptance of these materials by practicing engineers. One of the major hurdles to the development of reliable design criteria is a lack of understanding of the behavior of FRP materials under sustained loading. In addition, the types of FRP materials proposed for use in civil applications have shown a much greater sensitivity to

temperature variations than traditional construction materials. At elevated temperatures the resin matrix softens, which ultimately decreases ultimate strength and the modulus of elasticity. A reliable methodology to assess how these mechanical properties are diminished due to elevated temperatures is needed in order to develop more accurate predictive models of structural behavior over a normal service life.

1.1 Scopes and Objectives

This thesis presents the results of an experimental investigation into the behavior of a pultruded E-glass/polyester fiber reinforced polymer (FRP) composite under sustained loads at elevated temperatures in the range of those that might be seen in service. This investigation involved compression creep tests of material coupons performed at a constant stress level of 33% of ultimate strength and three temperatures levels; 23.3°C (74°F), 37.7°F (100°F), and 54.4°C (130°F). The results of these experiments were used in conjunction with the Findley power law and the Time-Temperature Superposition Principle (TTSP) to formulate a predictive curve for the long-term creep behavior of these pultruded sections. Further experiments were performed to investigate the effects of thermal cycles in order to better simulate service conditions.

CHAPTER II

PREVIOUS WORK

A large body of work currently exists on the time-dependent behavior of FRP composite materials. This chapter surveys those investigations deemed pertinent to the current study. An extensive survey of existing technical literature concerning creep behavior of FRP composites has previously been presented by Scott, Lai, and Zureick (1995). The current study reviewed a number of investigations pertaining to the creep of various FRP composites, the influence of elevated temperatures on creep behavior, and the techniques employed to model the creep behavior.

2.1 Ambient Temperature Studies

Findley (1944) formulated a power law equation to fit creep curves of various plastics previously tested by the author. The simplest form of the equation takes the form:

$$\varepsilon(t) = \varepsilon_o + mt^n \tag{2.1}$$

The recorded strain from creep tests can be plotted versus time on a log-log scale. The value of the power n can be determined by measuring the slope of the resulting line. The value of coefficient m can be determined as the y-intercept of the line at t = 1 hour. The material constant n was determined to be independent of stress while m is stress dependent. A 17,000 hour creep test of cellulose acetate was accurately modeled using the power law under low stresses. The author asserted from the various materials tested that as the modulus of elasticity decreased the resistance to creep also decreased. The

author concluded that the power law equation permitted reliable extrapolation of the data past the duration of available tests.

Spence (1990) tested a unidirectional glass/epoxy composite rod loaded to 30% of ultimate compressive strength. The specimen was tested at 21°C (70°F) and 207 MPa (30 ksi). The test specimen was a pultruded rod with a 0.635 cm (0.25 inch) diameter and a length of 1.90 cm (0.75 inch). The specimen consisted of S2 glass roving in an epoxy resin matrix. The fiber volume of the specimen was approximately 60%. The elastic modulus of the material was 41 GPa (5947 ksi), and the ultimate strength of 689 MPa (100 ksi). A constant load of 6.67 kN (1.5 kips) was placed on the specimen for 840 hours. After the loading period was over the specimen was then measured again to calculate the total deformation. The axial strain measured in the rod at the end of the test was found to be 0.04%.

The data was then extrapolated to 100,000 hours (10 years). Extrapolation of the data was carried out using the creep correlation method. The authors concluded that unidirectional composites are capable of sustaining stresses of 30% of ultimate while maintaining geometric stability.

Gibson et al (1991) characterized the creep behavior of glass/pps composites using the Frequency-Time Transformation (FTT) of frequency domain hysteresis loop measurements. These tests were performed in both wet and dry conditions in a servo-hydraulic testing machine. The specimens were comprised of 24 ply symmetric glass/pps laminates and were machined to the dimensions outlined in ASTM D-695. The specimens were subjected to a 100 pound pre-load and cyclic loading of +/- 80 pounds. This load range produced a very small strain and ensured linearity of the measurements.

The complex modulus was determined from the load-strain hysteresis loop measurements. The resulting compressive complex moduli were then transformed to the time domain compressive creep compliance using FTT method. This method was introduced as an alternative to the Time Temperature Superposition Principle (TTSP) which uses aggressive environmental conditions to accelerate the testing process. The aggressive elevated temperatures that are needed in order to use the TTSP can cause physical aging of the material which can cause a non-linear viscoelastic response of the material. This non-linearity can cause incorrect predictions of isothermal creep response of the material. The authors assert that the FTT method eliminates this non-linearity.

Five compression creep tests were performed in order to compare the results of FTT and actual creep response. Creep tests were performed for 4.636×10^6 seconds (1287 hrs). The FTT creep compliance curve, which is denoted as $J(t) = (\varepsilon(t) / \sigma_0)$, had good agreement with the actual creep tests which were slightly higher. As expected, the curves had better agreement at a time period less than 10^5 seconds. The authors assert that the FTT method is an efficient way of characterizing the creep behavior of composite materials without subjecting the material to aggressive climates.

McClure and Mohammadi (1995) investigated the creep behavior of three pultruded-angle FRP sections, reinforced with E-glass. The material was found to contain a fiber volume fraction V_f of 35-45%. The creep fixtures for this study utilized a cantilever arm device used to multiply the dead load applied to the end by a factor of 10. The same apparatus was used in the coupon and angle stub creep tests. The angle stub creep specimens were cut to dimensions of 152.4 mm (6 in.) in length and cross-sectional dimensions of 50.8 mm (2 in.) x 50.8 mm (2 in.) x 6.35 mm (0.25 in.). The specimens

were equipped with 12 strain gages (3 on each face). The stubs were subjected to a load of 23.2 kN (5.2 kips) after the cantilever action which corresponds to a stress of 44 MPa (18.26 ksi) which is approximately 45% of the initial buckling load. The coupon specimens used had cross-sectional dimensions of 12.7 mm (0.5 in.) x 6.35 mm (0.25 in.) and a length of 31.75 mm (1.25 in.). The coupons were equipped with two strain gages (one on each face). All of the specimens were cut from the stronger of the two legs of the single angle which was found to be leg number 1. The coupons were subjected to a stress of 146 MPa (21.2 ksi), approximately 45% of the average ultimate stress of the composite.

The Findley power law was used to model the time-dependent behavior of the material. Interestingly, the material constant n was not consistent for the two different tests. This was not desirable because Findley's theory defines n as a material constant independent of stress and environmental conditions. Further testing was suggested by the authors in order to assess the difference in n.

Still, the authors concluded that the Findley power law was an effective model of the creep behavior of the GFRP material. Notably, this model does not effectively model nonlinear tertiary creep; therefore the stress level must remain relatively low. Using the power law model, it was asserted that a full-sized structural element would only creep 0.3 mm after a 2,500 hour period. This was deemed acceptable from a civil engineering design perspective.

Wen, Gibson, and Sullivan (1995) utilized dynamic testing methods to characterize the creep behavior of polymer composites. The study used impulsive excitation of the specimens and their frequency response to determine the frequency

dependent storage modulus and loss factors. The Time-Temperature Superposition principle was applied to the frequency domain vibration test data to form a master curve. This curve was then transformed to the time domain to generate the creep compliance curve. The purpose of this study was to compare the results of the short term dynamic test method to the results of conventional long term static creep tests. The technique used by the authors is known as the impulse-frequency response technique. The authors asserted that it was known to work well in materials in their glassy state. Polyetherimide (PEI) neat resin and E-glass/PEI composites ($V_f = 35\%$) were selected as the material for this study. The material was cut into specimens that were 15cm in length by 1.27cm in width. The glass transition temperature of the material was estimated to be around 210°-215°C. Aging effects were eliminated by rejuvenating the specimens at 225°C for 3 hours. The authors concluded that the vibration tests could be used to predict creep compliance for a short amount of time, on the order of seconds, while creep tests showed longer periods; however, the time overlap show good correlation between the two methods. The authors emphasized that the preparation time and setup cost is much less for the vibration test than conventional creep tests.

Scott and Zureick (1998) investigated the compression creep of pultruded FRP composites at three different stress levels and time durations of up to 10, 000 hrs. Rectangular coupons were cut from the structural plate elements of a 102 mm (4 in.) x 102 mm (4 in.) x 6·4mm (.25 in.) pultruded FRP wide flange section. The material system consisted of a vinylester matrix reinforced with unidirectional E-glass roving and continuous filament mat. The fiber volume fraction was found to be 30% with a filler content of approximately 5% by volume.

The specimens were loaded using a lever arm creep fixture and concrete weights. Stress levels of 65 MPa (9.43 ksi), 129 MPa (18.7 ksi), and 194 MPa (28.1 ksi) were applied to the specimens. This corresponded to 20%, 40%, and 60% of the average ultimate compressive strength respectively. The stress levels of 20% and 40% are well within the linear-elastic range found in the short-term tests. The stress level of 60% is approximately where the material began to display non-linear behavior.

The data was modeled using the Findley power law. The model that was developed by Findley was based on an unreinforced thermoplastic material. Since the composite in this study possessed a low fiber volume fraction of 30%, the authors asserted that the creep behavior would be primarily matrix driven and therefore the Findley model would be an accurate approximation.

A predictive equation for the time-dependent elastic modulus was developed using a Taylor series expansion of the stress dependent terms ε_o and m. These terms can be expressed as hyperbolic functions of stress. The equation was simplified because the creep parameters are approximated as linear functions of stress so the cubic and higher terms in the Taylor series were neglected. This approximation may not be valid for higher stress levels where the relationship is no longer linear. The predictive equation proposed by Scott & Zureick was

$$E_L(t) = \frac{E_L^o}{1 + \frac{E_L^o}{E_t} t^n} = \frac{E_L^o}{1 + \frac{(8760)^{0.25}}{\beta} t^{0.25}} \approx \frac{E_L^o}{1 + \frac{10}{\beta} t^{0.25}} = \phi_t E_L^o \tag{2.2}$$

where

$$\phi_t = \frac{1}{1 + \frac{10}{\beta} t^{0.25}} \tag{2.3}$$

and $\beta = \frac{E_t}{E_L^o}$. The property E_t is the modulus that characterizes the time dependent behavior given by $\frac{f}{m}$ which is the applied stress divided by the material parameter m. The property E_L^o is the initial longitudinal elastic modulus of the material.

The predictive model showed a 28% reduction in longitudinal stiffness over a 75 year period. The predicted reduction in stiffness was not stress dependent. Thus the authors recommended that the sustained stress level remain under 33% of the ultimate stress to ensure that the Findley model provides an accurate model of the material behavior.

Papanicolaou, Zaoutsos, Cardon (1999) investigated the well-known Schapery formulation which models the non-linear viscoelastic response of any material using four stress and temperature dependent parameters and estimated them for FRP material using simple step creep-recovery curves. Previous research by Papanicolaou, Zaoutsos, Cardon (1998) predicted three out of the four parameters using step creep-recovery curves. In the later investigation the authors estimated the fourth nonlinear parameter, which accounts for the influence of the loading rate on creep, and depends on stress and temperature. The fourth parameter was found using a new methodology developed by the authors which is based on the Schapery model and assumes the material time-dependent compliance follows a power law.

Creep recovery data was obtained on unidirectional carbon-epoxy composite plates. The specimens were constructed using the hand lay-up technique with 12 plies in each. The specimens were 300mm (11.8 in.) in length, 17mm (0.67 in.) wide and 2mm (0.079 in.) thick. Short term tensile elastic modulus and ultimate tensile strength tests

were performed for five specimens. For the long-term loading the initial applied stress remained constant for 168 hrs followed by 168 hrs of recovery time. Six different stress levels were investigated: 30%, 40%, 50%, 55%, 60%, and 70% of the tensile rupture stress. The CF/Epoxy composite displayed strong viscoelastic behavior and was dominated by the matrix. The composite displayed a nonlinear viscoelastic strain response for applied stresses higher than 30% of the ultimate strength. Using the new methodology the authors asserted that the fourth parameter g_2 increased with increasing stress levels.

Haj-Ali and Muliana (2003) presented a new three-dimensional modeling approach to predict the non-linear viscoelastic behavior of pultruded composites. The material that was investigated consisted of a vinylester matrix reinforced with E-glass roving and a continuous filament mat (CFM) with an overall V_f of 34%. Micromechanical models, utilizing finite element, were formulated for the roving and CFM. A new iterative integration method applied to the Schapery three-dimensional model was used for the isotropic matrix. The matrix in both models had the same isotropic and nonlinear viscoelastic behavior. The fibers were taken as linearly elastic.

Uniaxial compression creep tests were performed on off-axis coupons at angles of 0, 45, and 90 degrees at room temperature for 1 hour. The coupons used for the creep tests were 177.8 mm (7 in.) in length x 31.75 mm (1.25 in.) x 12.7 mm (0.5 in.) thick. Multiple stress levels ranging from 10-60% of the ultimate strength of the material were used for the creep experiments. The short duration creep tests were used to calibrate the viscoelastic properties of the matrix and to assess the prediction capabilities of the models. The linear coefficients were determined from creep tests with low magnitudes of

applied stress. The nonlinear parameters of the Schapery model were calibrated based on the tests at the elevated stress levels. The authors asserted that the micromodels showed good prediction for all the linear and nonlinear curves except for the highest stress level. This was attributed to the calibration being based on a lower applied stress. The authors concluded that the nonlinear response was apparent in the off-axis creep tests and that the micromodel predictions produced a good match.

2.2 Elevated Temperature Studies

Findley and Worley (1951) investigated elevated temperature creep and fatigue properties of a polyester glass fabric laminate. The material was a glass fabric laminated with a polyester resin. The high temperature creep tests were conducted in a commercial creep testing machine. The specimens were tested at 25°C (77°F) and 204°C (400°F). The specimens were allowed to remain at temperature from 1 to 24 hours before the application of the load. Stress levels of 103.4 MPa (15,000 psi), 137.9 MPa (20,000 psi), and 172.4 MPa (25,000 psi) were tested at the elevated temperature. The 137.9 MPa (20,000 psi) test was continued as a step test to determine the stress level where fracture could be expected. The stress level was increased by 13.8 MPa (2,000 psi); fracture of the specimen occurred when the stress reached 179.3 MPa (26,000 psi). A test was also performed at a stress level of zero to determine the shrinkage at elevated temperature.

The test at the zero stress level showed significant shrinkage which would alter the creep curves if this adjustment was taken into account. The results indicated that the stiffness of the laminate increased with the duration of exposure to the elevated temperature. This was due to a change in the structure of the material due to post-cure effects. The data showed a 30 percent increase from an exposure of 16 hours to 262

hours. The authors concluded that the specimens must be exposed for the same amount of time if the results were to be comparable. The authors asserted that the strain at elevated temperatures is not only affected by temperature and stress but also shrinkage and stiffening of specimen.

Tuttle and Brinson (1986) investigated the prediction of the long-term creep compliance of general composite laminates using the Schapery non-linear viscoelastic theory. Specimens with 0, 45, and 90° fiber orientations were cut from 8-ply unidirectional panels of T300/5208 carbon epoxy composite. The fiber volume fraction of the material was found to be 65%. The specimens were cut to dimensions of 13 mm (0.51 in.) in width and the length ranged from 180 – 330 mm (7 – 13 in.). The thickness was 1 mm (0.04 in.). Short-term creep/creep recovery tests were performed on a creep machine with automatic loading with a lever arm amplification of 3:1. All tests were performed at 149°C (300°F). The creep portion of the test was 480 minutes and the recovery time was 120 minutes. These times were selected in order for the creep compliance to be accurate at times up to 10^5 minutes. The viscoelastic parameters in the Schapery equation were determined through a least-squares fit using the experimental data.

Five specimens were used for the long-term creep tests. The tests were performed at a stress level of 76 MPa (11,022 psi) and a temperature of 149°C (300°F). The tests were performed for a duration of 10^5 minutes. Comparison of the creep data with the Schapery prediction yielded reasonably accurate results up to a time period of 10^3 minutes. Predictions after 10^3 minutes fell below the measured values. The predicted response at 10^5 minutes fell 10-15 percent below the measured values. The authors

attributed the error to incorrect modeling of bi-axial stress interactions and damage accumulation within the plies.

Yen and Williamson (1990) tested creep and creep recovery of a unidirectional off-axis FRP composite that contained 50% by weight of continuous glass fiber in a polyester resin matrix. The composite had a fiber orientation of 15° with respect to the direction of the applied load. The specimens were cut into sections 203mm (8 in.) long and 12.7mm (0.5 in.) wide. The glass transition temperature for this material was reported to be 135°C (275°F). The ultimate stress at temperatures of 23°C (73.4°F), 38°C (100.4°F), 66°C (150.8°F), 93°C (199.4°F), 121°C (249.8°F), and 149°C (300.2°F) was determined through tensile testing of the material.

The test matrix for the creep experiments can be seen in Table 2.1. The different stress levels represented percentages of the average ultimate strength. The tests were conducted on a five-lever arm creep frame and each lever arm of the creep frame was equipped with an oven and temperature controller. Each test ran for a duration of 180 minutes with approximately 15 hours of recovery. According to the test matrix and the given glass transition temperature, samples were tested in the both the glassy and rubbery phases of the material. The authors asserted that the response of the material, at all temperatures, would be in the glassy state because of the presence of the fibers.

Table 2.1: Test Matrix of Creep Experiments (Yen & Williamson, 1990)

Stress Level (MPa)	***Temperature (°C)***					
	23	**52**	**79**	**107**	**135**	**149**
5.4						**X**
7.6					**X**	
9.0						**X**
10.8	**X**	**X**	**X**	**X**		
12.7					**X**	**X**
16.3		**X**				**X**
17.6					**X**	
18.0			**X**			
21.5				**X**		
22.7					**X**	
32.3	**X**	**X**	**X**	**X**		
36.5				**X**		
42.1			**X**			
53.8	**X**	**X**	**X**			
75.4	**X**					
96.5	**X**					

The collected data was modeled using the Findley equation along with the Time-Temperature-Stress Superposition principle to create master curves to model the long-term creep response. Curves were created for 57 days and 400 days based on the aforementioned 180 min short-term creep tests. The measured strain response was used to estimate the parameters in the Findley equation. Creep data showed very small deviation from the results of the Findley equation.

The time exponent, n, was found to have little variation with a change in the stress which is concurrent with Findley's observations that n is stress independent. The test data showed that n increased non-linearly with temperature which conflicts with

Findley's findings that n is almost independent of temperature. The value of ε_o showed a non-linear increase with stress; however, the rate of increase was found to decline as the stress increased. The value of m showed an increase with both temperature and stress level. Master curves were found using horizontal and vertical shift factors on the data collected at different temperatures and relating them to the reference temperature. The authors asserted that a 28 hour creep test at 149°C (300°F) could be use to predict the 10-year creep response for the material.

The authors stressed that this duration of testing does not take into account the physical aging of the specimen which can change the creep response of a material. The authors suggested longer testing periods in order for the aging effect to be included. The maximum error that was found between the master curve and the Findley equation was 5%. The accelerated tests make it possible to predict the response of the material up to 3200 times the duration of the original test.

Gates (1993) investigated two types of FRP material to establish non-linear time-dependent relationships for stress/strain over a range of temperatures. The first material system was comprised of an amorphous graphite/thermoplastic composed of Hercules® IM7fiber and Amoco® 8320 matrix. The second FRP was a graphite/bismaleimide composed of Hercules® IM7 fibers and Narmco® 5260 matrix. Both specimens had a glass transition temperature of 220°C (428°F). The constitutive model that was developed accounted for temperature dependency through the variation of material properties with respect to temperature. The model would therefore be applicable to both tensile and compressive loading. The model was designed to predict the non-linear rate-dependent behavior such as creep.

The six temperatures selected for the study were 23°C (73.4°F), 70°C (158°F), 125°C (257°F), 150°C (302°F), 175°C (347°F), and 200°C (392°F). Rectangular test specimens were cut following ASTM D3039-76 which consisted of 12 plys measuring 2.54 cm (1 in.) by 24.1 cm (9.5 in.). Elastic material constants were determined on specimens 0, +/-45, and 90 degree orientations in order to determine the elastic modulus and the shear modulus of the material. For the three elastic/plastic and two elastic/viscoplastic material parameters, off-axis tests were performed on 15, 30, and 40 degree coupons.

The trends of the different temperature tests showed that transverse and shear moduli stiffness decreased with increased temperature. Both materials displayed an increase in ductility as the temperature increased. The authors found the results indicated that the analytical model provided reasonable predictions of material behavior in load or strain controlled tests.

Katouzian and Bruller (1995) investigated the effect of temperature on the creep behavior of neat and carbon fiber-reinforced PEEK and epoxy resins. Two composite materials were used in this investigation. One was an epoxy resin matrix reinforced with T800 carbon fibers and the other was a semi-crystalline PEEK matrix reinforced with IM6 carbon fibers. The fiber volume for each of the composites tested was approximately 60%. The neat resin matrices for each composite were also tested.

Creep experiments were performed in creep fixtures utilizing lever arm action with force amplifications of 10:1 and 25:1. Dead weights acting at the ends of the lever arms generated the tensile force needed for the experiments. The high temperature tests were performed in thermostatically controlled chambers. The creep specimens used in

the experiments had a length of 150 mm (5.9 in.), a width of 10 mm (0.394 in.), and a thickness of 1 mm (0.039 in.). Fiberglass end tabs were used on all specimens. The test duration for all creep tests was 10 hours.

The temperatures tested for the neat PEEK matrix were 23°C (73.4°F), 60°C (140°F), 80°C (176°F), and 100°C (212°F) while the reinforced material was tested at 23°C (73.4°F), 80°C (176°F), 100°C (212°F), and 120°C (248°F). The neat and reinforced epoxy materials were tested at 23°C (73.4°F), 80°C (176°F), 120°C (248°F) and 140°C (284°F). The room temperature (23°C (73.4°F)) tests were conducted at five stress levels ranging between 10 and 70% of the ultimate tensile strength. The load levels were reduced with increasing test temperature. The test specimens were allowed to cure at the test temperature to ensure even heat distribution throughout the specimens.

The authors used the well known Schapery equation to model the results of the creep experiments. It was discovered that the linear viscoelastic limit shifted to lower values with increasing temperature for the neat epoxy and reinforced epoxy. It was also found that the instantaneous creep response is far less sensitive to temperature than the transient response. The instantaneous creep response showed slight increases with increasing temperature and was found to be linear up to stress levels of 20 MPa (2,900 psi) for the epoxy resin and reinforced epoxy. The transient creep response showed a nonlinear dependence of temperature. The transient creep response showed very little influence from temperature between 23°C (73.4°F) and 80°C (176°F) but increases to 140°C (284°F) showed significant effects for the neat epoxy and reinforced epoxy. A comparison between the two resins showed that the influence of temperature on the creep response in the PEEK resin was greater than the epoxy resin. The results of the PEEK

resin showed that the linear viscoelastic limit shifted to lower values with increasing temperature. This was not evident in the reinforced PEEK resin where the linear limit was approximately 25 MPa (3,625 psi) for all tests.

The authors asserted that the Schapery approach provided a good approximation of the experimental results with a maximum error of less than 3%. The authors also stated that the instantaneous response is linear and temperature-independent over the stress levels used in practical applications. Finally, the authors claimed that the influence of temperature on the time-dependent response of the materials was found to be nonlinear.

Raghavan and Meshii (1997) presented a model to predict creep of unidirectional, continuous carbon-fiber-reinforced polymer composite and its epoxy matrix. Creep was studied over a wide range of stress levels (10-80%) and temperatures ranging from 295K (71.3°F) to 433 K (319.7°F).

Laminates were made in house in an autoclave. Eight plies were used for the 0, 10, 30, and 60 degree laminates. Sixteen plies were used for the 90 degree laminates. The fiber volume fraction was 62%. The 0, 10, and 90 degree laminates were used to measure longitudinal, shear and transverse properties. The 30 and 60 degree laminates were used in the creep testing. Tensile test coupons 167 mm in length and 12.7 mm in width were used. The coupon dimensions were based on the measurements provided by ASTM D638M-96 (1996). Thermal activation energy was used to model the behavior of the material. This was used as opposed to the time-temperature-stress superposition principle (TTSSP) because it can be used to model non-linear viscoelastic materials.

The four temperatures that were tested were 295K (71.3°F), 373K (211.7°F), 403K (265.7°F), and 433K (319.7°F). Creep experiments were performed for a maximum duration of 24hrs. Three moduli were calculated from short term tests. They were the instantaneous modulus, the rubbery modulus and the viscous modulus. These represented the modulus with respect to the temperature which the specimen was being tested. The authors asserted that the model provided good correlation with the creep data for the unidirectional composite for the temperature range that was tested and stress levels up to 80% of the ultimate strength. The model showed reasonable quantitative agreement with predicted results being higher by 15 – 23%.

Bradley et. al. (1998) investigated creep characteristics of neat thermosets and thermosets reinforced with E-glass. Vinylester samples were machined to dimensions of 1.27 cm (0.5 in.) wide by 10.2cm (4.02 in.) long and 0.318 cm (0.125 in.) thick. The specimens were tested in flexural creep and displacements were measured using dial gages. The specimens were post-cured at temperatures of 48.9°C (120°F), 71.1°C (160°F), and 93.3°C (200°F) for time durations of 2 and 4 hours. The purpose of the experiments was to determine the effect of temperature and time of cure on the creep compliance of the materials. Loading and unloading of the specimens was performed in order to determine the initial creep compliance *D*o.

The creep data was modeled using a form of the Findley equation taking the form:

$$D(t) = \frac{\varepsilon(t)}{\sigma} = D_o + D_t t^n \tag{2.2}$$

where

D(t) = total time-dependent creep compliance
ε(t) = total time-dependent creep strain
σ = applied stress

D_o = instantaneous creep compliance
D_t = transient creep compliance
t = load time
n = stress –independent material constant

The authors observed that an increase in curing temperature resulted in a reduction in the creep compliance as well as a reduction in the time exponent n.

Saadatmanesh (1999) investigated the long-term behavior of plastic tendons reinforced with aramid fibers. The Aramid Fiber Reinforced Plastic (AFRP) tendons had a fiber volume fraction of 50% with a filament diameter of .012mm (0.00047 in.). Five specimens were tested until failure to evaluate the mechanical properties. The short-term testing resulted in a tensile strength of 91.2kN (20.5 kips), an ultimate stress of 2324 MPa (337 ksi), and an ultimate strain of 2.1%. The modulus of elasticity of the AFRP tendons was 120.7 GPa (17,500 ksi) with a Poisson's of 0.36. The average diameter of the tendon was 10mm (0.39 in.) and across-sectional area of 78.5 mm^2 (0.12 $in.^2$). Twelve specimens were tested in air temperatures of -30°C (-86°F), 25°C (77°F), and 60°C 140°F), and 24 specimens were tested in alkaline, acidic, and salt solutions at temperatures of 25°C (77°F) and 60°C (160°F) to evaluate the relaxation behavior. Six specimens were tested under sustained load to evaluate creep at room temperature, and 45 specimens were tested to evaluate fatigue behavior.

The creep investigation was just a preliminary investigation. Samples were subjected to a load of 40% of ultimate load. The average initial strains were 0.82, 0.84, and 0.83 percent creep for samples in air, alkaline solution, and acidic solution. The specimens were put into tension using a hanging dead weight to create the stress on the specimens. The specimens were subjected to the load for up to 3000 hrs and the strains were recorded on one hour intervals. The author asserted that the specimens exhibited

good creep characteristics in air and alkaline solutions and to a lesser degree in acidic solutions.

Dutta and Hui (2000) asserted that the behavior of FRP material at elevated temperatures is essential for assessing the survival time of a structure undergoing a fire. The purpose of this study was to develop engineering constants that can be used as material parameters, allowing for the assessment of heat durability. The strength degradation and final collapse of FRP structures due to the increase in temperature in a fire was investigated. An isothermal curve can be created by running a simple creep test at constant stress and temperature while recording the strain.

The time-temperature superposition principle was decided against because it was too complex and did not meet the desired simplified method. The method that was decided upon was an adaptation of the Findley equation.

Short-term tests were performed at room temperature (25°C (77°F)) in order to establish mechanical properties of the FRP. The specimens were then tested at sustained loads in the range of 60-80% of ultimate load at 25°C (77°F), 50°C (122°F), and 80°C (176°F). The failure mode was semi-brittle. The average failure strength at 25°C (77°F) was 304.4 MPa (44.1 ksi) in compression and 271.5 MPa (39.4 ksi) in tension. The 25°C (77°F) specimens continued to strain under creep loads for over 30 min. The 50°C (122°F) and 80°C (176°F) specimens were tested until failure because they typically broke before the 30 minute test period. A semi-empirical equation was developed using Findley's power law. The two creep constants were replaced with functions of time ratios and temperature ratios. The resulting equation was compared with data collected in this experiment and experiments performed by other researchers, with good agreement.

CHAPTER III

SHORT-TERM TESTING

3.1 Tested Specimens

All tested specimens in the current investigation were manufactured using an isophthalic polyester resin matrix containing UV radiation inhibitors reinforced with unidirectional E-glass roving and a continuous filament mat. Specimens were cut from 101.6 mm (4 in.) wide square tube structural elements with a wall thickness of 6.35 mm (0.25 in.). Results from previous work indicated that the fiber volume fraction for the material is approximately 35%, with 9% filler and 1.7% voids by volume (Kang, 2001).

3.2 Characterization of Elastic Material Properties

Short-term tests were conducted in both compression and tension in order to determine modulus of elasticity, ultimate strength, and ultimate strain of the material. The results of the short-term tests were used to set the parameters for the long-term experiments. The specimens were tested in both compression and in tension to ensure the composite performed the same in both loading conditions. The specimens in the following tables will be designated by resin type, reinforcement type, test type, specimen, section designator, and panel number. For example, PGT-A1-1, would denote Polyester, Glass, Tension, square tube A, section 1, panel number 1.

Short-term material properties were investigated for each panel of the structural members that were to be used in the long-term investigation. This was done to ensure all of the structural members were similar and did not contain discontinuities that could cause premature failure when tested in the long-term.

3.2.1 Determination of Longitudinal Tensile Properties

A total of 16 uniaxial tension tests were performed in order to determine the longitudinal tensile properties of the square tube sections used in this study. Three different square tube sections were used, with a specimen being cut from each of the four panels as shown in Figure 3.1. Two sections were cut from specimen A to confirm the accuracy and repeatability of the test results. All longitudinal tension tests were performed using a hydraulic testing machine with pneumatic grips. Coupon preparation, loading procedure and data reduction were performed in accordance with ASTM D3039 (1993).

Guided by previous work by Butz (1997) and Kang (2001) the tensile properties were determined using prismatic coupons without end tabs. The nominal dimensions for the tensile coupons used in the current study are given in Table 3.1. A schematic of the coupons used in the short-term tensile tests can be found in Figure 3.2. The gage length of the tensile coupons was 203 mm (8 in.) with approximately 127 mm (5 in.) being added to guarantee adequate seating in the pneumatic grips. A single uniaxial extensometer was used to measure the longitudinal strain in the coupon. The extensometer was removed at a predetermined stress of 241MPa (35,000 psi) to prevent damage to the extensometer. Due to the absence of the extensometer for the remainder of the test, strain at failure was estimated based on an assumed linearity of the stress-strain response of the composite material. A photograph of the short-term tensile test setup can be found in Figure 3.3. A typical stress-strain diagram for the short-term coupon tests can be found in Figure 3.4 and all others can be found in Appendix B.

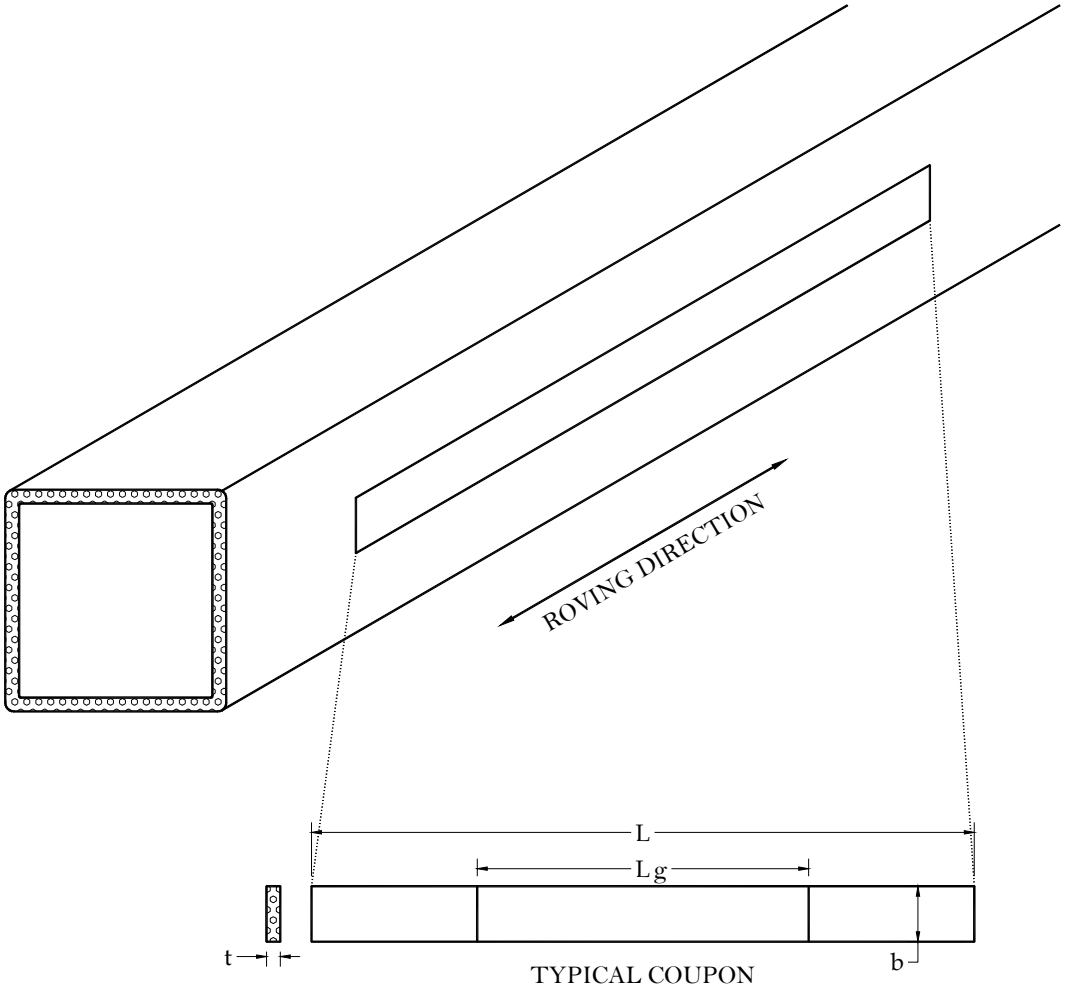

Figure 3.1 – Short-Term Coupons

Table 3.1- Nominal Coupon Dimensions

Test Type	t		L		L_g		b	
	mm	in.	mm	in.	mm	in.	mm	in.
Tension	6.35	0.25	330	13	203	8	25	0.984
Compression	6.35	0.25	127	5	51	2	25	0.984
Compression (Strain Readings)	6.35	0.25	127	5	51	2	38	1.5

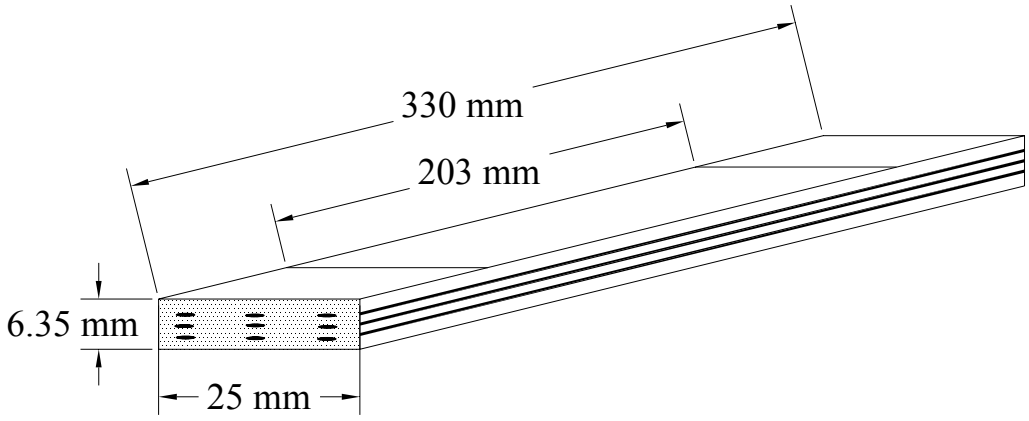

Figure 3.2 - Nominal Tensile Coupon Dimensions

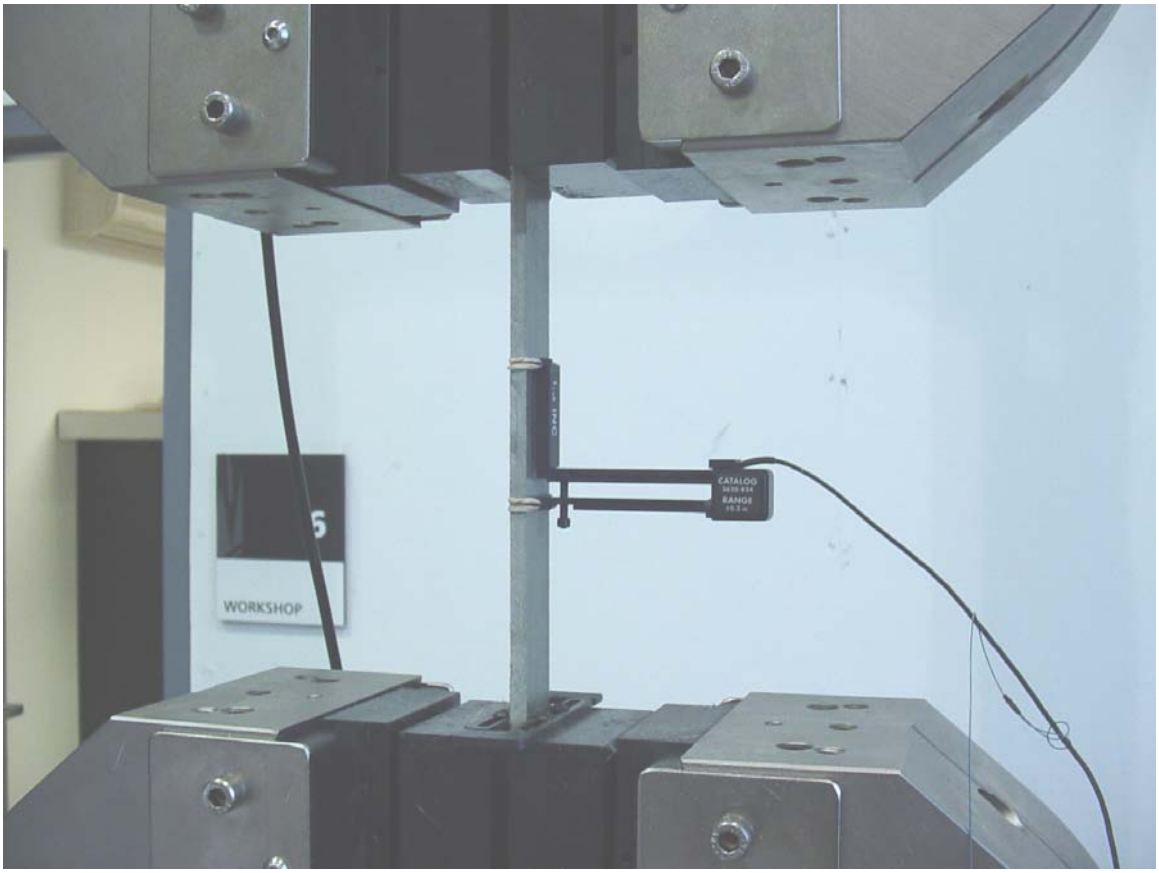

Figure 3.3 - Short-term Tensile Testing Setup

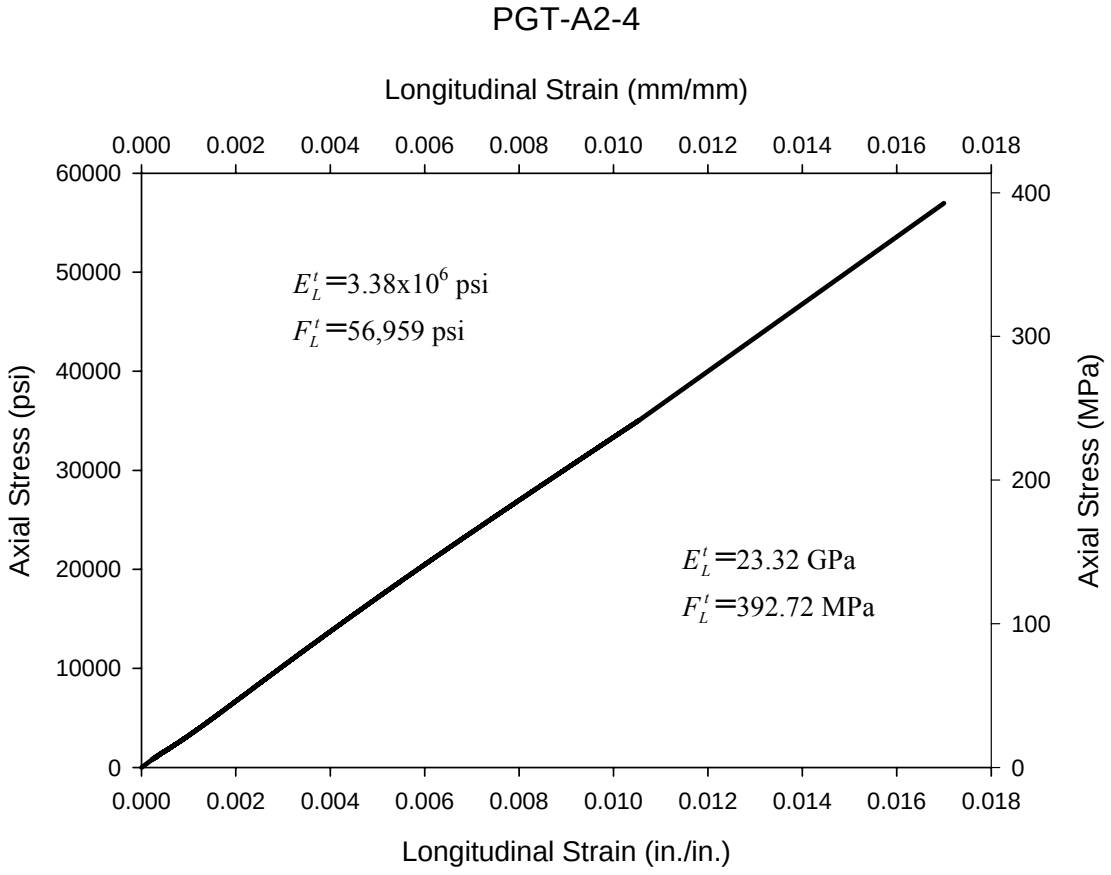

Figure 3.4 - Typical Tensile Coupon Stress-Strain Curve

3.2.2 Determination of Longitudinal Compressive Properties

In order to determine the longitudinal properties in compression, prismatic coupons were cut to lengths that would ensure that material failure would occur before buckling of the specimen. This length was determined using a simple stability analysis (ASTM D3410):

$$l_g \le t\left(.9069\sqrt{\left(1-\frac{1.2F_L^c}{G_{LT}}\right)\left(\frac{E_L^c}{F_L^c}\right)}\right) \tag{3.1}$$

where

l_g = coupon gage length
t = coupon thickness
F_L^c = ultimate longitudinal compressive stress
E_L^c = longitudinal compressive modulus
G_{LT} = shear modulus

This equation yields a conservative estimate of the buckling load for pinned end constraints. For Equation 3.1, the ultimate longitudinal compressive stress and the longitudinal compressive modulus were estimated using the results of the tension tests. It was determined that the same size coupons from Scott and Zureick (1998) could effectively be used in the current investigation. The nominal dimensions for the compression coupons are given in Table 3.1 and a schematic illustration of the coupons can be found in Figure 3.5.

A total of 18 uniaxial compression tests were performed in order to determine the longitudinal compressive properties of the square tube sections used in this study. Three different square tube sections were used with a specimen being cut from each of the four panels. An additional section was cut from specimen A, from which two coupons were cut to confirm the accuracy and repeatability of the test results. These specimens were

tested with the same boundary conditions that would later be used in the long-term creep study. The samples were tested until failure and the ultimate stress was recorded. In addition to these samples, four coupons were cut to the dimensions of the creep specimens that were to be used in the long-term creep analysis. These specimens were 13 mm wider than those outlined in ASTM D3410. This was done in order to accurately simulate the conditions found in the creep fixtures which were constructed for 38 mm wide coupons. The dimensions of these specimens can be found in Table 3.1 and a schematic illustration can be found in Figure 3.6. The specimens were equipped with a single uniaxial extensometer that was removed at a predetermined stress of 138 MPa (20 ksi) to prevent damage of the extensometer. These additional tests were performed in order to collect strain data to allow the stress-strain curves to be plotted and the compressive modulus to be calculated. Due to the absence of the extensometer for the remainder of the test, strain at failure was estimated based on an assumed linearity of the stress-strain response of the composite material. A photograph of the short-term tensile test setup can be found in Figure 3.7. A typical stress-strain diagram for the short-term compressive coupon tests can be found in Figure 3.8 and all others can be found in Appendix B. All longitudinal compression tests were performed using a hydraulic testing machine and specimens without end tabs. Coupon preparation, loading procedure and data reduction were performed in accordance with ASTM D3410 excluding the change in width of the four coupons used for strain measurements.

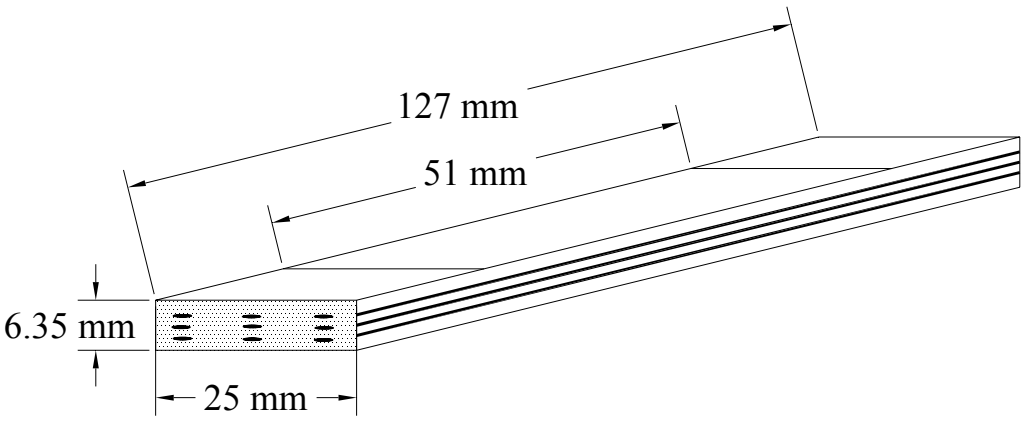

Figure 3.5 - Nominal Compression Coupon Dimensions

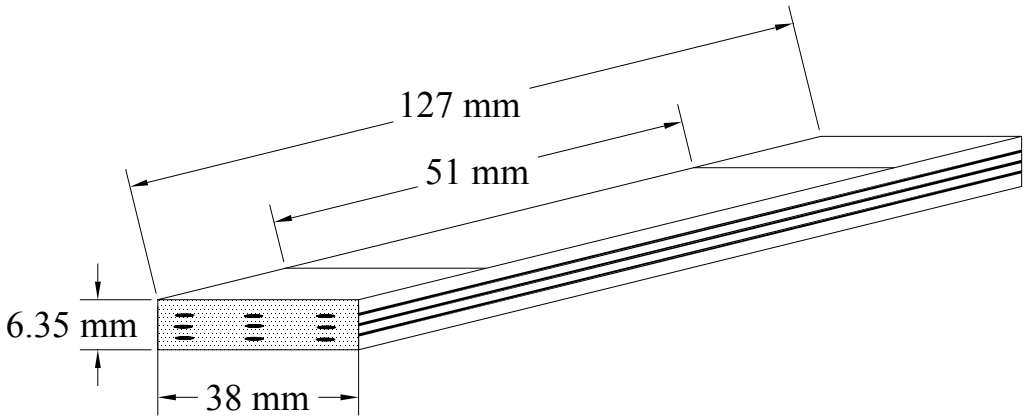

Figure 3.6 - Nominal Compression Coupon Tested with Extensometer

Figure 3.7 - Short-term Compression Test Setup

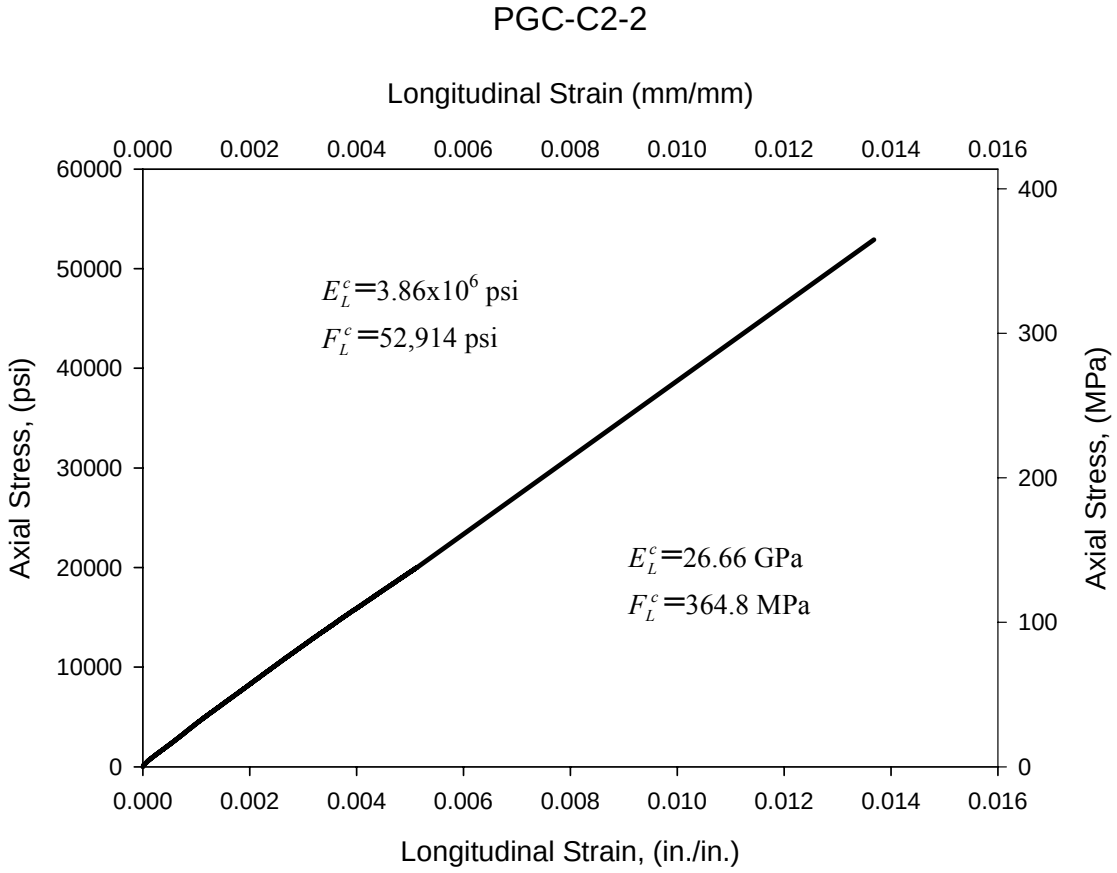

Figure 3.8 - Typical Compression Coupon Stress-Strain Curve

3.2.3 Coupon Test Results

The following tables contain the dimensions of the coupons that were used and the results of the short-term tensile and compressive coupon tests. The dimensions of the coupons can be found in Table 3.2 and the results for each sample can be found in Tables 3.3 and 3.4. Average values for the longitudinal modulus (tension) $E_L{}^t$, longitudinal modulus (compression) $E_L{}^c$, ultimate stress (tension) $F_L{}^t$, and the ultimate stress (compression) $F_L{}^c$ can be found in Table 3.5. Short-term tests of the same material were performed in previous works by Butz (1997) and Kang (2001). Thirty uniaxial compression tests were performed by Butz and thirty uniaxial tensile tests were performed by Kang. The values found in these studies are comparable to the values found from short-term tests in the current investigation. The results of the current study and these previous works can be found in Table 3.5.

Table 3.2 – Measured Coupon Dimensions

Specimen	Thickness		Width		Area	
	mm	in.	mm	in.	mm^2	$in.^2$
Tension						
PGT-A1-1	6.09	0.240	25.87	1.019	157.58	0.244
PGT-A1-2	6.26	0.246	25.81	1.016	161.54	0.250
PGT-A1-3	6.42	0.253	25.88	1.019	166.24	0.258
PGT-A1-4	6.41	0.253	25.78	1.015	165.36	0.256
PGT-A2-1	6.14	0.242	26.57	1.046	163.05	0.253
PGT-A2-2	6.27	0.247	25.92	1.020	162.45	0.252
PGT-A2-3	6.12	0.241	25.89	1.019	158.51	0.246
PGT-A2-4	6.16	0.242	25.96	1.022	159.89	0.248
PGT-C-1	6.21	0.245	25.35	0.998	157.55	0.244
PGT-C-2	6.29	0.248	25.24	0.994	158.84	0.246
PGT-C-3	6.35	0.250	25.32	0.997	160.74	0.249
PGT-C-4	6.12	0.241	25.08	0.987	153.42	0.238
PGT-D-1	6.14	0.242	25.36	0.999	155.62	0.241
PGT-D-2	6.41	0.252	25.40	1.000	162.80	0.252
PGT-D-3	6.29	0.248	25.28	0.995	158.95	0.246
PGT-D-4	6.19	0.244	25.36	0.998	157.01	0.243
Compression						
PGC-A1-1	6.17	0.243	25.50	1.004	157.40	0.244
PGC-A1-4	6.17	0.243	25.53	1.005	157.56	0.244
PGC-A2-1	6.02	0.237	25.37	0.999	152.75	0.237
PGC-A2-2	6.10	0.240	25.22	0.993	153.75	0.238
PGC-A2-3	6.38	0.251	24.79	0.976	158.05	0.245
PGC-A2-4	6.32	0.249	24.64	0.970	155.83	0.242
PGC-C1-1	6.27	0.247	25.45	1.002	159.67	0.247
PGC-C1-2	6.25	0.246	25.50	1.004	159.34	0.247
PGC-C1-3	6.68	0.263	25.40	1.000	169.68	0.263
PGC-C1-4	6.53	0.257	25.43	1.001	165.97	0.257
PGC-D1-1	6.30	0.248	25.48	1.003	160.48	0.249
PGC-D1-2	6.22	0.245	24.97	0.983	155.38	0.241
PGC-D1-3	6.30	0.248	25.22	0.993	158.88	0.246
PGC-D1-4	6.35	0.250	25.32	0.997	160.81	0.249
PGC-C2-1	6.02	0.237	38.10	1.50	229.4	0.356
PGC-C2-2	6.31	0.248	38.32	1.51	241.8	0.374
PGC-C2-3	6.29	0.247	38.43	1.51	241.7	0.373
PGC-A1-3	6.15	0.242	38.22	1.50	235	0.363

Table 3.3 – Results of Short-Term Tensile Tests

	Tension			
Specimen	F_L^t		E_L^t	
	MPa	**psi**	**GPa**	**(10^3ksi)**
~~**PGT-A1-1***~~	~~314.55~~	~~45621~~	~~8.34~~	~~1.21~~
PGT-A1-2	384.39	55750	21.31	3.09
PGT-A1-3	361.19	52386	22.02	3.19
PGT-A1-4	417.69	60580	23.51	3.41
PGT-A2-1	350.62	50853	24.72	3.58
PGT-A2-2	413.41	59960	24.03	3.48
PGT-A2-3	365.85	53062	24.50	3.55
PGT-A2-4	392.72	56959	23.34	3.38
PGT-C-1	320.66	46508	21.89	3.17
PGT-C-2	332.69	48252	20.85	3.02
PGT-C-3	358.01	51924	21.45	3.11
PGT-C-4	396.22	57466	23.53	3.41
PGT-D-1	343.05	49755	20.23	2.93
PGT-D-2	448.36	65028	26.34	3.82
PGT-D-3	383.98	55691	21.83	3.16
PGT-D-4	382.99	55547	21.98	3.19
Average	**376.79**	**54648**	**22.77**	**3.30**

*Values were disregarded due to dramatic slipping of the extensometer

Table 3.4 – Results of Short-Term Compression Tests

	Compression			
Specimen	F_L^c		E_L^c	
	MPa	**psi**	**GPa**	**(10^3ksi)**
PGC-A1-1	384.47	55763	-	-
PGC-A1-4	434.12	62963	-	-
PGC-A2-1	316.97	45972	-	-
PGC-A2-2	296.61	43020	-	-
PGC-A2-3	384.95	55832	-	-
PGC-A2-4	396.29	57477	-	-
PGC-C1-1	355.32	51534	-	-
PGC-C1-2	385.77	55951	-	-
PGC-C1-3	458.77	66539	-	-
PGC-C1-4	359.92	52202	-	-
PGC-D1-1	329.74	47824	-	-
PGC-D1-2	412.70	59857	-	-
PGC-D1-3	358.41	51983	-	-
PGC-D1-4	367.55	53309	-	-
PGC-C2-1	324.60	47079	20.73	3.00
PGC-C2-2	364.83	52914	26.68	3.87
PGC-C2-3	334.53	48519	24.55	3.56
PGC-A1-3	289.08	41928	22.64	3.28
Average	**364.15**	**52815**	**23.65**	**3.43**

Table 3.5- Average Values from Short-Term Testing

	F_L		E_L	
	MPa	**psi**	**GPa**	**(10^3ksi)**
Tension	**376**	**54648**	**22.8**	**3.30**
STD	34.4	4986	1.68	.244
C.O.V.	9.1%		7.4%	
Compression	**364**	**52815**	**23.7**	**3.43**
STD	45.2	6557	2.55	.373
C.O.V.	12.4%		10.8%	
Tension (Kang 2001)	**372**	**54070**	**23.8**	**3.45**
STD	25.6	3712	1.5	0.217
C.O.V.	6.9%		6.3%	
Compression (Butz 1997)	**380**	**55114**	**23.8**	**3.46**
STD	45.4	6583	0.96	.140
C.O.V.	12%		4%	

3.3 Short-Term Elevated Temperature Tests

Compression tests were conducted at elevated temperatures to observe the effects of temperature on the modulus of elasticity and the ultimate strength of the E-glass polyester composite under short-term loading. Coupon specimens were tested in compression at temperatures of 38°C (100°F), 54°C(130°F) and 65°C (150°F) until failure. An environmental chamber was constructed on the base plate of a universal testing machine that was capable of maintaining the desired temperatures. The chamber was heated using a 450 watt finned strip heater and the temperature was regulated by a remote bulb thermostat. Coupons were placed in the same fixture as used in the previous compression tests. The coupons used for the elevated temperature tests were the same

dimensions as the previous compression tests with one notable exception; the length was shortened from 127 mm (5 in.) to 114 mm (4.5 in.), which in turn shortened the gage length from 51mm (2 in.) to 38 mm (1.5 in.). This reduction in length was based on the stability Equation (3.1) and the expected reduction in modulus of elasticity at the higher temperatures. The reduction in modulus was approximated using the manufacturer's design guidelines. The shortened sample ensured that the coupon would undergo material failure rather than buckling. The coupons were equipped with strain gages and tested until failure. The coupons were allowed to cure at their specified testing temperature for 2 hours before the tests were started. This ensured that the heat was completely distributed throughout the specimen. A picture of the environmental chamber and test setup can be found in Figure 3.9. A typical stress-strain curve for each temperature is shown in Figures 3.10 with all others appearing in Appendix B. The results of all elevated temperature tests can be found in Table 3.6. The elevated temperature tests showed appreciable reductions in both modulus of elasticity and ultimate strength with increasing temperature. The percent reduction in these properties from those found at room temperature can be found in Table 3.7.

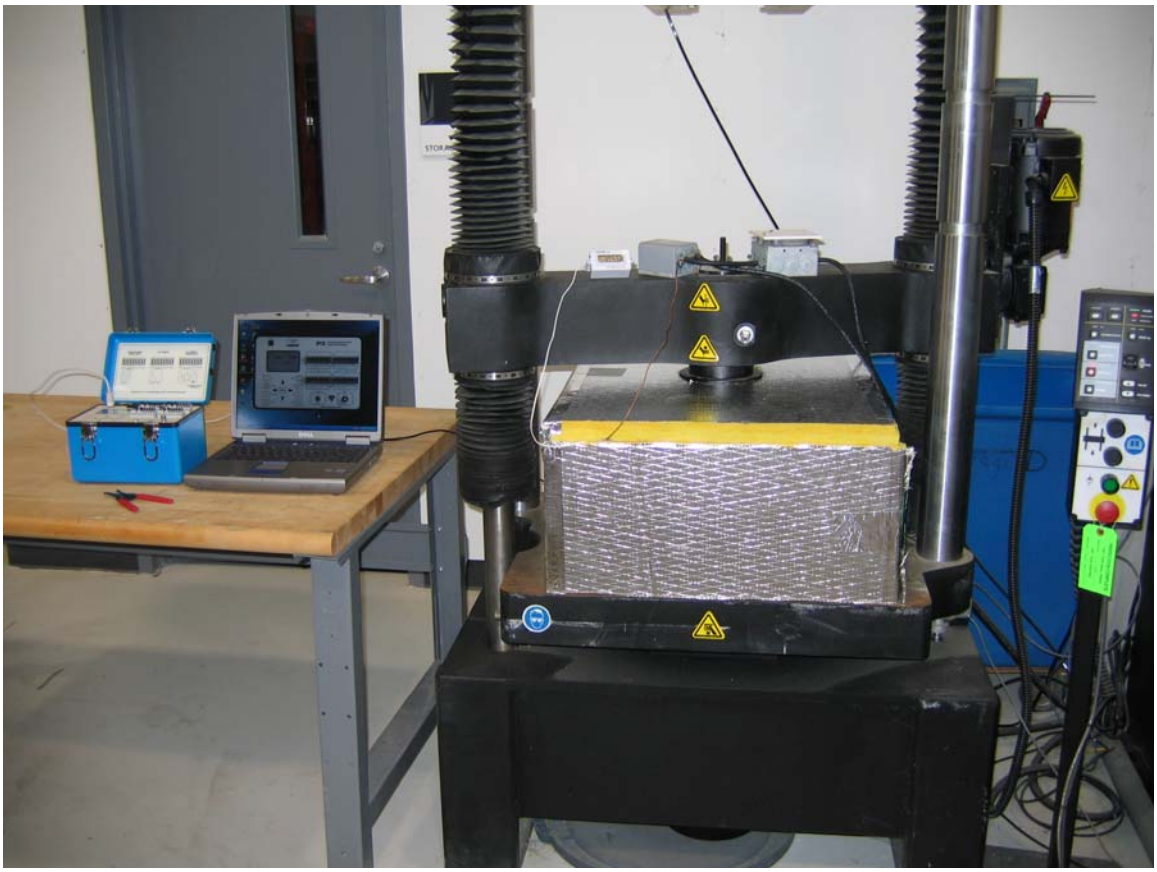

Figure 3.9 – Test Setup for Short-Term Elevated Temperature Tests

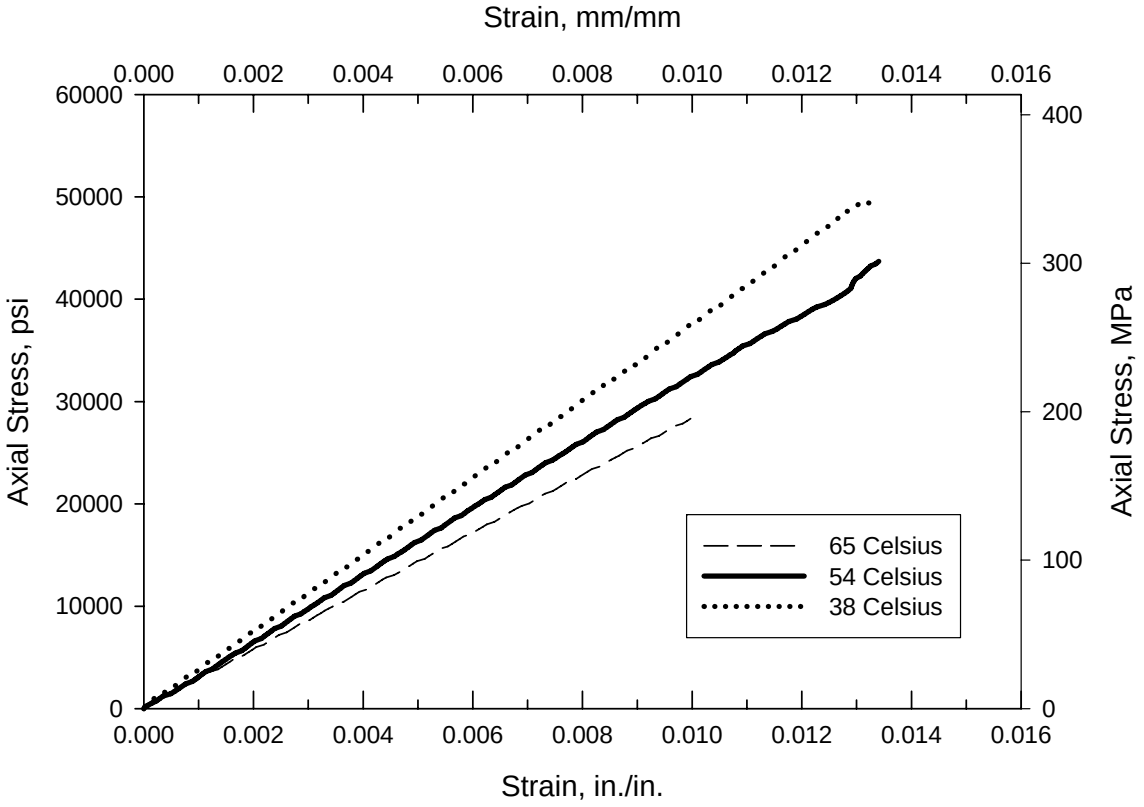

Figure 3.10 – Typical Stress-Strain Curves at Elevated Temperatures

Table 3.6 – Results of Short-Term Elevated Temperature Tests

Specimen	Temp (°C)	F_L^c MPa (psi)	ε_L^c (mm/mm)	E_L^c GPa (ksi)
C1	**65**	**233** (33737)	0.0118	**20.9** (3032)
C2	**54**	**301** (43708)	0.0134	**22.4** (3256)
C3	**38**	**361** (52423)	0.0175	**20.6** (2987)
D1	**65**	**195** (28335)	0.0100	**19.5** (2828)
D2	**54**	**364** (52746)	0.0158	**23.0** (3329)
D3	**54**	**240** (34825)	0.0129	**18.6** (2695)
D4	**38**	**342** (49691)	0.0132	**25.9** (3758)
65°C Average		**214** (31036)	**0.0109**	**20.2** (2930)
54°C Average		**302** (43760)	**0.0140**	**21.3** (3093)
38°C Average		**352** (51057)	**0.0154**	**23.3** (3373)
23°C Average		**364** (52815)	**0.0140**	**23.65** (3430)

Table 3.7 – Reduction of Mechanical Properties Due to Temperature

Temperature	% Reduction in F_L^c	% Reduction in E_L^c
65°C Average	**41.2**	**14.6**
54°C Average	**17.5**	**9.9**
38°C Average	**3.3**	**1.5**

CHAPTER IV

LONG-TERM EXPERIMENTAL PROGRAM

4.1 Introduction

This chapter presents an investigation into the creep behavior of a pultruded E-glass/polyester composite under sustained compressive loading and elevated temperatures. The experiments were conducted at a stress level of 0.33 F_L^c and three different temperatures. The temperatures investigated were 23.3°C (74°F), 37.7°C (100°F), and 54.4°C (130°F). In addition to the tests conducted at these constant temperatures, two tests were conducted under cyclic heating. All experiments were performed for a minimum duration of 1,000 hours.

4.2 Specimen Details

The rectangular prismatic coupons used in this investigation were cut from the panels of a 102 mm (4 in.) x 102 mm (4 in.) x 6.4 mm (0.25 in.) pultruded FRP square tube. The gage length of the coupons was determined using the stability equation, Equation (3.1), to prevent buckling and ensure compressive failure of the specimen. This approach led to the specimen dimensions found in Table 4.1. It is notable that the coupon gage length is shorter for the elevated temperature tests due to the expected decrease in longitudinal modulus. This expected loss was based on the findings of the short-term elevated temperature tests that were performed in this study. The specimen dimensions can be seen in the schematic illustrations in Figures 4.1 and 4.2.

Table 4.1 – Nominal Coupon Dimensions for Creep Studies

Test Type	**t**		**l**		**l_g**		**b**	
	mm	in.	mm	in.	mm	in.	mm	in.
Room Temp.	6.35	0.25	127	5	51	2	38	1.5
Elevated Temp.	6.35	0.25	114	4.5	38	1.5	38	1.5

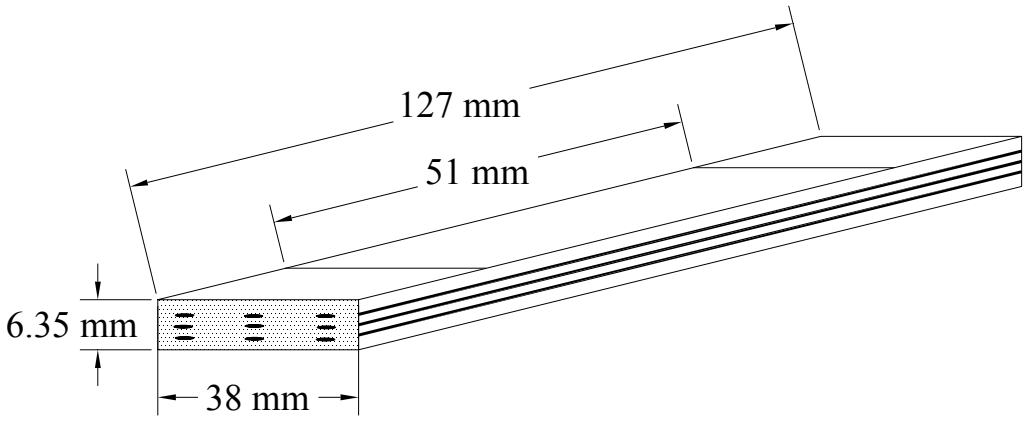

Figure 4.1 – Typical Room Temperature Creep Coupon

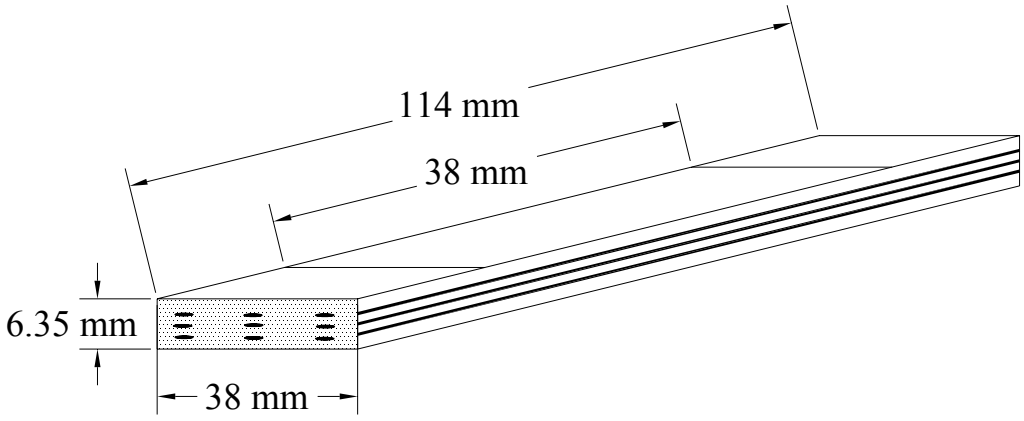

Figure 4.2 – Typical Elevated Temperature Creep Coupon

4.3 Long-Term Experimental Setup

The long-term experimental program utilized dead weight lever arm creep fixtures to apply a compressive load to the coupons. A schematic of the creep fixtures can be found in Figure 4.3. The fixture was constructed of structural steel and pillow block roller bearings were used as the fulcrum for the lever arm. The dimension of the lever arm allowed the dead weight load to be amplified by a factor of 10 on the coupons. The cages in which the coupons were placed were designed to transfer the tensile load that was placed on the fixture by the lever arm into compression on the coupons. Figure 4.4 shows a typical compression cage. Three such cages were placed inside each creep fixture which allowed the simultaneous loading of three coupons with the same stress level.

Two creep fixtures were outfitted to perform the elevated temperature tests. To accomplish this, 38 mm (1.5 in.) thick fiberglass duct board insulation was cut and taped around the outside of the creep fixture using foil tape to secure the corners and edges. The rear of the creep fixture housed two 450 watt finned strip heaters which supplied the heat to the chamber through an opening in the back of the heating chamber. Air was circulated through the creep fixture using a high temperature blower. The blower removed air from the top of the fixture and circulated it back through the chamber that contained the heating strips for the air to be reheated. The temperature inside the environmental chamber was monitored using a panel thermometer and regulated with a remote bulb thermostat. Figure 4.5A shows a creep fixture without the environmental chamber was assembled and Figure 4.5B shows the fixture after assembly.

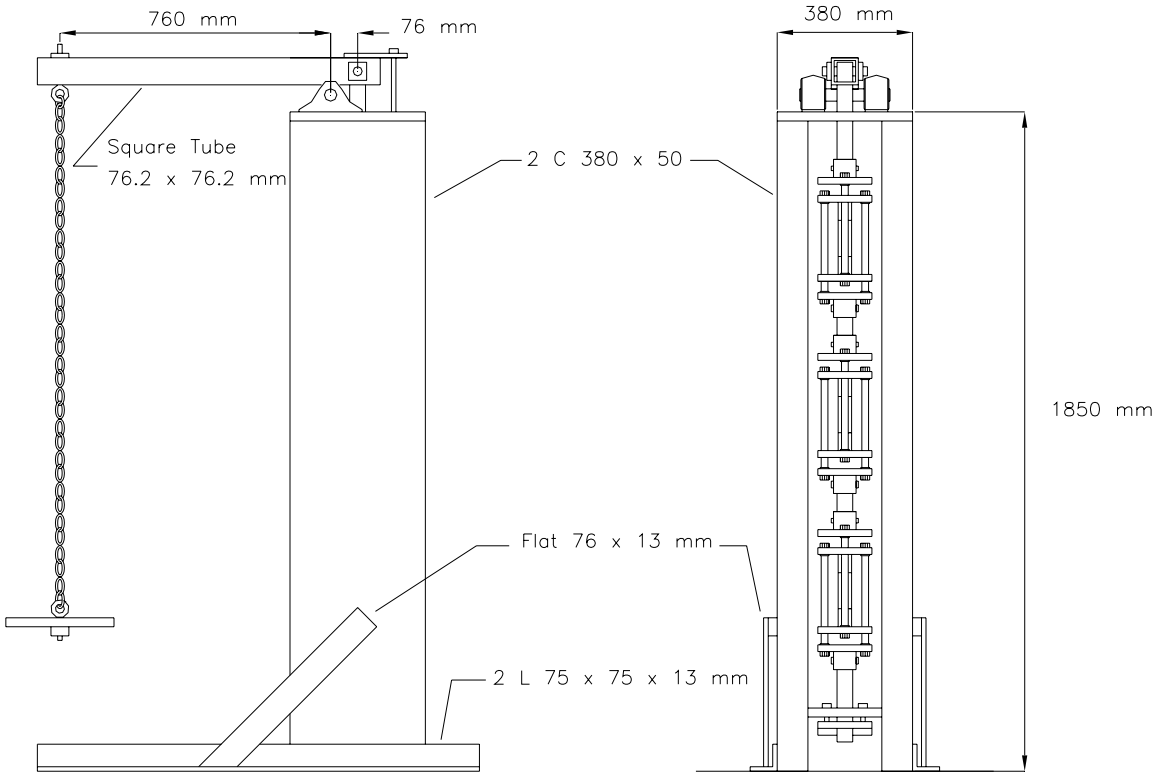

Figure 4.3 – Schematic of Creep Fixture (from Scott and Zureick (1998))

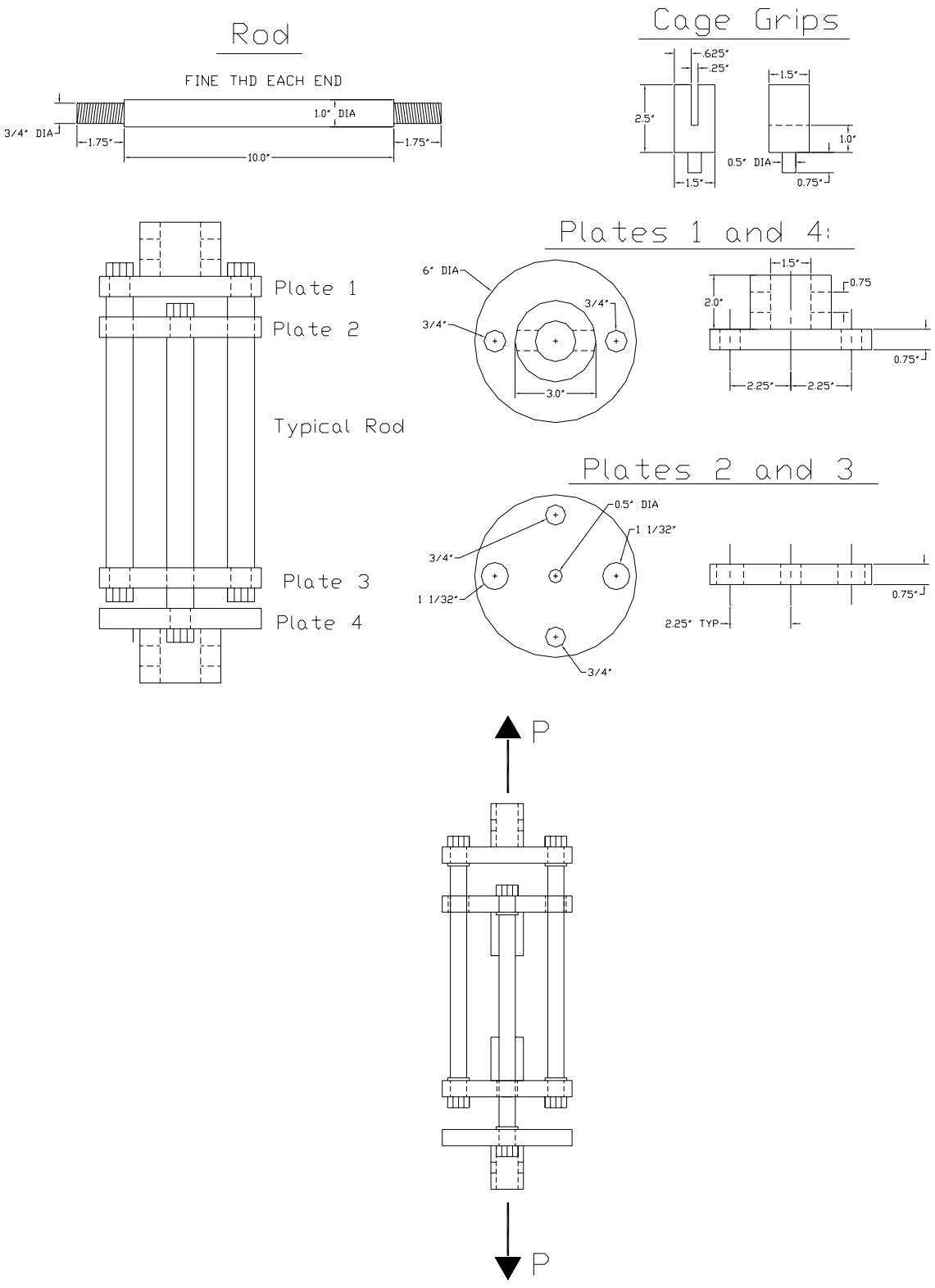

Figure 4.4 – Typical Compression Cage (from Scott and Zureick (1998))

Figure 4.5A– (Left) Creep Fixture with Environmental Chamber

Figure 4.5B – (Right) Room Temperature Creep Fixture

A stress level of 126MPa (18.3 ksi) was used for all creep tests. This value represents approximately 33% of the ultimate stress that was determined in the short-term testing. This percentage of the ultimate stress was chosen based on the manufacturer's design guidelines (Strongwell (1998)) in which a factor of safety of 3 is suggested for structural elements in compression. This stress level also ensured that the test would be conducted in the linear-elastic range of the material.

The three temperatures under investigation were 23.3°C (74°F), 37.7°C (100°F), and 54.4°C (130°F). These temperatures were selected based on possible real world applications of this material and the manufacturer guidelines. The manufacturer does not recommend the use of this composite material above 65.5°C (150°F). The temperatures that were selected are meant to reflect situations such as attics or crawlspaces which can easily reach 54.4°C (130°F) in the summer months.

The coupons were inserted into the cage grips and aligned. After the coupons were seated in the grips, concrete dead weights were added to reach the desired stress level. The elevated temperature specimens were allowed 1 hour to acclimate to the temperature before the concrete weights were applied. The specimen and cage dimensions allowed for two specimens to be tested simultaneously at elevated temperature.

Cyclically heated creep tests were performed at maximum temperatures of 37.7°C (100°F), and 54.4°C (130°F). For these experiments the heat was applied for 8 hours and then the heat was terminated for 16 hours. This was controlled using a timer which controlled the power supply to the finned strip heaters. The load was applied to the

specimens at the beginning of the first heat cycle and the specimens were not allowed to acclimate to the elevated temperature.

Figure 4.6 shows a creep fixture after the concrete weights have been applied. Previous work by Scott and Zureick (1998) with the same creep fixtures showed that the creep fixtures did not induce bending of the specimens. Therefore, the room temperature coupons were equipped with a single uniaxial strain gage. Strain gages were used on both sides of the elevated coupons to ensure that the elevated temperature did not induce bending of the specimen. Strain readings for the room temperature coupons were based on the previous work by Scott and Zureick (1998) and were recorded at the following intervals:

Period 1: Once each six minutes (0.1 hours) for the first hour

Period 2: Once each 15 minutes for the next three hours

Period 3: Once each hour for the following 24 hours

Period 4: Once each day thereafter

The tests at elevated temperatures had periods that differed slightly and were as follows:

Period 1: Once each two minutes for the first hour

Period 2: Once each six minutes for the next hour

Period 3: Once each 15 minutes for the next three hours

Period 4: Once each hour for the next 24 hours

Period 5: Once each day thereafter

The specimen strain readings for each of the three temperatures and the cyclic heating are shown in Figures 4.7, 4.8, 4.9, and 4.10.

Figure 4.6 – Creep Fixture with Applied Dead Load

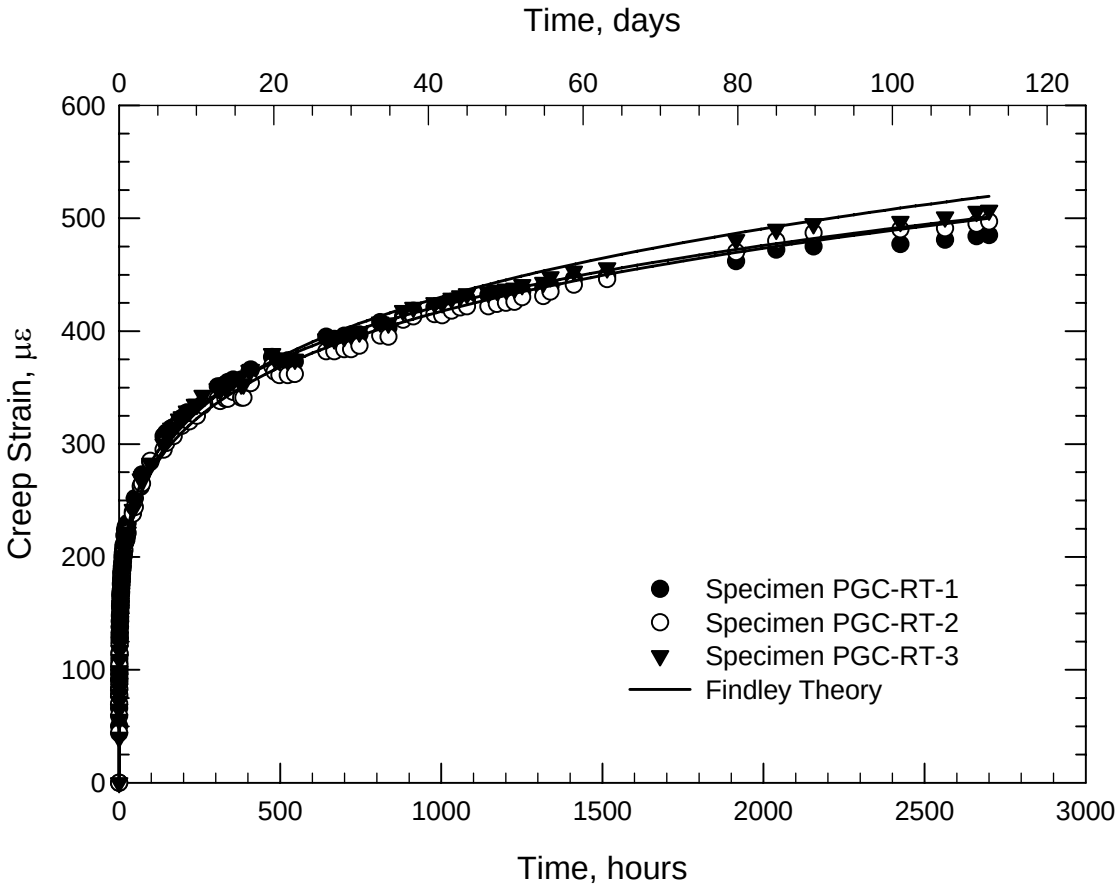

Figure 4.7 – Creep Strains for Coupons at Room Temp. 23.3°C (74°F) and 0.33 F_L^c

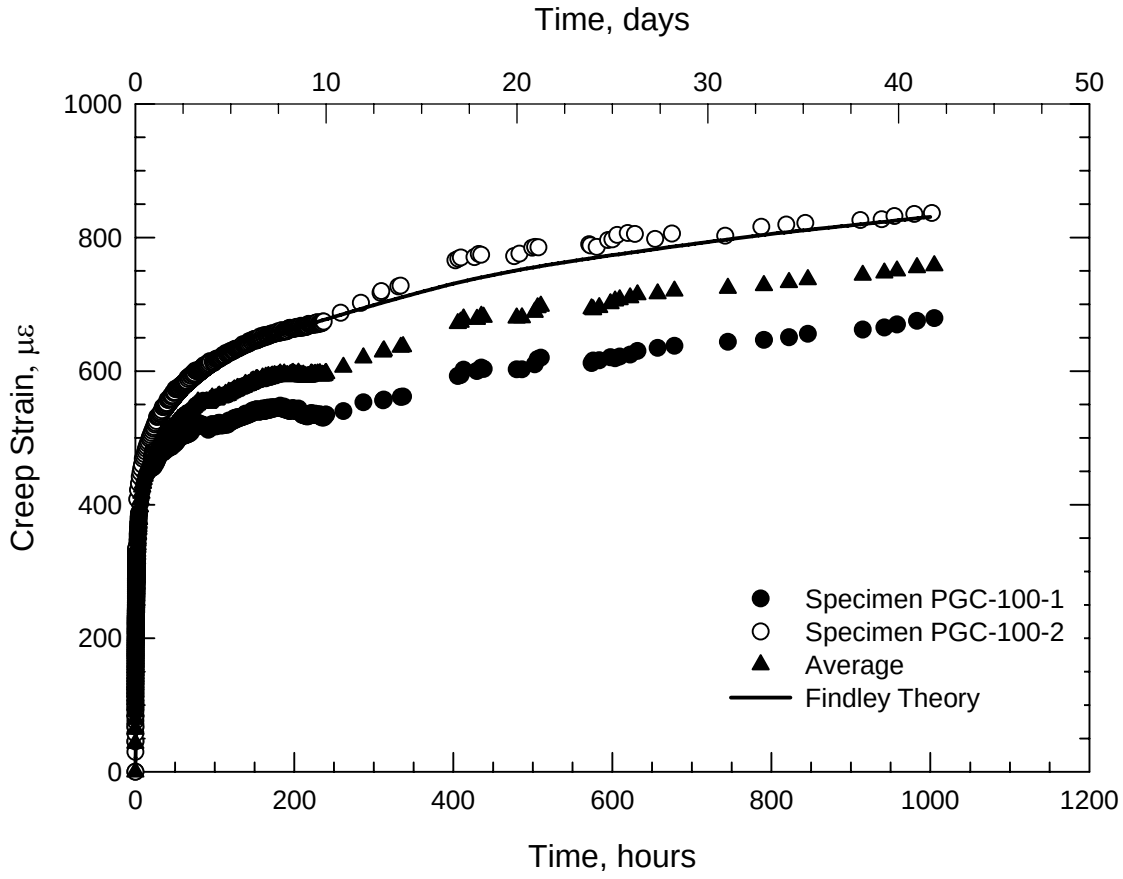

Figure 4.8 – Creep Strains for Coupons at 37.7°C (100°F) and 0.33 F_L^c

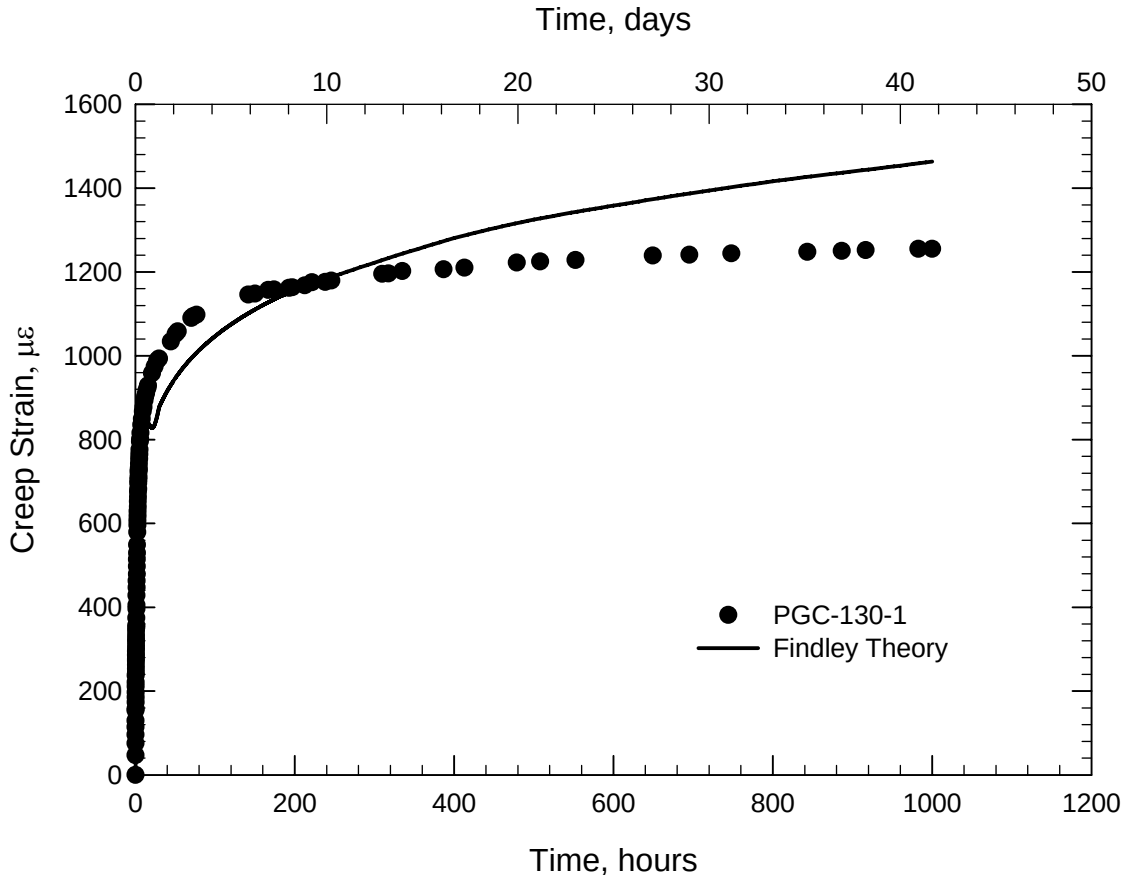

Figure 4.9 – Creep Strains for Coupons at 54.4°C (130°F) and 0.33 F_L^c

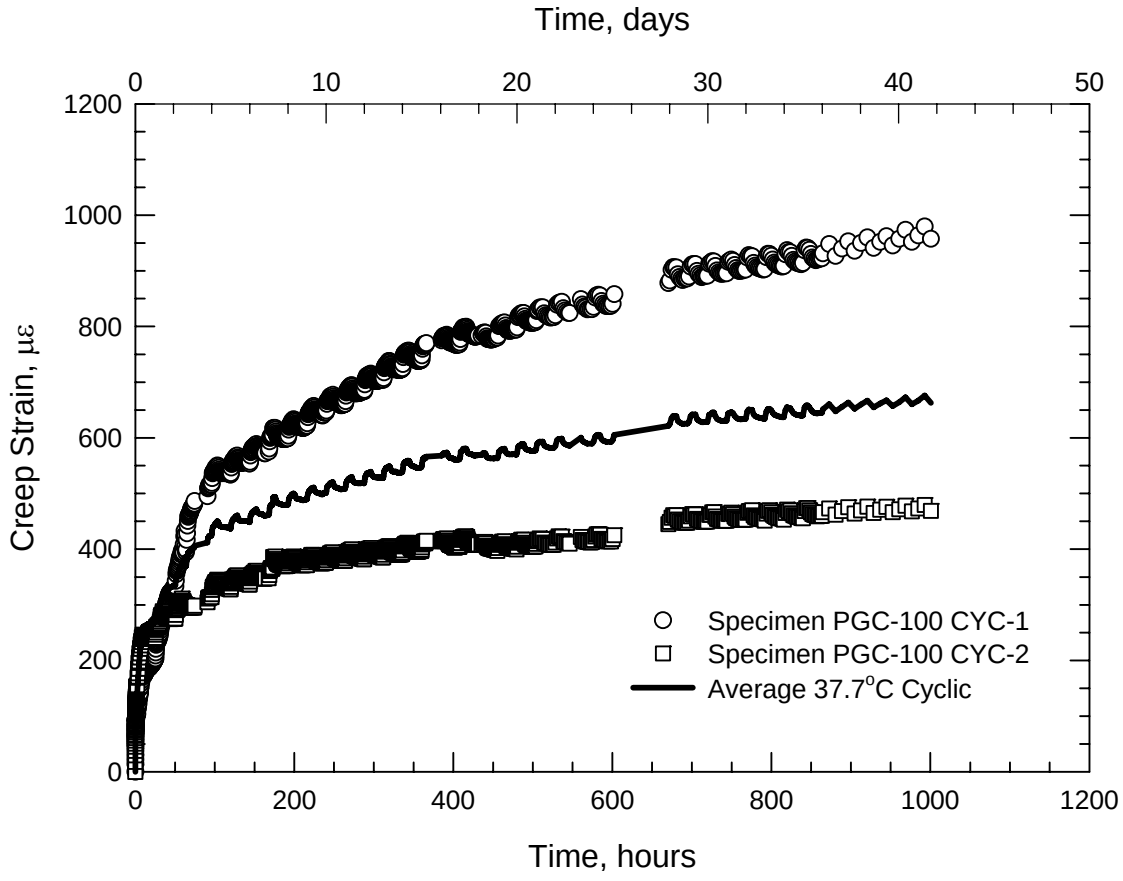

Figure 4.10 – Creep Strains for Coupons under Cyclic Heating at 37.7°C (100°F) and 0.33 F_L^c

4.4 Development of a Semi-Empirical Viscoelastic Model

The current investigation involved both time-dependent and temperature-dependent behavior that needed to be incorporated into the viscoelastic model. Findley, Lai, and Onaran (1976) asserted that the total strain ε under a given temperature *T*, and a given stress *f* can be represented by:

$$\varepsilon = \varepsilon^T + \varepsilon^t \tag{4.1}$$

where ε^t is the strain due to stress over time and ε^T is the tensor of thermal expansion. Therefore the time-dependent and the temperature-dependent behavior could be modeled separately and then summed to reach the total creep strain.

The time-dependent behavior of the material was modeled using the power law developed by Findley (1944). This model provided an accurate model for the 26 year creep data of an unreinforced thermoplastic material (Findley 1987). The Findley power law also proved to be a good approximation for creep in a pultruded E-glass/vinylester composite with a V_f of 30% (Scott and Zureick (1998)). As noted earlier, the material in the current investigation had fiber volume fraction V_f of approximately 35% by volume. Therefore, the creep deformation was assumed to be primarily matrix driven and as a result the Findley power law would provide an accurate approximation of the data. The simplest form of the Findley power law can be written as:

$$\varepsilon(t) = \varepsilon_o + mt^n \tag{4.2}$$

where

ε(t) = total time-dependent strain

ε_o = stress-dependent initial elastic strain

m = stress-dependent and temperature-dependent coefficient

n = stress-independent and temperature independent material constant

t = time after loading

Since the total viscoelastic model has been separated into two distinct parts, time-dependent behavior and temperature-dependent behavior, the room temperature creep tests were used to model the time-dependent behavior only. Effectively, ε^T in Equation (4.1) was considered to be zero and therefore the total strain was equal to the time-dependent strain. The room temperature (23.3°C) model would serve as a reference for the temperature-dependent studies. The empirical constants, m and n, needed to formulate the power law can be found from the experimental creep data, rearranging Equation (4.2) and taking the logarithm of both sides:

$$\log\left[\varepsilon(t) - \varepsilon_o\right] = \log(m) + n\log(t) \tag{4.3}$$

Plotting Equation (4.3) on a log-log scale yields a straight line from which the empirical constants can be calculated. From the resulting line, the y-intercept at t = 1 hour is equivalent to the value of m and the slope of the line is the material constant n.

The creep strain data for the room temperature coupons are plotted on a logarithmic scale in Figure 4.11. The values obtained for the constants m and n are given in Table 4.2. The Findley models produced by these constants are plotted alongside the experimental creep strain data in Figure 4.7. The power law model proved to be a good approximation of the creep behavior of the E-glass/polyester material at room temperature. Comparisons of n values from previous work can be found in Table 4.3.

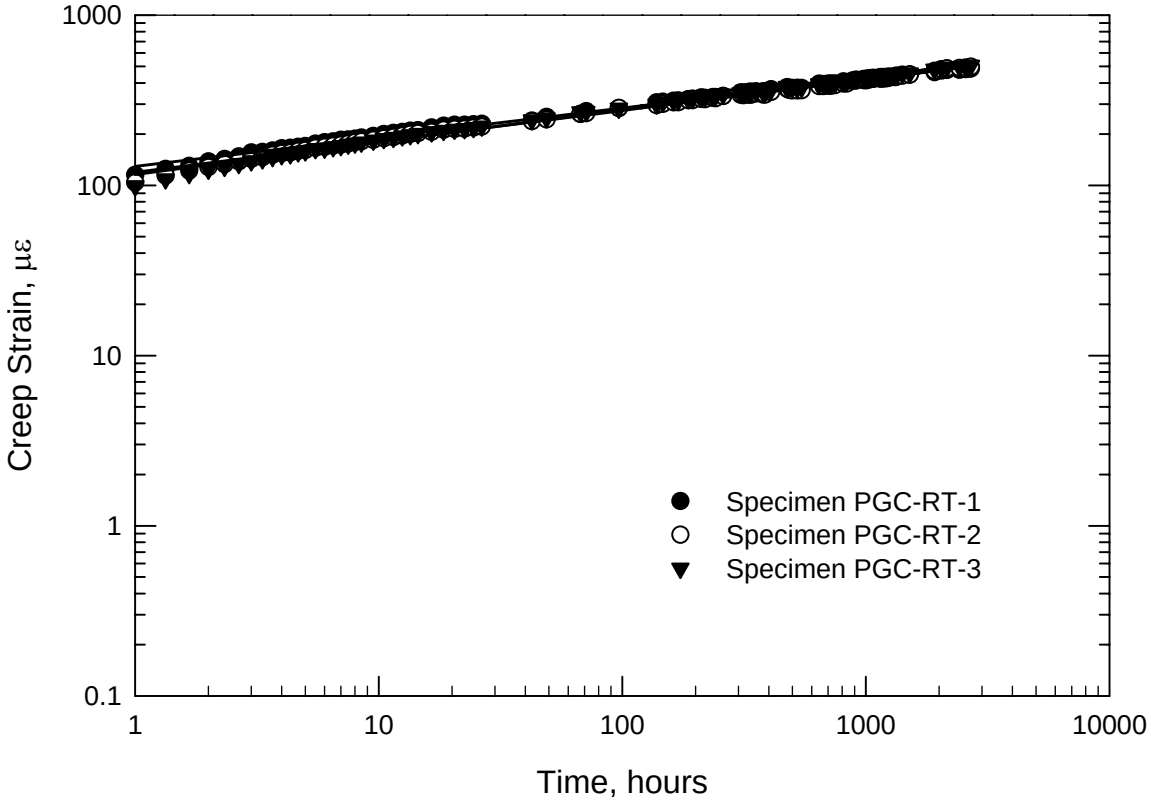

Figure 4.11 – Logarithmic Plot for Evaluation of Constants m and n at 23.3°C

Table 4.2 – Creep Constants *m* and *n* from Equation (4.3) at 0.33 F_L^c and Room Temperature

Specimen	ε_o (με)	*m* (με)	*n*
PGC-RT-1	5339	129	.172
PGC-RT-2	5176	119	.181
PGC-RT-3	4854	116	.190
Average	**5123**	**121**	**.183**

Table 4.3 – Average values for the Material Constant *n* from Previous Works

Investigator	Loading Regime	*n*
McClure and Mohammadi (1995)	Compression (Angles)	0.17
McClure and Mohammadi (1995)	Compression	0.25
Scott and Zureick (1998)	Compression	0.23
Current Investigation	Compression	0.18

Using the average values of the empirical parameters m and n, the Findley power law model using Equation (4.2) is equated to the time-dependent behavior of the material that is currently been investigated. Due to the relationship shown in Equation (4.1), the temperature-dependent behavior of the material can be found by subtracting the time-dependent strains from the total strain recorded in the experimental data as follows:

$$\varepsilon^T = \varepsilon - \varepsilon^t \tag{4.4}$$

Using the results of Equation (4.4), a secondary Findley power law can be used to express the temperature-dependent behavior of the material. To accomplish this, the results of Equation (4.4) are found using the recorded strains at the elevated temperatures as ε and the recorded strains at room temperature as ε^t. These results are then plotted on a logarithmic scale and the values for m and n are taken in the same manner as described earlier, where m is the y-intercept at t = 1 hour and n is the slope of the resulting straight line. For the temperature-dependent model, these parameters will be designated as m_T and n_T. The results from Equation (4.4) for the 37.7°C (100°F) and the 54.4°C (130°F) experiments can be found in Figure 4.12 and the logarithmic plot can be found in Figure 4.13. Using the empirical constants m_T and n_T , given in Table 4.4, the temperature-dependent creep strains can be modeled using a power law model where:

$$\varepsilon(T) = \varepsilon_o + m_T t^{n_T} \tag{4.5}$$

Thus, the strain as a function of time and temperature can be modeled by summing the results of the room temperature and the temperature-dependent Findley power law models:

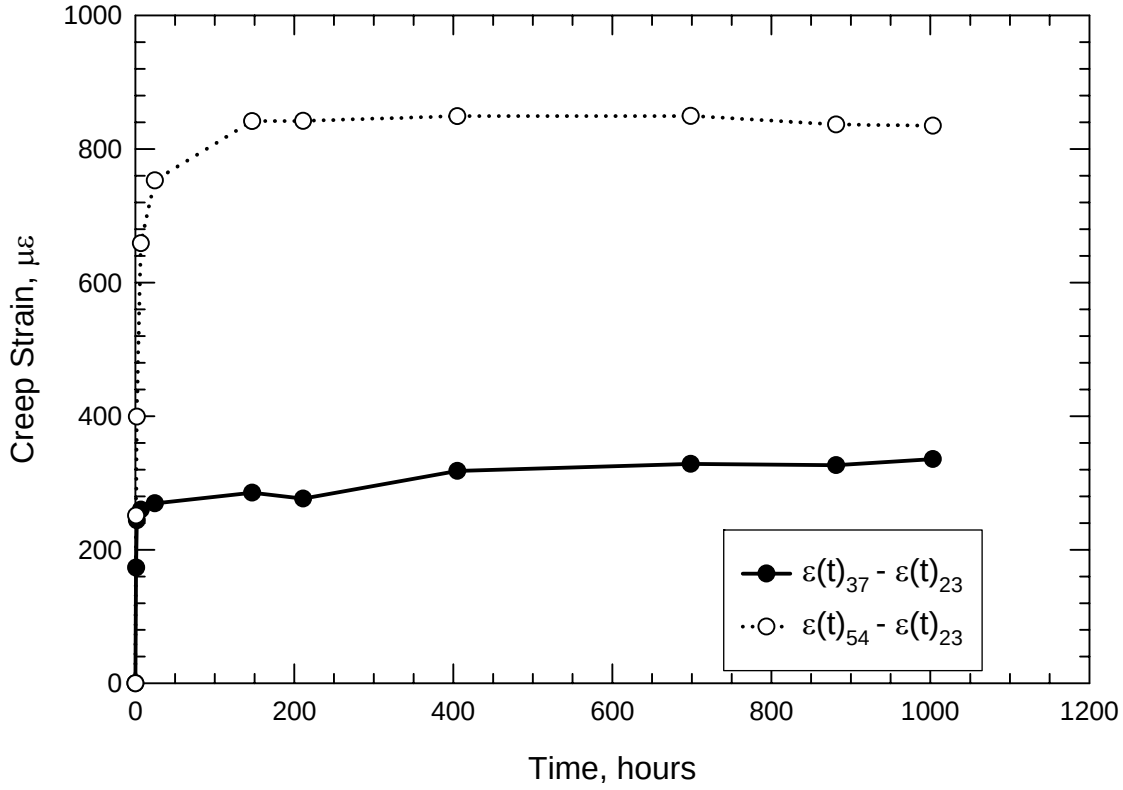

Figure 4.12 – Plot of Creep Strain at Elevated Temp., minus Creep Strain Measured at Room Temp.

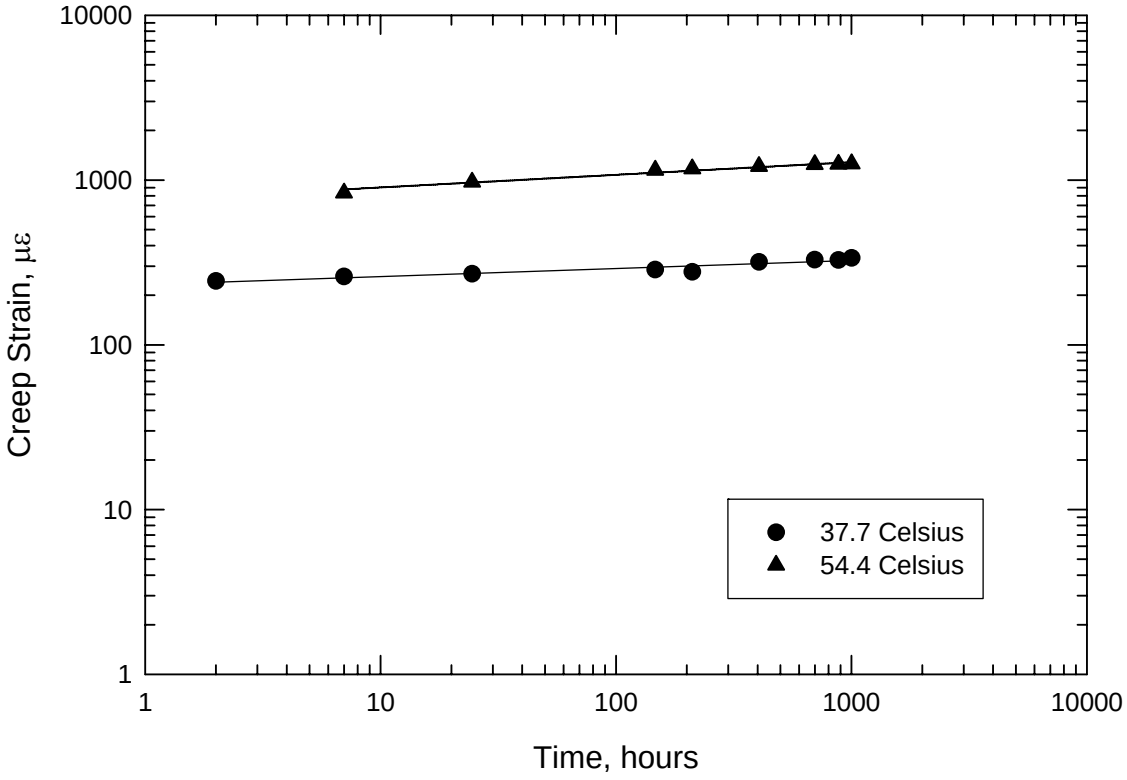

Figure 4.13 – Logarithmic Plot of Creep Strain at Elevated Temp., minus Creep Strain Measured at Room Temp.

Table 4.4 –Constants m_T and n_T

Temperature	m_T	n_T
37.7°C (100°F)	231	0.0489
54.4°C (130°F)	635.7	0.0453
37.7°C (100°F) Cyclic	27.6	0.336

$$\varepsilon(T,t) = \varepsilon_o + m_{RT} t^{n_{RT}} + m_T t^{n_T} \tag{4.6}$$

where

$\varepsilon(T,t)$ = total time and temperature dependent strain

ε_o = stress-dependent initial elastic strain

m_{RT} = stress-dependent and temperature-dependent coefficient at 23.3°C

n_{RT} = stress independent material constant at 23.3°C

m_T = stress and temperature-dependent coefficient at elevated temperature

n_T = stress independent material constant at elevated temperature

t = time after loading

This model can be used to predict the strain response of the elevated temperature specimens in the current study. Figure 4.14 shows the time and temperature dependent model alongside the experimental creep data for all tests. It should be noted that the initial elastic strains for all experiments were very similar and were found to be independent of temperature for the range of temperatures in this study. Table 4.5 shows the initial elastic strains for all coupons.

The same modeling procedure is also applicable to the cyclically heated specimens as can be seen in Figure 4.15 which contains the experimental creep data and the comprehensive model. The time and temperature dependent model was a very close approximation of the creep data using the parameters m_T and n_T, found using the same methods as the constant heat procedure. However, the parameters m_T and n_T did not correlate with the parameters found from the constant heat experiments. Due to the

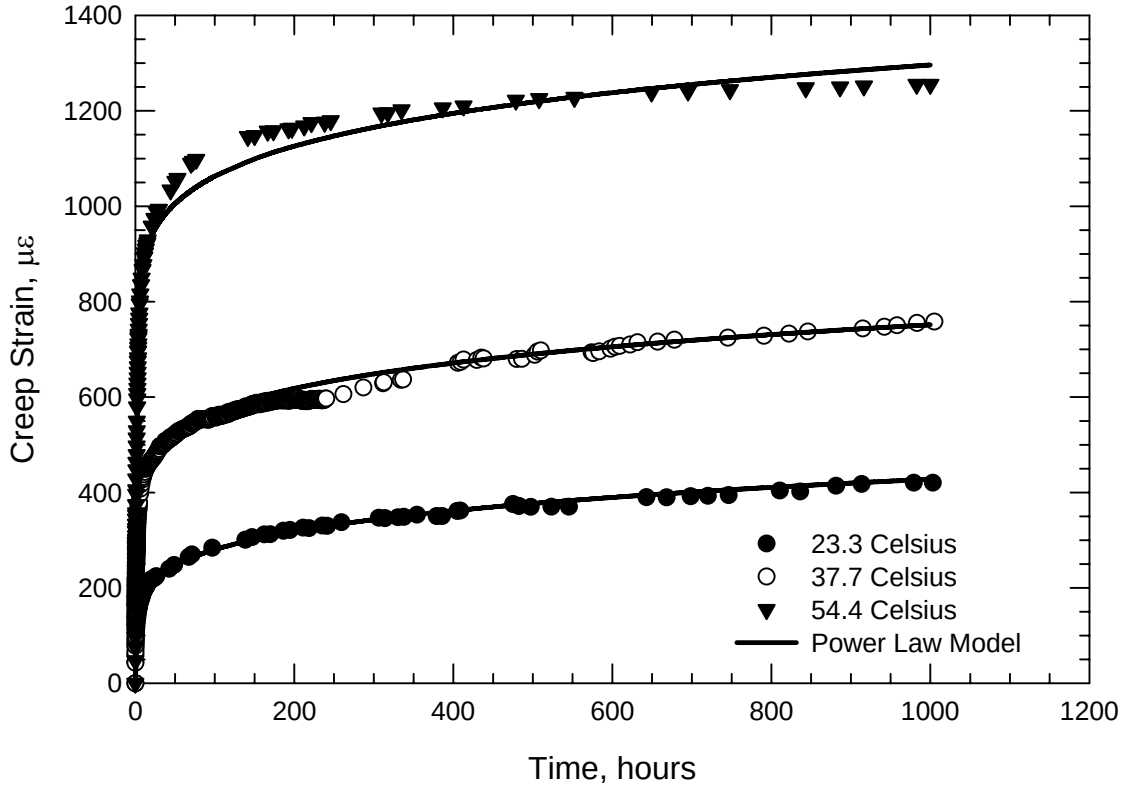

Figure 4.14 – Experimental Creep Strain with Time/Temperature-Dependent Model

Table 4.5 – Initial Elastic Strains

Temperature (°C)	Specimen	ε_0 (με)
23.3	1	5339
23.3	2	5176
23.3	3	4854
37.7	1	5157
37.7	2	4843
54.4	1	5195
54.4	2	4958
37.7 Cyclic	1	5376
37.7 Cyclic	2	4818
Average		**5079**
STD		**216**
COV		**4.3%**

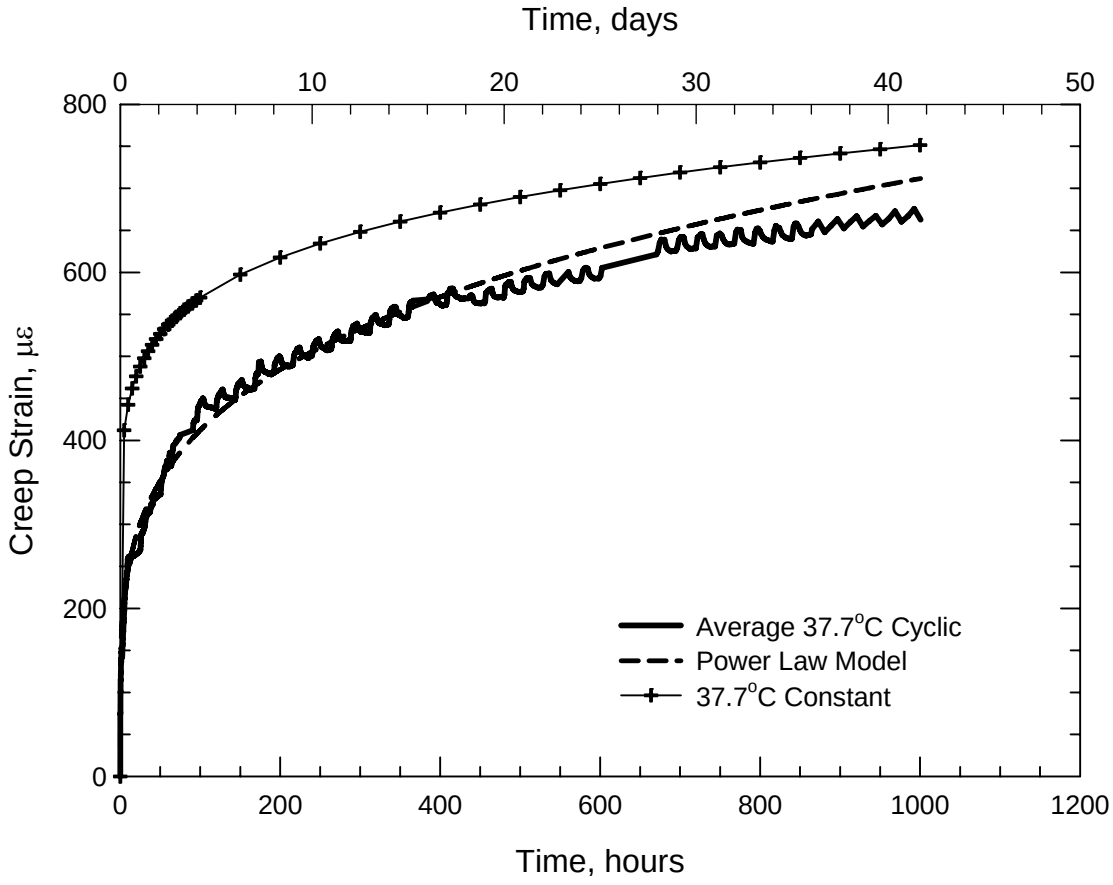

Figure 4.15 – 37.7°C Cyclic Heat Creep Strains with Power Law Model

greatly different values of m_T and n_T it was difficult to make comparisons between the cyclically heated specimens and the constant heat experiments. The values of m_T and n_T are shown in Table 4.4 for comparison. The 37.7°C (100°F) cyclically heated test performed much as expected. The strain data is below the 37.7°C (100°F) constant heat curve and increased slowly to approximately the same magnitude as the constant heat test. This can be seen in Figure 4.15.

A creep test was performed under cyclic heat at 54.4°C (130°F) for comparison with the 37.7°C (100°F) cyclic test in order to form an equation to predict the behavior of cyclically heated specimens. However, the results were very erratic which can be attributed to an error somewhere in the data acquisition process. Based on the strain readings, the problem was most likely a cold solder joint where the lead wires were attached to the strain gages or a pre-existing problem with the lead wires. This is apparent due to the sporadic readings that were collected. A cold solder joint causes an insufficient connection that can cause erratic readings due to small changes in the current being passed through the strain gage.

As can be seen from Figure 4.15 the cyclic heating on the 37.7°C (100°F) specimen caused a stair step effect in the strain values. The strain increased as the heat was added and then decreased during a period of recovery when the heat was removed. Figure 4.15 also indicates that the behavior of the cyclically heated specimens may eventually converge with the behavior of the constant heat specimens. The strains recorded in the later points are less influenced by temperature, which can be seen by the smaller increases in strain during the heating cycles.

Equation (4.6) can be used to estimate the longitudinal strain over the possible service life of the material as used in construction. The total creep strain can then be compared to the short-term data to evaluate the possibility of material failure over a structure's service life. The predicted results may also be compared to the short-term elevated temperature tests. Since total strains will be needed and the data revealed a relatively consistent value for ε_o regardless of temperature, ε_o will be given a value of 5000 με for all temperature models. This value was established as the average throughout all of the tests. Figure 4.16 shows the strain data extrapolated to 50 years. Table 4.6 shows the increase in strain over the 50 year period. Table 4.7 shows the comparisons between the predicted strains and the results of the short-term testing at both room temperature and elevated temperature. As can be seen in Table 4.7, the total strain approaches approximately half of the strain at failure seen in the short-term tests. In the most extreme creep case, the 54.4°C (130°F) test, the strain was predicted to increase to 7,900 με after 50 years, which is just slightly more than half of the total strain at failure in the short-term test. Under the stress level of 0.33 F_L^c, recommended by the manufacturer, the total strain over a 50 year service life would not approach the short-term ultimate strain. However, if the stress level was increased, the total strain could easily approach the strain at failure in the short-term tests. These conclusions are applicable only to the materials and temperatures used in the current investigation. Further research is needed on a wider range of pultruded materials and environmental conditions to assess the general applicability of creep models developed using Equation (4.6).

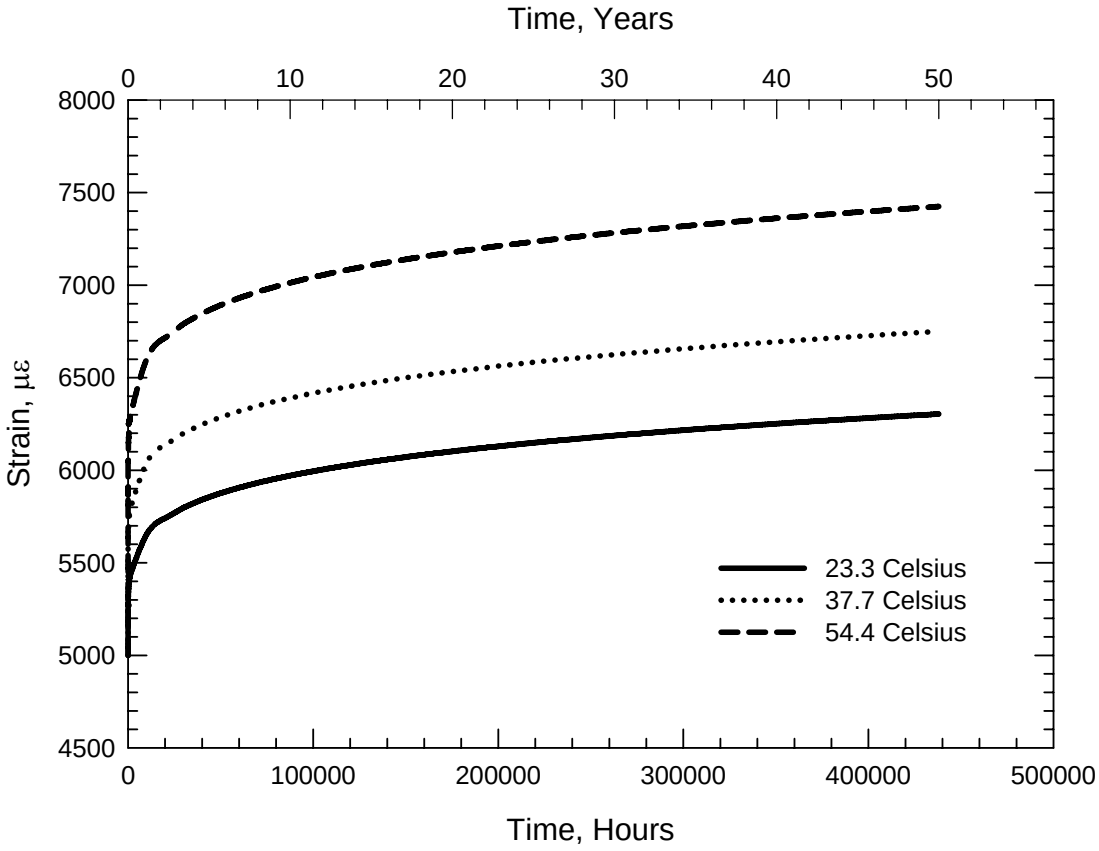

Figure 4.16 – Predicted Strains over a 50 Year Service Life

Table 4.6 – Increase in Longitudinal Strain over a 50 Year Service Life

	23.3°C (Room Temperature)	37.7°C	54.4°C
Time	$\frac{\varepsilon(T,t)-\varepsilon_o}{\varepsilon_o}$	$\frac{\varepsilon(T,t)-\varepsilon_o}{\varepsilon_o}$	$\frac{\varepsilon(T,t)-\varepsilon_o}{\varepsilon_o}$
Years	%	%	%
1	12.7	20.4	39.2
5	17.1	25.3	45.5
10	19.4	27.8	48.6
25	23.0	31.6	53.4
50	26.1	35.0	57.4

Table 4.7 – Comparison of Short-Term Strain Values with Creep Values

	Temperature	Strain (με)
Short-Term (Strain at Failure)	23.3°C	16,600
	37.7°C	15,400
	54.4°C	14,000
	65.6°C	10,900
Creep (50 years)	23.3°C	6,300
	37.7°C	6,700
	54.4°C	7,900

4.5 Time-Temperature Superposition Principle

Another approach to modeling the long-term performance of the FRP material is to use the Time-Temperature Superposition Principle (TTSP) introduced in Chapter II. The TTSP states that the effect of temperature on the time-dependent mechanical behavior of the material is equivalent to a stretching of the real time for temperatures above the given reference temperature (Findley, Lai, and Onaran (1976)), which in this case is room temperature (23.3°C (74°F)). Since creep tests were performed at one stress level and multiple temperatures above the reference temperature, a master curve can be made by shifting the elevated temperatures curves using a modification factor. This states that the following relationship exists:

$$\varepsilon(T,t) = \varepsilon(T_o,\zeta) \tag{4.7}$$

$$\zeta = \frac{t}{a_T(T)} \tag{4.8}$$

where

t = time after loading
T = temperature
T_o = reference temperature
ζ = "reduced time"
a_T = shift factor

The creep curves in the current study were only shifted horizontally; however, the TTSP does allow for vertical shifts. The three creep curves from the current investigation are plotted on a log-log scale in Figure 4.17. The data from the room temperature (23°C(74°F)) test will be considered the reference temperature. The data for the room temperature test extends to 2700 hours and a creep strain of 496 με. The time when the

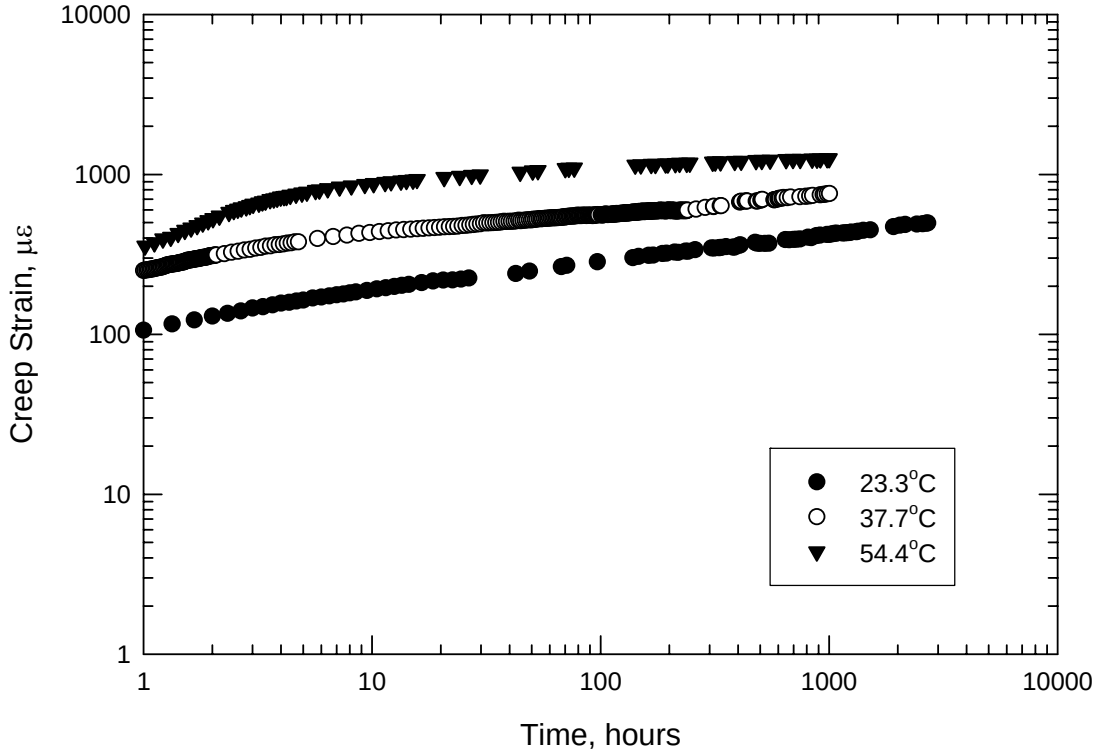

Figure 4.17 – Creep Strain for Temperature of 23.3°C, 37.7°C, and 54.4°C

specimen tested at 37.7°C (100°F) reached the same level of strain was identified from the data as t ≈ 30 hours. Thus the data from the 37.7°C (100°F) test was shifted horizontally at this point and joined to the reference temperature curve after the appropriate shift factor was determined. The shift factor was determined by taking the time that it took for the 37.7°C (100°F) test to reach 496 με and dividing it by the time for the reference temperature to reach the same value. For this case it was:

$$a_T = \frac{30.8}{2700} = 0.0114$$

After the determination of the shift factor each subsequent time interval between strain readings was divided by the shift factor and added to the previous time starting at 2700 hours. The data from the 37.7°C (100°F) test was stretched to a time period of 88,190 hours (10.1 years). The results of this shift can be seen in Figure 4.18. The same methodology was employed for the 54.4°C (130°F) curve. A strain value of 757 με was determined to be the shift point of the 54.4°C (130°F) curve. The shift factor was determined to be 5.273×10^{-5}. This shift stretched the master curve to a time period of 2,165 years, which is far beyond any reasonable time duration. However, it did increase the model beyond the 50 year service life, which is valuable for comparison with the Findley power law model developed in Section 4.4. The results of this shift formed the master curve which can be seen in Figure 4.19. A plot of the reciprocal of the shift factors (logarithmic scale) versus (T-T_o) is given in Figure 4.20. The reference temperature, T_o, was given a shift factor value of 1. The shift factors displayed a linear increase with increasing temperature. A second master curve with a reference temperature of 37.7°C (100°F) was also created using the same methodology and can be seen in Figure 4.21.

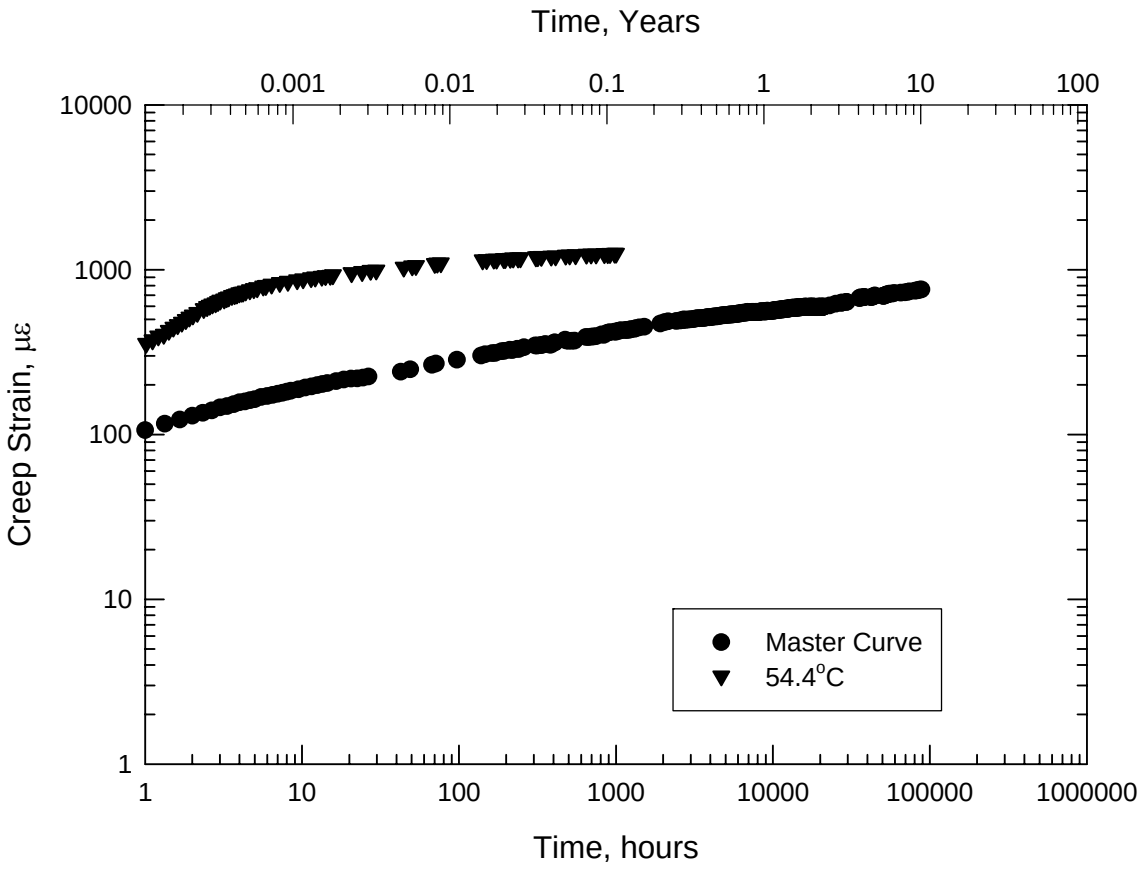

Figure 4.18 – Master Curve Including Shift of 37.7°C Curve

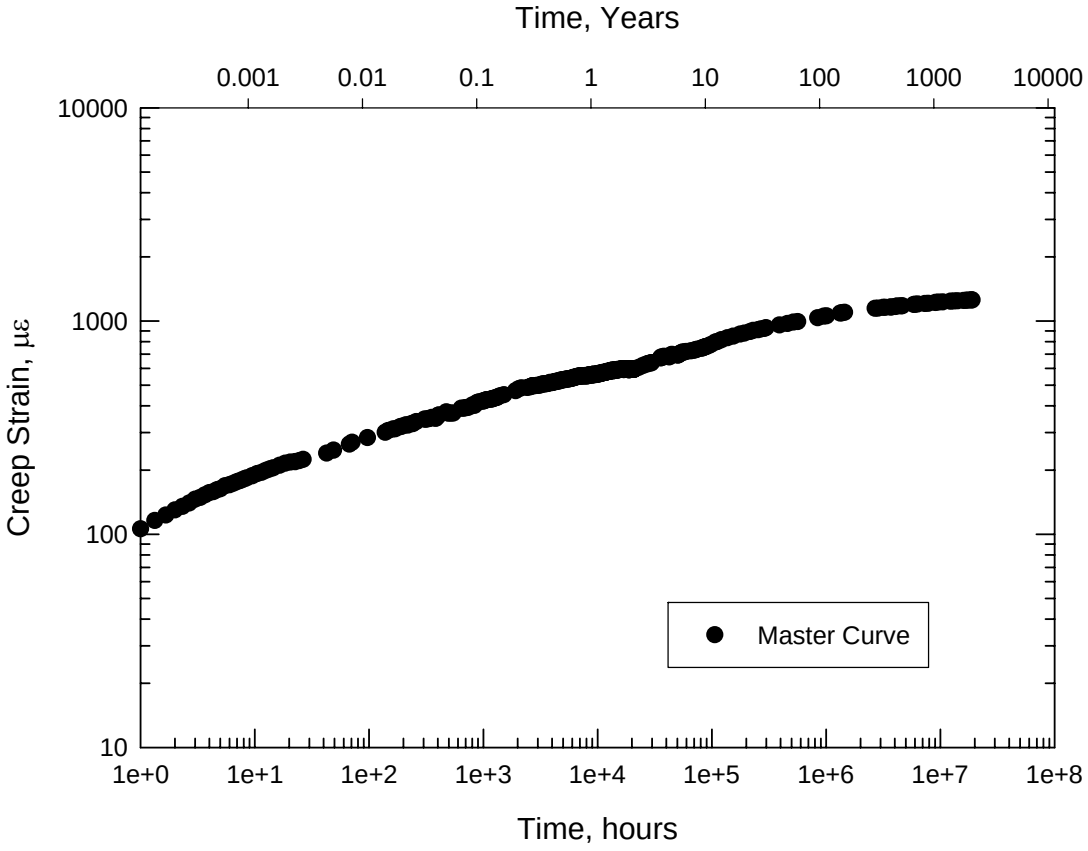

Figure 4.19 – Master Curve for T_o (23.3°C) Including Shifts of Creep Data at 37.7°C an 54.4°C

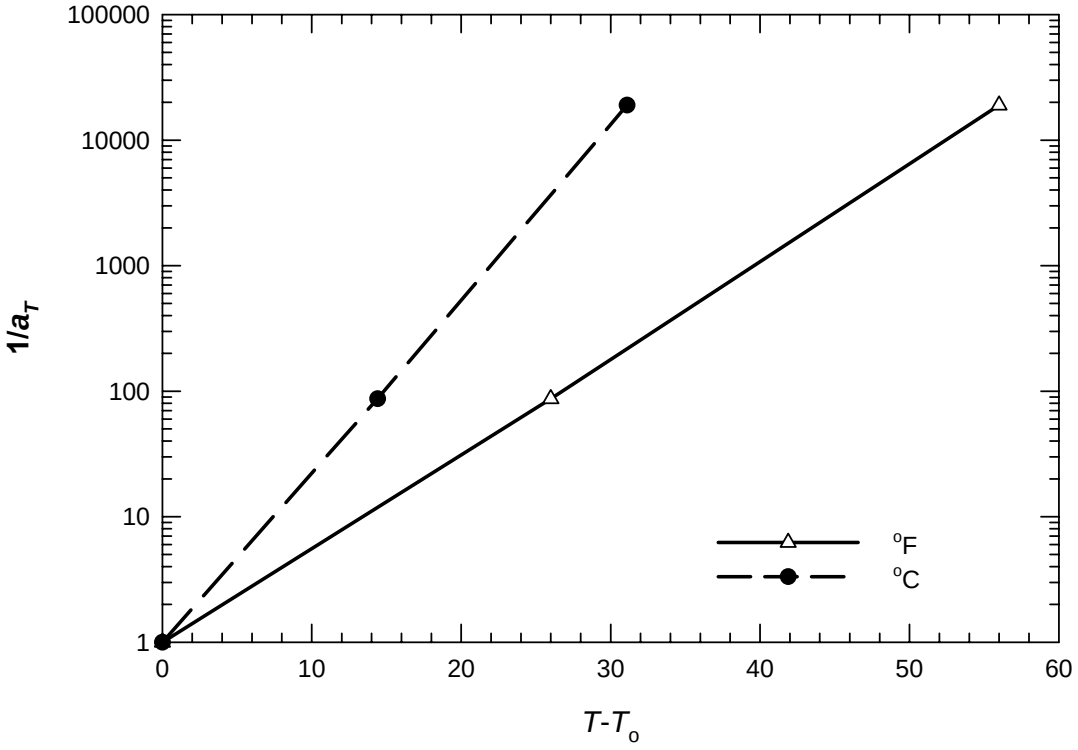

Figure 4.20 – Shift Factors for TTSP

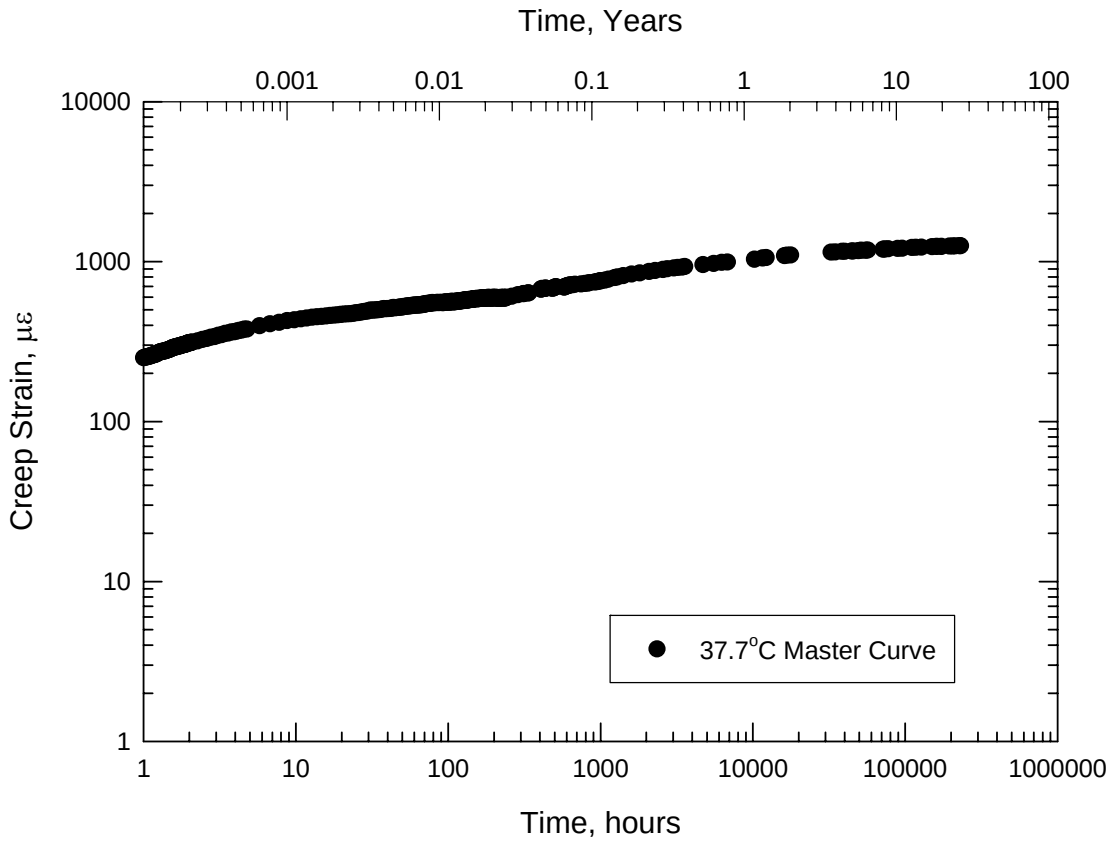

Figure 4.21 – Master Curve for T_o (37.7°C) Including Shift of Creep Data at 54.4°C

The Time-Temperature Superposition Principle applied to the data from the creep tests in the current investigation was capable of modeling the time-dependent behavior of the material well past the time period of interest for the 23.3°C (74°F) reference temperature. The shifted curves formed reasonably smooth master curves from which creep strain could be predicted for the reference temperatures, T_o, which were 23.3°C (74°F) and 37.7°C (100°F) for this study. Comparisons of the predicted creep strains from the TTSP and the semi-empirical Equation (4.6) can be seen in Table 4.8. The table shows that the semi-empirical Findley model consistently predicted higher creep strain values than the TTSP master curve. The difference between the two models increased with the length of time predicted. The difference in the room temperature models can possibly be attributed to physical aging of the elevated temperature specimens which is not accounted for in the Findley model.

Table 4.8 – Predicted Strains for Material Using Two Methods

Time (Years)	23.3°C Semi-Empirical Model (με)	23.3°C TTSP (με)	% Diff.	37.7°C Semi-Empirical Model (με)	37.7°C TTSP (με)	% Diff.
1	638	558	12.5	997	1016	1.9
5	856	688	19.6	1244	1161	6.7
25	1148	895	22	1569	1253	20.1
50	1303	969	25.6	1740	N/A	N/A

The Time-Temperature Superposition Principle can be used to characterize the behavior of the material at 50 years utilizing shorter duration tests than the experiments performed in the current study. The current study durations of 1,000 hours produced a estimation of the creep strain over a period of 2,165 years. Analysis of the creep data in this investigation reveals that three creep tests of 120 hours (5 days) would be sufficient to provide an estimation of the strain response over a 50 year service life as shown in Figures 4.22 and 4.23. Applying the TTSP to the measured data, the shorter testing period yielded estimations of creep strain more consistent with the strains predicted by the semi-empirical model, as shown in Table 4.9. Further research must be conducted in order to confirm this test duration is sufficient for estimation of other materials.

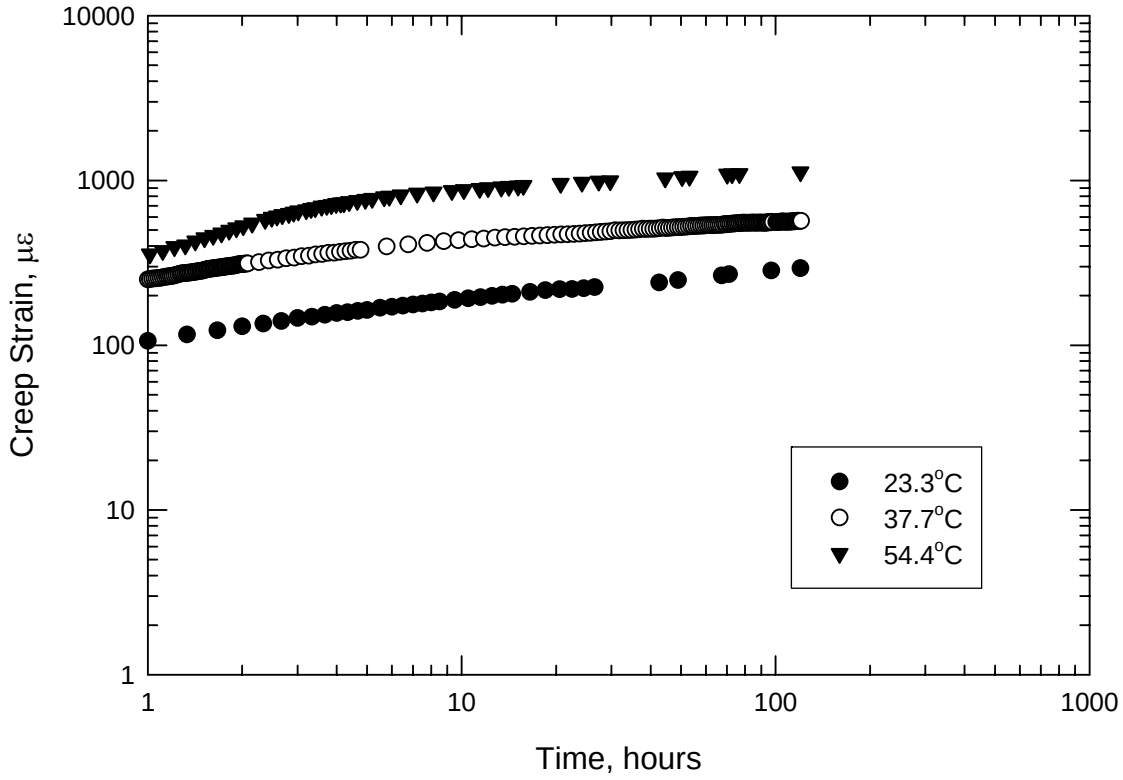

Figure 4.22 - Recorded Creep Strain for 120 hours

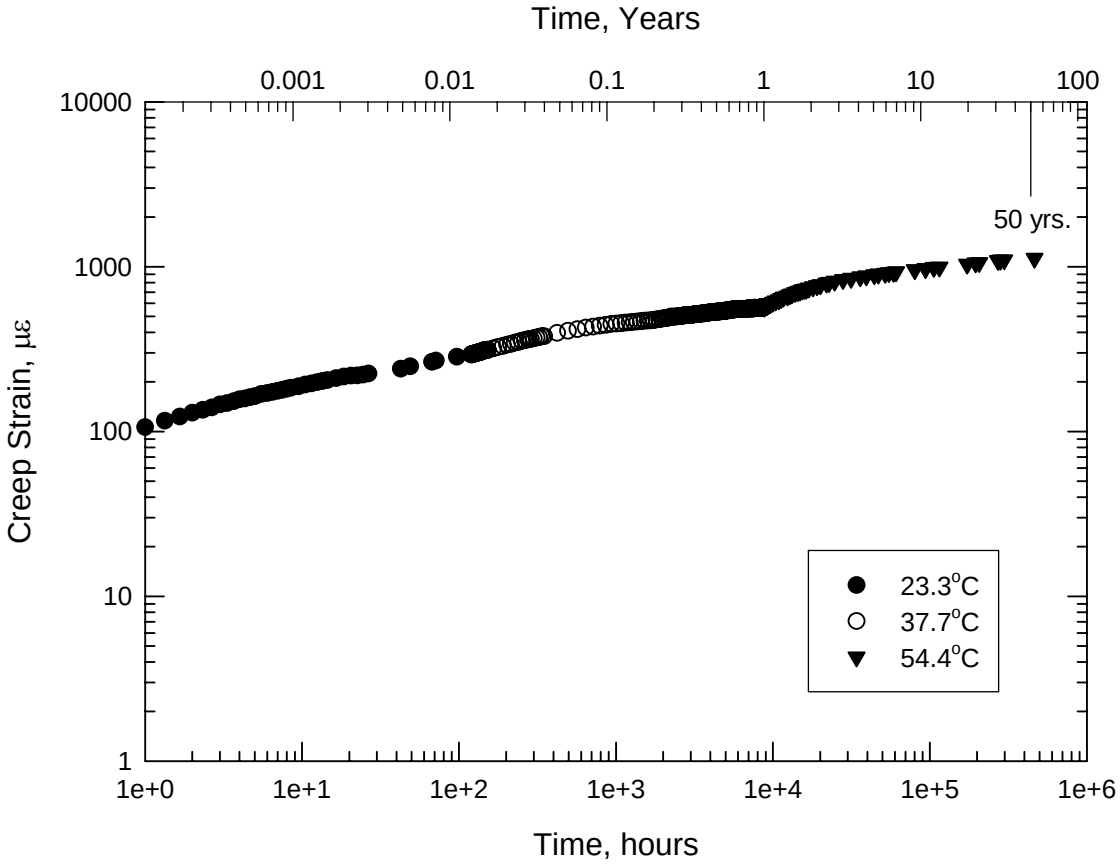

Figure 4.23 - TTSP Master Curve for Test Durations of 120 Hours, Allowing Prediction of Strain Response over a 50 Year Service Life

Table 4.9 – Predicted Strains Utilizing 120 Hour TTSP Curves and Semi-Empirical Model

Time (Years)	23.3°C Semi-Empirical Model (με)	23.3°C TTSP (με)	% Diff.
1	638	568	11
5	856	893	4.3
25	1148	1085	5.5
50	1303	1118	14.2

4.6 Prediction of Time and Temperature Dependent Modulus

The constant m_T in Equation (4.6) can be expressed as a hyperbolic function of temperature as shown:

$$m_T = m' \sinh\left(\frac{\Delta T}{T_o}\right) = m'\left[\left(\frac{\Delta T}{T_o}\right) + \frac{1}{3!}\left(\frac{\Delta T}{T_o}\right)^3 + \ldots\right] \tag{4.9}$$

Substituting this into Equation (4.6) yields:

$$\varepsilon(T,t) = \varepsilon_o + m_{RT} t^{n_{RT}} + m' t^{n_T} \sinh\left(\frac{\Delta T}{T_o}\right) \tag{4.10}$$

The parameters m' and T_o are material constants determined from creep experiments at various temperatures. The parameter ΔT is the temperature being modeled, T, minus the material constant T_o. These material constants were determined from a plot of Equation (4.9) as shown in Figure 4.24. The value of T_o was selected to ensure linearity and the value of m' was taken as the slope of the resulting line. From the curve T_o was determined to be 23.3°C (74°F), which is equal to room temperature, and m' was determined to be 360 με for °C and 746 με for °F. Either temperature units may be used as long as the correct value of m' is used.

Previous work by Scott and Zureick (1998) provided a model for the time-dependent modulus based on the material parameter m as a function of stress. The current investigation extends this model to include the reduction in modulus due to elevated temperatures. The original equation can be written as:

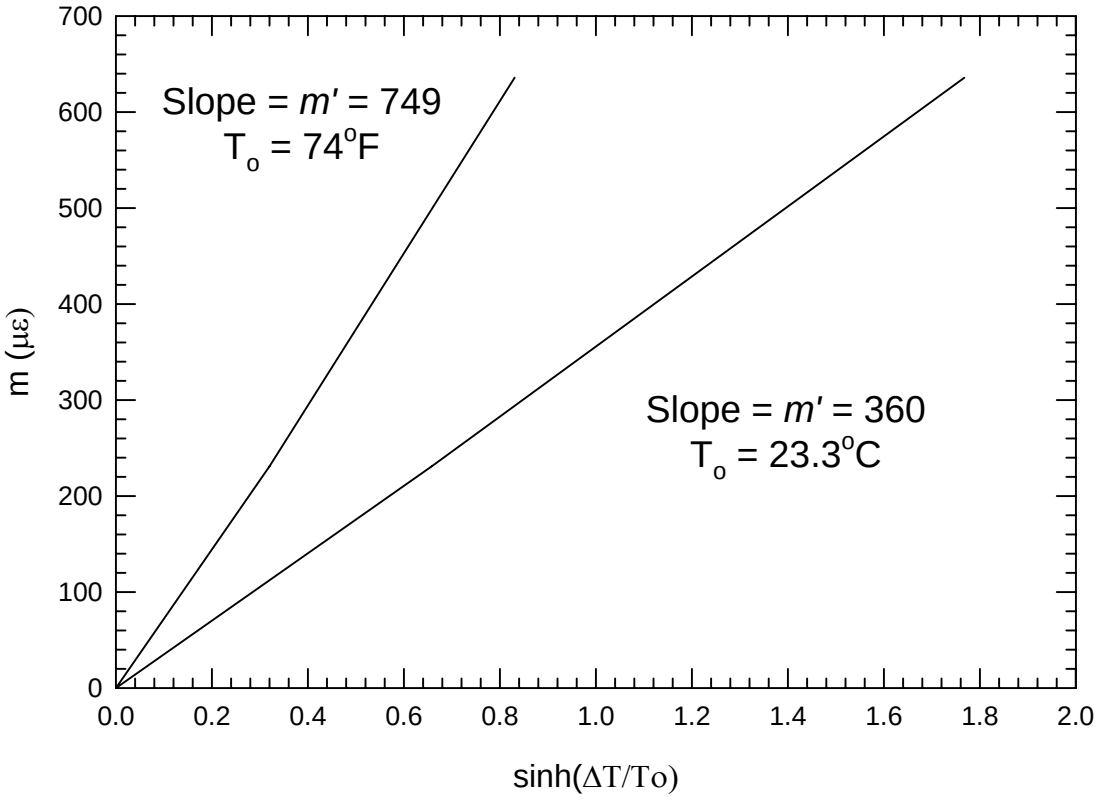

Figure 4.24 – Evaluation of Creep Parameter *m*' and T_o

$$E_L(t) = \frac{E_L^o}{1 + \frac{E_L^o}{E_t} t^n} \tag{4.11}$$

where

$E_L(t)$ = time-dependent longitudinal modulus of elasticity

E_L^o = initial elastic longitudinal modulus independent of time

E_t = modulus which characterizes only the time-dependent behavior

n = stress independent material constant

t = time after loading (hours)

and

$$E_t = \frac{f}{m} \tag{4.12}$$

where

f = applied stress

m = stress and temperature-dependent coefficient

For this investigation Equation (4.11) will be used to define the reduction in modulus of elasticity over time and then extended to include the reduction due to temperature. The material parameters m_T and n_T are substituted into Equations (4.11) and (4.12) to provide an equation for the reduction in modulus due to temperature. When the parameters are incorporated Equation (4.11) then becomes:

$$E_L(T) = \frac{E_L^o}{1 + \frac{E_L^o}{E_T} t^{n_T}} \tag{4.13}$$

where

$$E_T = \frac{f}{m' \sinh\left(\frac{\Delta T}{T_o}\right)} = \frac{f}{m_T} \tag{4.14}$$

Therefore, the reduced modulus of elasticity due to time and temperature may be expressed as:

$$E_L(T,t) = E_L^o - (\Delta E_L(T)) - (\Delta E_L(t)) \tag{4.15}$$

where

$$\Delta E_L(T) = E_L^o - \frac{E_L^o}{1 + \frac{E_L^o}{E_T} t^{n_T}} \tag{4.16}$$

and

$$\Delta E_L(t) = E_L^o - \frac{E_L^o}{1 + \frac{E_L^o}{E_t} t^{n}} \tag{4.17}$$

Tables 4.10, 4.11 and 4.12 give predicted values of E_L(T, t) for time periods of 1, 5, 10, 25, and 50 years. All predicted modulus values are based on a stress level of 0.33 F_L^c. Figure 4.25 shows the total reduction in modulus values over a 50 year service period. Equation (4.11) was used to predict the reduction in modulus for the 23.3°C (74°F) coupons. Table 4.13 shows a comparison of modulus reduction at 50 years of service life. The reduction in modulus of a similar material subjected to sustained loads at room temperature (Scott and Zureick (1998)) is also included in Table 4.13.

Table 4.10- Predicted Modulus Reduction for Material at Room Temperature

	23.3°C Average	
E_L^o **GPa** (ksi)	**23.1** (3345)	
f **MPa** (ksi)	**126** (18.333)	
m **(με)**	121	
n	0.183	
E_t **GPa** (ksi)	**1044** (151512)	
Time (Years)	$E_L(t)$ **GPa** (ksi)	**Decrease (%)**
0	**23.1** (3345)	0
1	**20.7** (2997)	10.4
5	**19.9** (2893)	13.5
10	**19.6** (2842)	15.1
25	**19.1** (2766)	17.3
50	**18.6** (2702)	19.2

Table 4.11 – Predicted Modulus Reduction for Material at 37.7°C

	37.7°C Average	
E_L^o **GPa** (ksi)	**23.1** (3345)	
f **MPa** (ksi)	**126** (18.333)	
m_T **(με)**	268.55	
n_T	0.0391	
E_T **GPa** (ksi)	**470.7** (68266)	
Time (Years)	$E_L(T, t)$ **GPa** (ksi)	**Decrease (%)**
0	**23.1** (3345)	0
1	**19.2** (2778)	16.9
5	**18.4** (2662)	20.4
10	**18.0** (2604)	22.2
25	**17.4** (2520)	24.7
50	**16.9** (2450)	26.7

Table 4.12 – Predicted Modulus Reduction for Material at 54.4°C

	54.4°C Average	
E_L^o GPa (ksi)	**23.1** (3345)	
f MPa (ksi)	**126** (18.333)	
m_T (με)	622.34	
n_T	0.0453	
E_T GPa (ksi)	**203.1** (29458)	
Time (Years)	$E_L(T, t)$ GPa (ksi)	Decrease (%)
0	**23.1** (3345)	0
1	**17.3** (2507)	25.0
5	**16.4** (2373)	29.1
10	**15.9** (2307)	31.0
25	**15.3** (2212)	33.9
50	**14.7** (2134)	36.2

Table 4.l3 – Predicted 50 Year Reduction in Modulus

Investigation	Stress Level	Reduction in Modulus (50 years)
Scott and Zureick (1998)	0.40 F_L^c	21%
23.3°C (74°F)	0.33 F_L^c	19.2 %
37.7°C (100°F)	0.33 F_L^c	26.4 %
54.4°C (130°F)	0.33 F_L^c	35.8 %

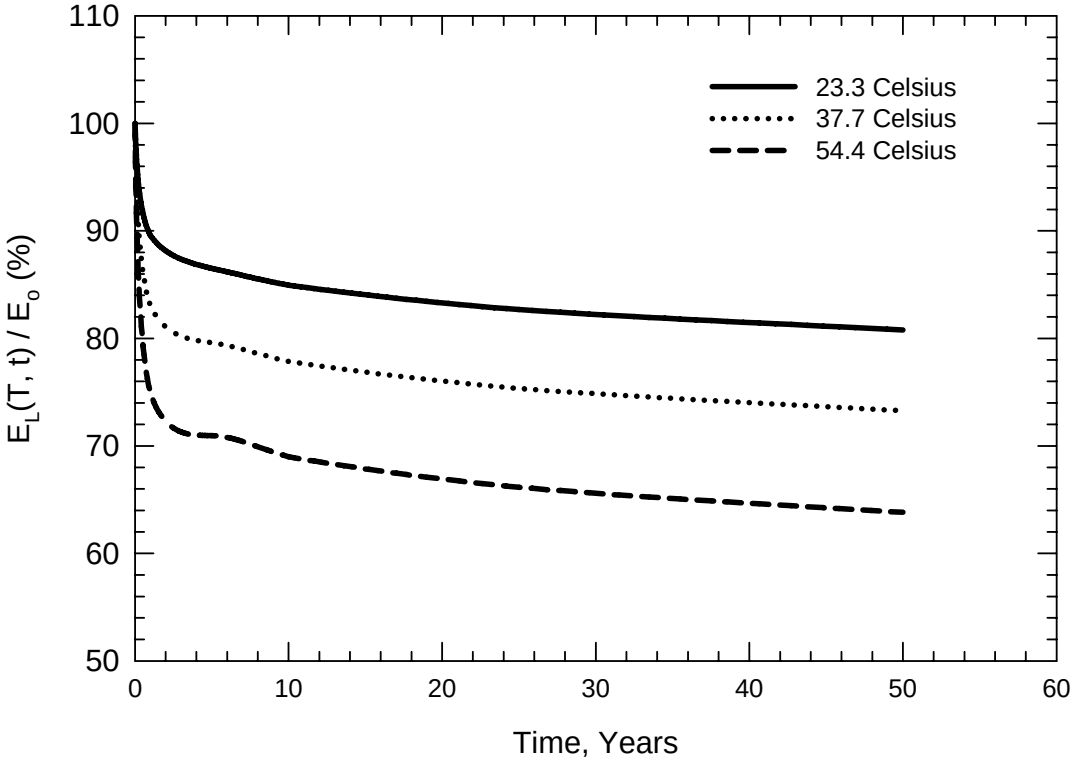

Figure 4.25 – Predicted Reduction in Modulus of Elasticity

Over a 50 Year Service Life

CHAPTER V

CONCLUSIONS AND PROPOSED DESIGN EQUATION

5.1 Conclusions

Based on the results of the short-term and long-term experimental program, the following observations can be made:

1. The short-term elevated temperature tests performed at 37.7°C (100°F), 54.4°C (130°F), and 65.6°C (150°F) revealed a noticeable decrease in the ultimate strength and modulus of elasticity. The 65.6°C test showed a decrease in ultimate strength of 43.5% and a decrease in modulus of 13%. These values are in general agreement with the manufacturer's design guidelines (STRONGWELL (1998)), which predict a decrease of 50% in strength and 15% in modulus of elasticity for the material subjected to a temperature of 65.6°C (150°F).
2. The Findley power law provides an accurate model of the creep performance of the room temperature creep experiments. The power law modeled the strain in the FRP material within 3.5% over a time duration of 2700 hours. All room temperature creep tests yielded power law coefficients comparable to previous work.
3. The time and temperature-dependent power law model provided a reasonably accurate model of the creep strain in the pultruded FRP material for the time duration studied. The temperature-dependent portion of the creep behavior could be modeled using the Findley power law with the unique material parameters m_T and n_T. The parameter m_T could be expressed as a hyperbolic function of temperature with an m' value of 360 for temperatures given in degrees Celsius.

The value of m' was 746 for temperatures given in degrees Fahrenheit. The value used for T_o to ensure linearity of the plot of the parameter m_T with temperature was equal to room temperature, 23.3°C (74°F). This effectively made the temperature-dependent portion of the power law model equal to zero at room temperature, which was assumed early in the investigation. The values for n_T were very similar for both elevated temperature experiments and could be given a value of 0.05 for practical use. Thus, the equation for the time and temperature-dependent model could be expressed as:

$$\varepsilon(T,t) = \varepsilon_o + 121t^{0.18} + m't^{0.05}\sinh\left(\frac{T-T_o}{T_o}\right) \tag{5.1}$$

where t is expressed in hours. This model can be used to predict the time-dependent strain of the material under a given elevated temperature, T, and a stress of 0.33 F_L^c.

4. The Time-Temperature Superposition Principle provided a reasonable model of the long-term behavior of the material. Two master curves were made for the 23.3°C (74°F) and 37.7°C (100°F) specimens. The resulting predicted strain values were reasonably close to the strain predicted by the Findley model for shorter time periods of 1 to 5 years but diverged as the predicted time increased. The TTSP model for the 37.7°C (100°F) specimen was closer to the results predicted by the Findley model. The difference in the TTSP model and the Findley model for the 23.3°C (74°F) case can possibly be attributed to physical aging at the elevated temperatures used for the TTSP curve fitting. Analysis of

the creep data revealed that shorter creep test durations of 120 hours would be sufficient to provide an estimation of the 50 year strain response of the material.

5. Equation (4.15) can be used to predict the reduction in modulus due to both time and temperature. This equation is based on Equation (4.11) which was proposed by Scott and Zureick (1998). Equation (4.15) incorporates the two temperature parameters m_T and n_T to predict the reduction in modulus due to temperature.

5.2 Proposed Design Equation for the Time and Temperature-Dependent Modulus

Based on the data presented in this study, it is possible to formulate a design equation that predicts the longitudinal elastic modulus $E_L(T, t)$ due to temperature and time. This predictive equation can be achieved by simplifying Equations (4.15), (4.16), and (4.17). This equation would allow the user to predict the modulus of elasticity at a given temperature T and a stress level of 0.33 F_L^c, which is recommended by the manufacturer, for the service life of the material.

For design purposes, it is more practical to have the time t in years rather than hours. Rearranging Equation (4.15) yields:

$$E_L(T,t) = \left(\frac{E_L^o}{1 + \frac{E_L^o}{E_T}(8760t)^{n_T}} \right) + \left(\frac{E_L^o}{1 + \frac{E_L^o}{E_t}(8760t)^{n}} \right) - E_L^o \qquad (5.2)$$

Due to the consistency of the room temperature creep tests for this material the empirical parameter n can be given a conservative value of 0.20. The constant $\beta = \frac{E_t}{E_L^o}$ can be

introduced to further simplify the equation. The parameter n_T can also be given a conservative value of 0.05. This yields:

$$E_L(T,t) = \left(\frac{E_L^o}{1 + \frac{1.6E_L^o}{E_T} t^{0.05}} \right) + \left(\frac{E_L^o}{1 + \frac{5}{\beta} t^{0.20}} \right) - E_L^o \tag{5.3}$$

where

$$E_T = \frac{f}{m' \sinh\left(\frac{T}{T_o} - 1 \right)} \tag{5.4}$$

For this work the stress level did not change, therefore the value of E_t will remain the same and can be calculated using Equation (4.12). If E_L^o is known then the constant β can be calculated and used in Equation (5.3). Since the values of m' and T_o for both degrees Celsius and degrees Fahrenheit are known they can be used in Equation (5.4) to develop equations for SI units and English units. The resulting equations may be written as:

(SI) $$E_L(T,t) = \left(\frac{E_L^o}{1 + 0.1 \sinh\left(\frac{T}{T_o} - 1 \right) t^{0.05}} \right) + \left(\frac{E_L^o}{1 + \frac{5}{\beta} t^{0.20}} \right) - E_L^o \tag{5.5}$$

(Eng.) $$E_L(T,t) = \left(\frac{E_L^o}{1 + 0.22 \sinh\left(\frac{T}{T_o} - 1 \right) t^{0.05}} \right) + \left(\frac{E_L^o}{1 + \frac{5}{\beta} t^{0.20}} \right) - E_L^o \tag{5.6}$$

Further simplification of Equation (5.5) and (5.6) yields:

$$E_L(T,t) = \phi_{(T,t)} E_L^o \tag{5.7}$$

where $\Phi_{(T,t)}$ is a time and temperature dependent reduction factor given by:

(SI)
$$\phi_{(T,t)} = \left(\frac{1}{1 + 0.1 \sinh\left(\frac{T}{T_o} - 1 \right) t^{0.05}} \right) + \left(\frac{1}{1 + \frac{5}{\beta} t^{0.20}} \right) - 1 \tag{5.8}$$

(Eng.)
$$\phi_{(T,t)} = \left(\frac{1}{1 + 0.22 \sinh\left(\frac{T}{T_o} - 1 \right) t^{0.05}} \right) + \left(\frac{1}{1 + \frac{5}{\beta} t^{0.20}} \right) - 1 \tag{5.9}$$

For the current investigation β can be given a value of 45 for both Equations (5.8) and (5.9). This value of β is determined based on the stress level of 0.33 F_L^c and the value of E_L^o determined in the short-term material testing. The simplifications performed in the earlier steps are meant to approximate the lower bound of the reduction in modulus while at the same time simplifying the equation for design use. The results of the simplified Equation (5.7) can be compared to the values found using Equation (5.2) in Figure 5.1. A design example that utilizes the predictive equation for the modulus of elasticity can be found in Appendix A.

It must be emphasized that this model is unique to the material, stress level, and temperatures studied in the current investigation. Studies on other FRP materials at a variety of stress levels and temperatures must be conducted in order to determine the general applicability of the model.

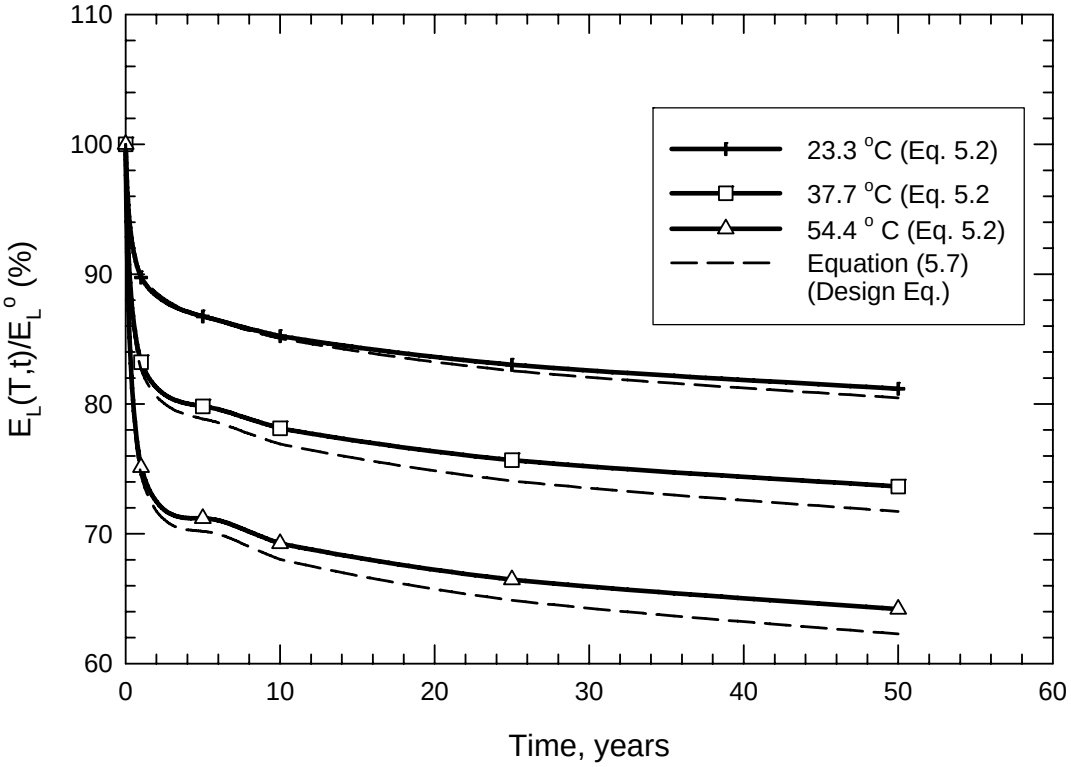

Figure 5.1 – Reduction in Modulus with Simplified Design Equation

5.3 Suggestions for Further Research

1. The 37.7°C (100°F) cyclically heated specimens yielded interesting results that need additional research to further understand and model the creep behavior. The behavior progressed as expected with the cyclically heated curve occurring below the constant 37.7°C (100°F) curve. However, the cyclic data did approach the same strain value as the constant heat curve after several hundred hours. Further cyclically heated experiments performed at additional elevated temperatures would allow an equation to be formulated to predict behavior under cyclic heat.
2. Additional research could include the variation of heat cycle durations. The current study investigated durations of 8 hours which could be modified to be longer or shorter to see the effect on the creep behavior.
3. Higher elevated temperatures could also be studied to see the effectiveness of the model proposed in this study to predict temperatures outside of the manufacturer's suggested range. The investigation could determine the effective range of the proposed model and how accurate it is within that range.
4. Multiple stress levels must also be investigated in order to observe the applicability of the model to those stress levels. The parameter m could then possibly be expressed as a function of both stress and temperature. Thus, yielding a wider range of applicability of the model proposed in the current study.
5. Future studies could also incorporate the impact of moisture with elevated temperatures, which is a combination often seen in the service life of a structure.

APPENDIX A

DESIGN EXAMPLE – LONG-TERM BEAM DEFLECTION

Check the adequacy of a unidirectionally reinforced pultruded wide flange section, shown in Figure A1, for serviceability conditions for a 50 year service life in a constant climate of 37.7°C (100°F). The beam is subjected to the loads as shown in Figure A1. The initial deflection, the deflection due to time and temperature, and the maximum deflection after 50 years must be in accordance with the EUROCOMP design code (1996). The initial modulus of elasticity, E_L^o, of the member is determined from coupon tests to be 23.1 GPa (3345 ksi) and the moment of inertia is 0.000792 m^4 (1903 in^4). The ultimate stress, F_L^c, is determined to be 186 MPa (27,000 psi). A maximum deflection of $L/250$ is specified for general public access flooring. The design code also specifies a limit state of $L/300$ for the time and temperature-dependent behavior after the initial deflection without exceeding the maximum allowable deflection. Effectively: $\Delta_{max} - \Delta_o = \Delta_{(T,t)} = L/300$.

Solution:

Step 1: Determine limit states for beam deflection:

$$L/250 = \frac{3}{250} = .012 \text{ m} = 12 \text{ mm (0.47 in.)} = \Delta_{max}$$

$$L/300 = \frac{3}{300} = .010 \text{ m} = 10 \text{ mm (0.39 in.)} = \Delta_{(T,t)}$$

Step 2: Estimate initial deflection using classic beam theory:

$$\Delta_o = \frac{5wl^4}{384EI} = \frac{5(143kN)(3)^4}{384(23.1GPa)(.000792m^4)} = .0082 \text{ m} = 8.2 \text{ mm}$$

8.2 mm (0.32 in.) < 12 mm (0.47 in.)

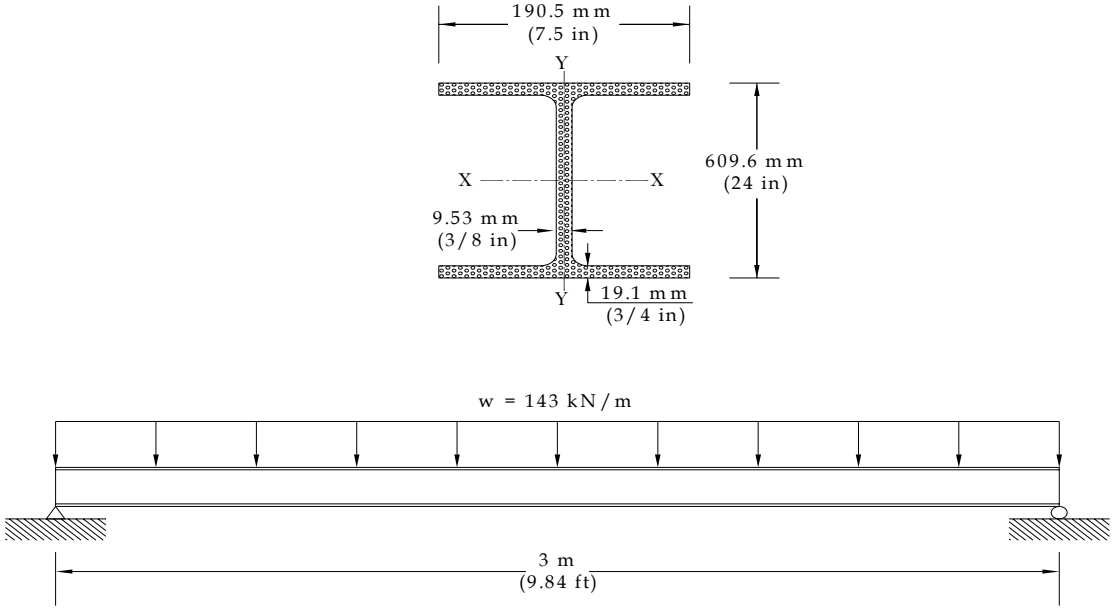

Figure A1 – Beam Deflection Example

Step 3: Determine the stress in the wide flange section

$$M = \frac{wl^2}{8} = \frac{(143kN)(3)^2}{8} = 160{,}875 \text{ N-m (118 kip-ft)}$$

$$f = \frac{Mc}{I} = \frac{(160{,}875)(.3048)}{.000792} = 62 \text{ MPa (9,000 psi)}$$

$$\frac{f}{F_L^t} = \frac{62}{186} = 33 \text{ \% of ultimate strength*}$$

* Proposed predictive modulus equation can be used

Step 4: Determine time and temperature-dependent modulus

$$E_L(T,t) = \phi_{(T,t)} E_L^o$$

$$\phi_{(T,t)} = \left(\frac{1}{1 + 0.1\sinh\left(\frac{T}{T_o} - 1\right) t^{0.05}} \right) + \left(\frac{1}{1 + \frac{5}{\beta} t^{0.20}} \right) - 1$$

$$\phi_{(T,t)} = \left(\frac{1}{1 + 0.1\sinh\left(\frac{37.7}{23.3} - 1\right) 50^{0.05}} \right) + \left(\frac{1}{1 + \frac{5}{45} 50^{0.20}} \right) - 1$$

$$\phi_{(T,t)} = 0.73$$

$$E_L(T,t) = \phi_{(T,t)} E_L^o = 0.73 \text{ (23.1 GPa)} = 16.86 \text{ GPa (2,445 ksi)}$$

Step 5: Determine deflection with reduced modulus

$$\Delta_{max} = \frac{5wl^4}{384EI} = \frac{5(143kN)(3)^4}{384(16.9GPa)(.000792m^4)} = .0113 = 11.3 \text{ mm}$$

11.3 mm (0.44 in) < 12 mm (0.47 in)

Step 6: Check deflection due to time and temperature dependent behavior with serviceability conditions

$\Delta_{max} - \Delta_o = \Delta_{(T,t)} = 11.3 \text{ mm} - 8.2 \text{ mm} = 3.1 \text{ mm}$ (0.12 in.)

3.1 mm (0.12 in.) < 10 mm (0.39 in.)

The design of the current beam satisfies the serviceability criteria proposed by the EUROCOMP design guide. The beam satisfies these criteria for the initial deflection and the maximum deflection after 50 years with time and temperature-dependent behavior included. The design also satisfies the limit state for deflection due only to time and temperature-dependent behavior.

APPENDIX B

STRESS VS. STRAIN CURVES FROM SHORT-TERM TESTING

SHORT-TERM TENSILE TESTS

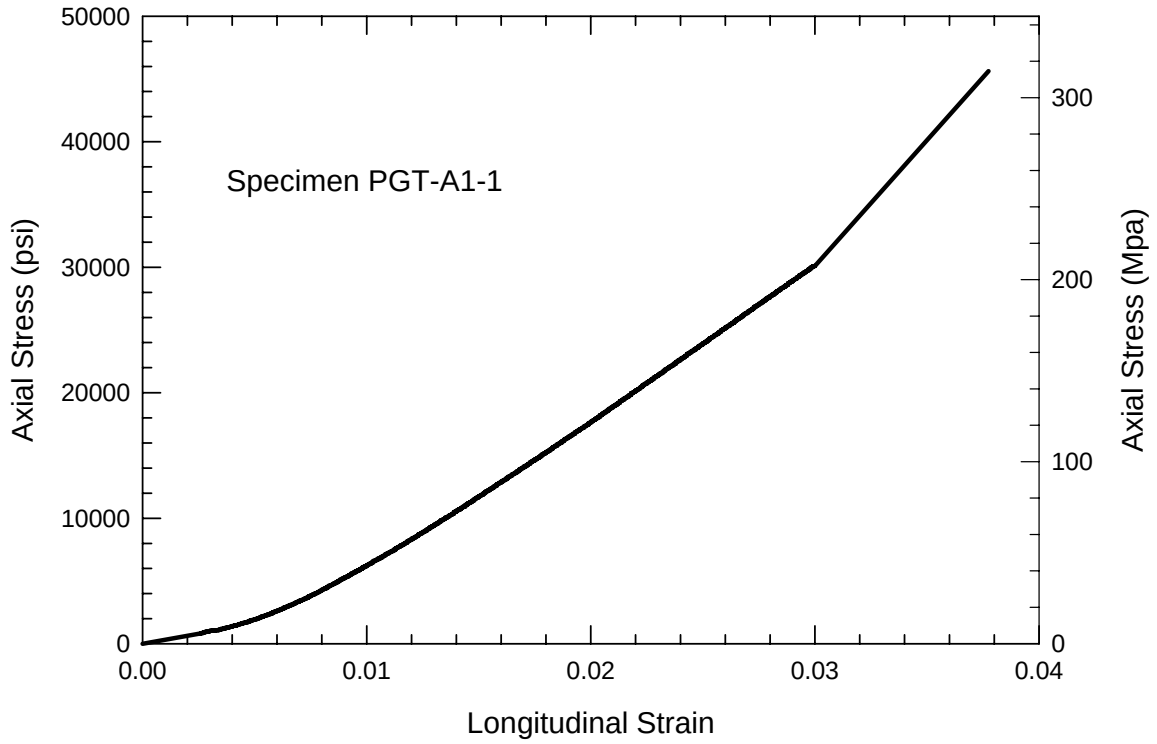

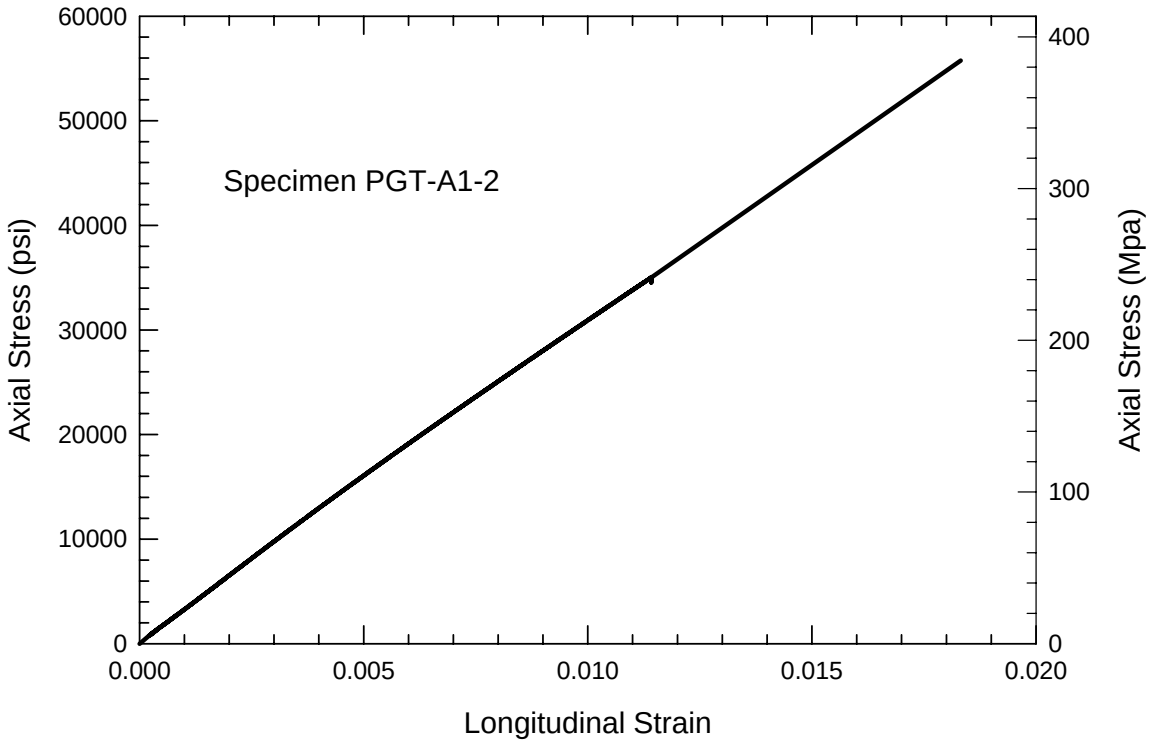
Specimen PGT-A1-2
Axial Stress (psi)
Axial Stress (Mpa)
Longitudinal Strain
60000
50000
40000
30000
20000
10000
0
400
300
200
100
0
0.000
0.005
0.010
0.015
0.020

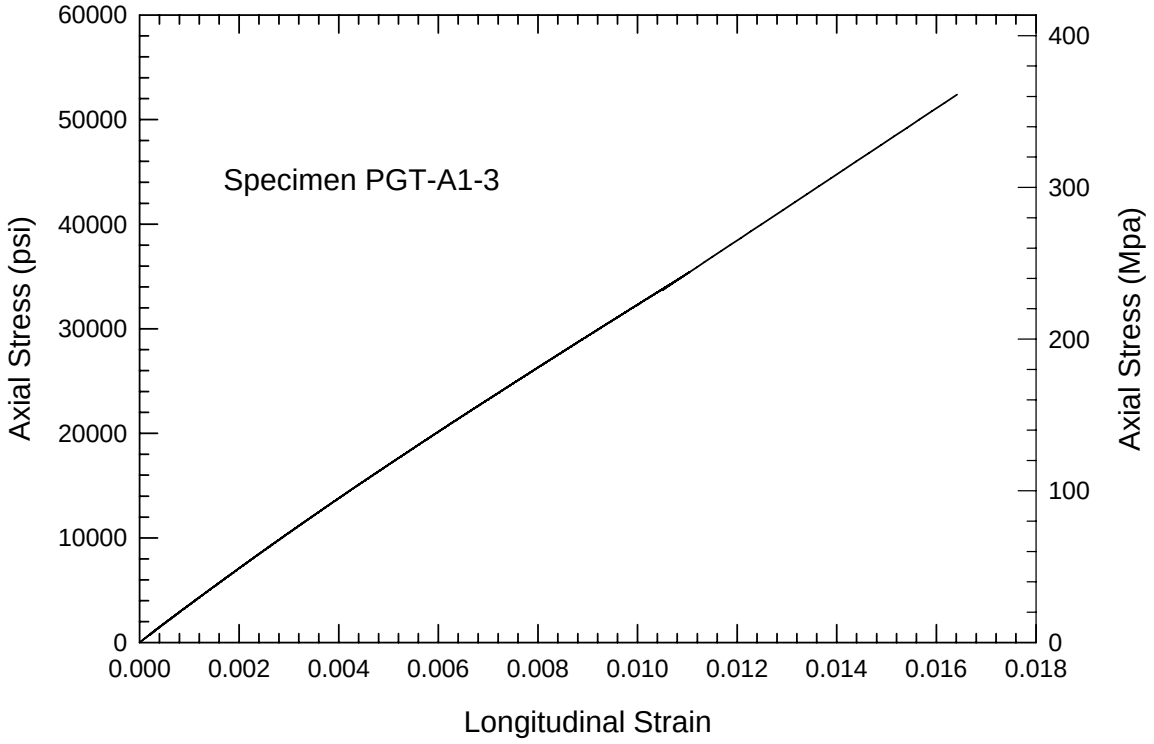
Specimen PGT-A1-3
Axial Stress (psi)
Axial Stress (Mpa)
Longitudinal Strain
60000
50000
40000
30000
20000
10000
0
400
300
200
100
0
0.000
0.002
0.004
0.006
0.008
0.010
0.012
0.014
0.016
0.018

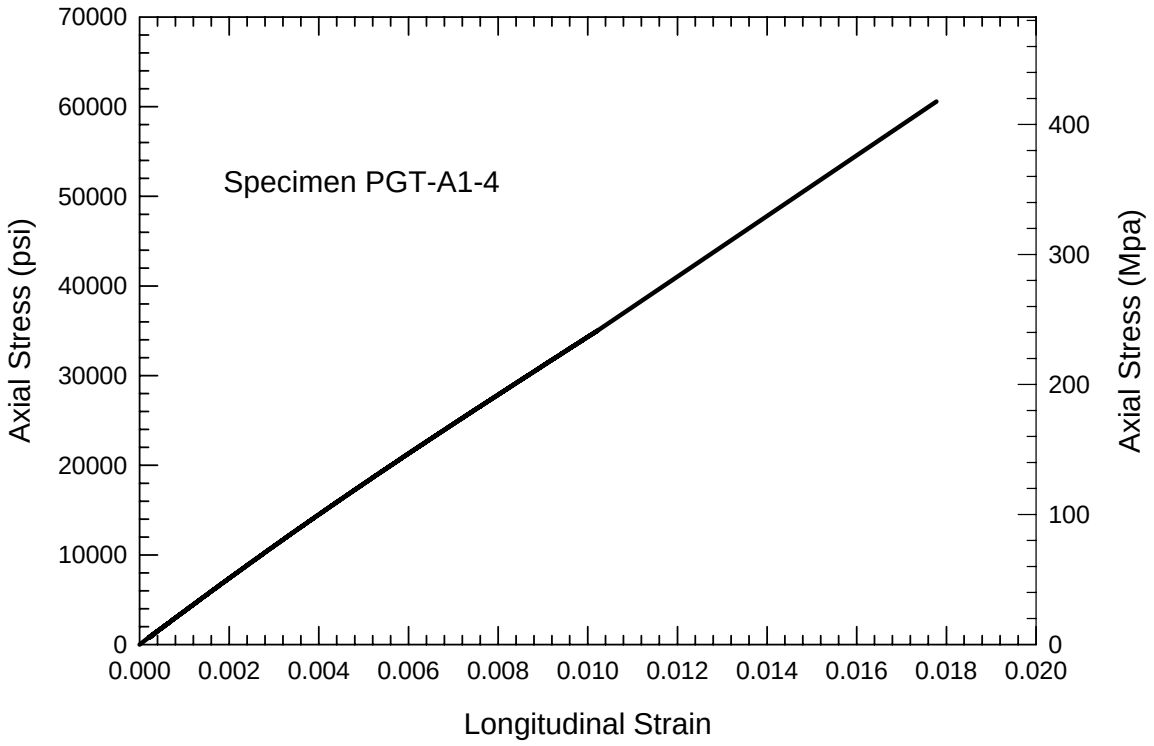
Specimen PGT-A1-4
Axial Stress (psi)
Axial Stress (Mpa)
Longitudinal Strain
70000
60000
50000
40000
30000
20000
10000
0
400
300
200
100
0
0.000
0.002
0.004
0.006
0.008
0.010
0.012
0.014
0.016
0.018
0.020

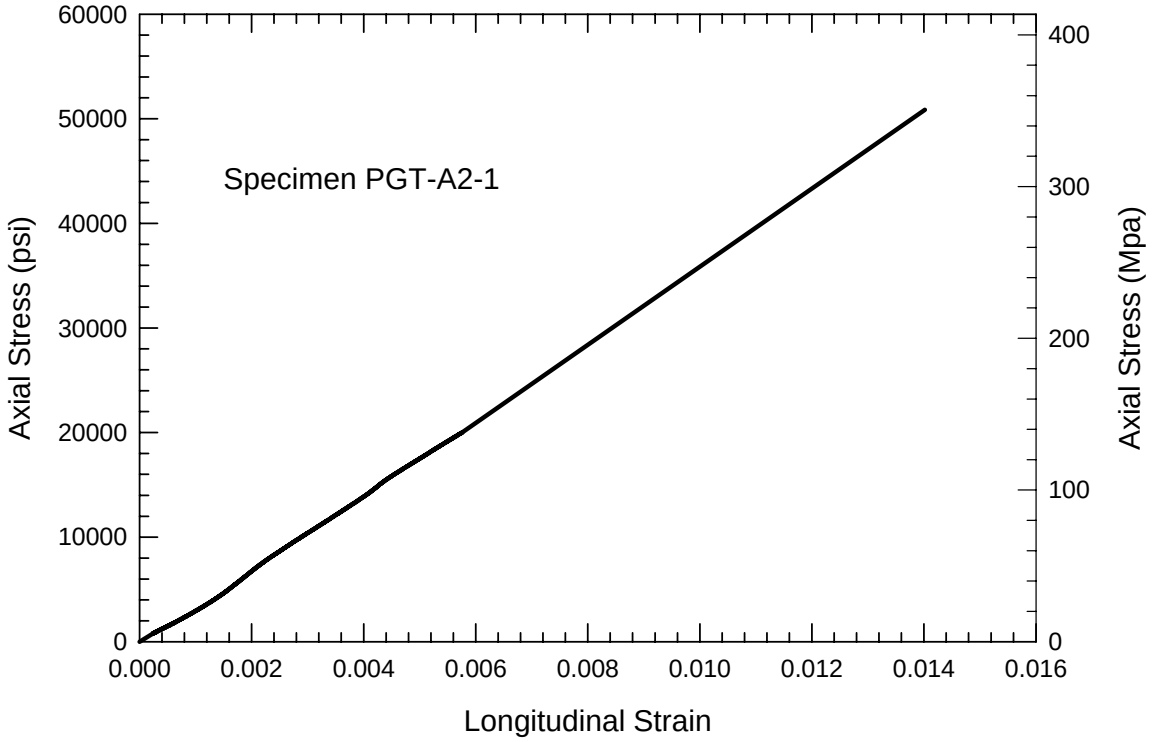
Specimen PGT-A2-1
Axial Stress (psi)
Axial Stress (Mpa)
Longitudinal Strain
60000
50000
40000
30000
20000
10000
0
400
300
200
100
0
0.000
0.002
0.004
0.006
0.008
0.010
0.012
0.014
0.016

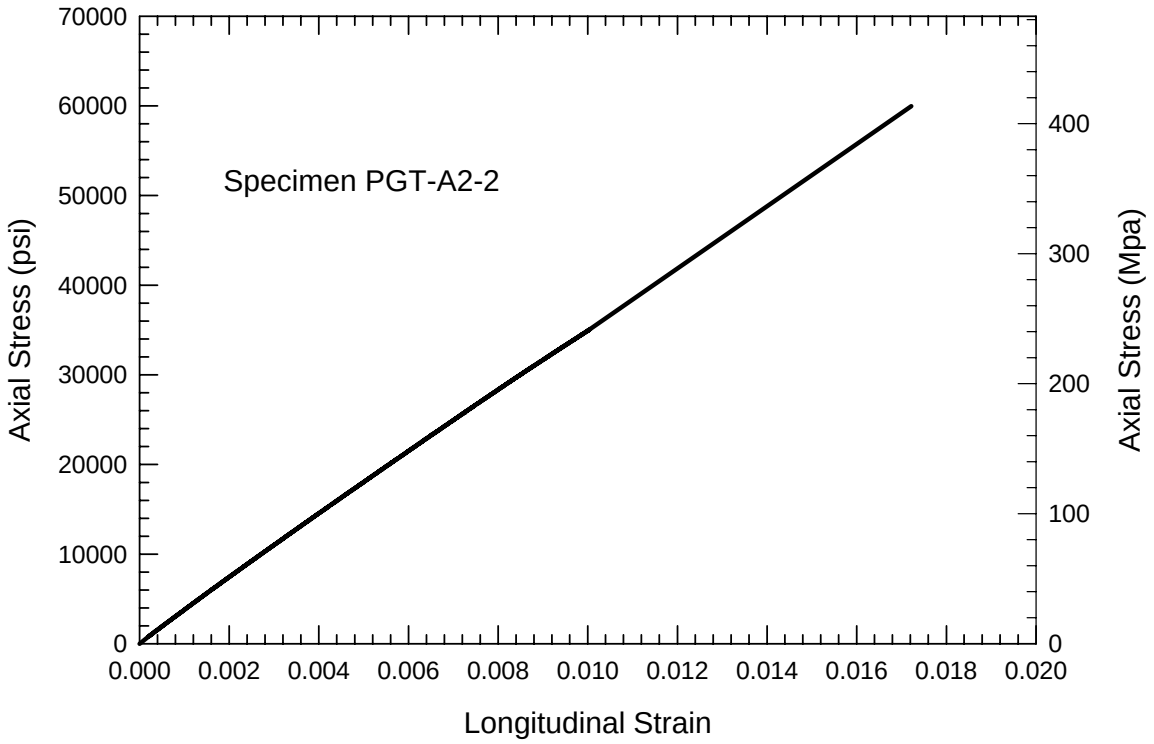
Specimen PGT-A2-2
Axial Stress (psi)
Axial Stress (Mpa)
Longitudinal Strain
70000
60000
50000
40000
30000
20000
10000
0
400
300
200
100
0
0.000
0.002
0.004
0.006
0.008
0.010
0.012
0.014
0.016
0.018
0.020

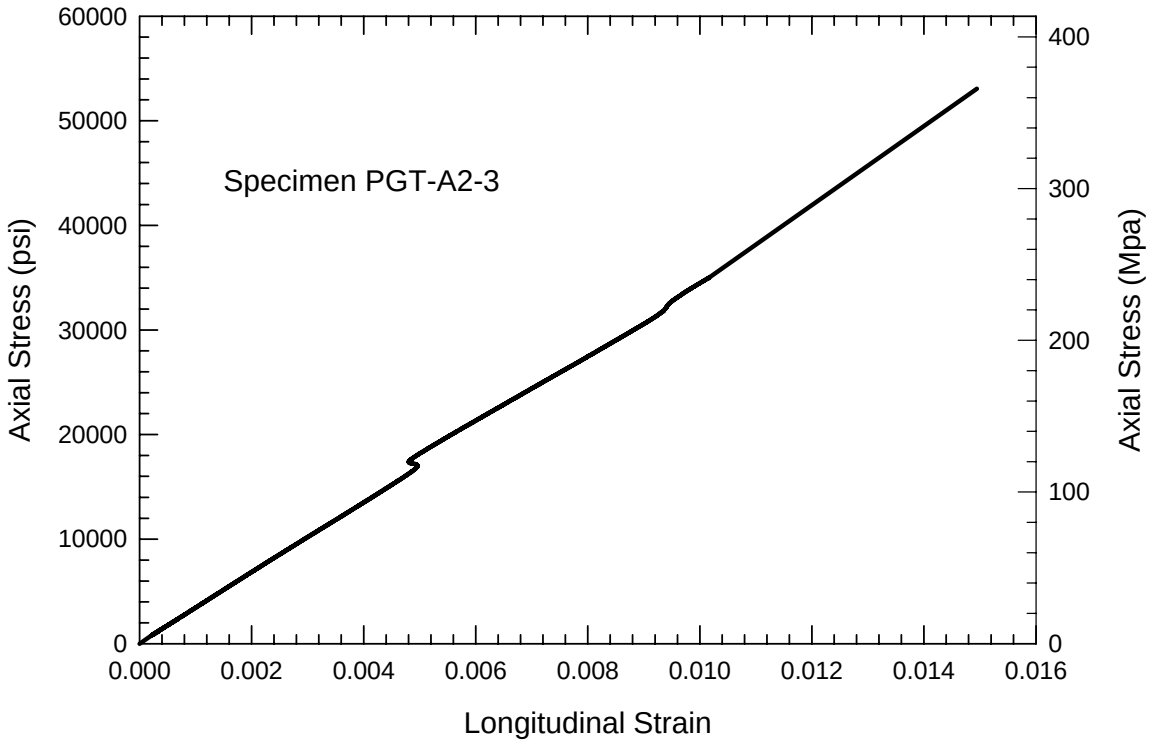
Specimen PGT-A2-3
Axial Stress (psi)
Axial Stress (Mpa)
Longitudinal Strain
60000
50000
40000
30000
20000
10000
0
400
300
200
100
0
0.000
0.002
0.004
0.006
0.008
0.010
0.012
0.014
0.016

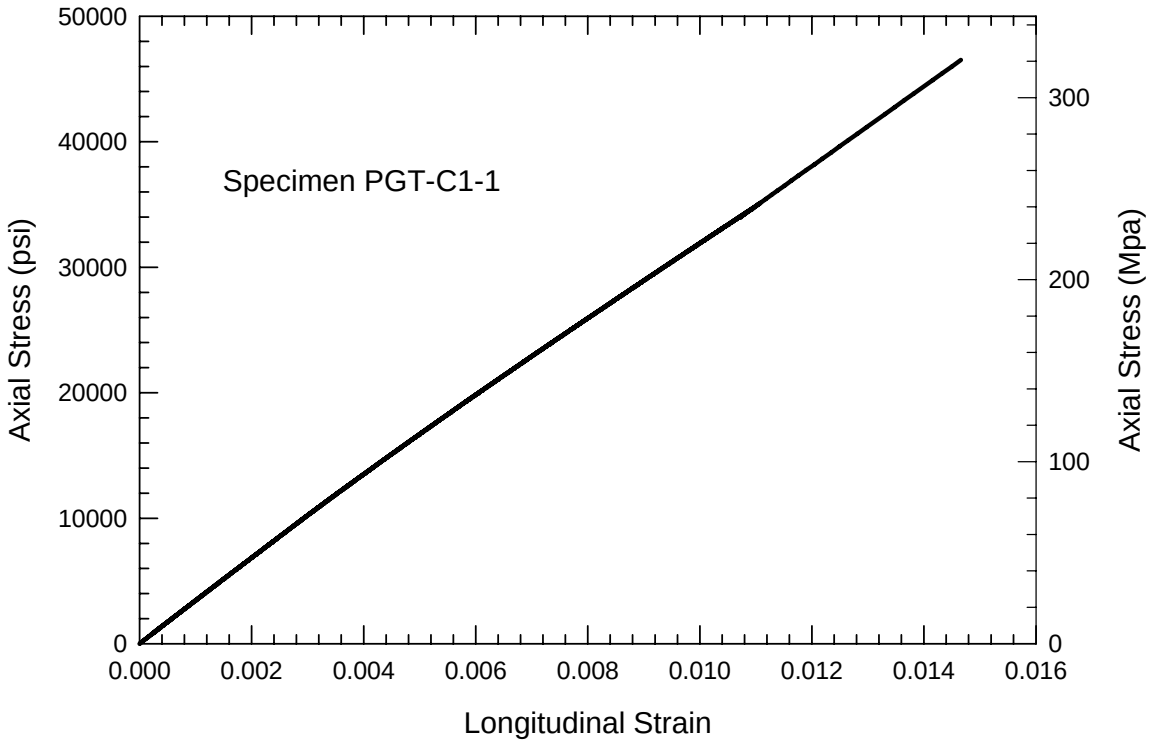
Specimen PGT-C1-1
Axial Stress (psi)
Axial Stress (Mpa)
Longitudinal Strain
50000
40000
30000
20000
10000
0
300
200
100
0
0.000
0.002
0.004
0.006
0.008
0.010
0.012
0.014
0.016

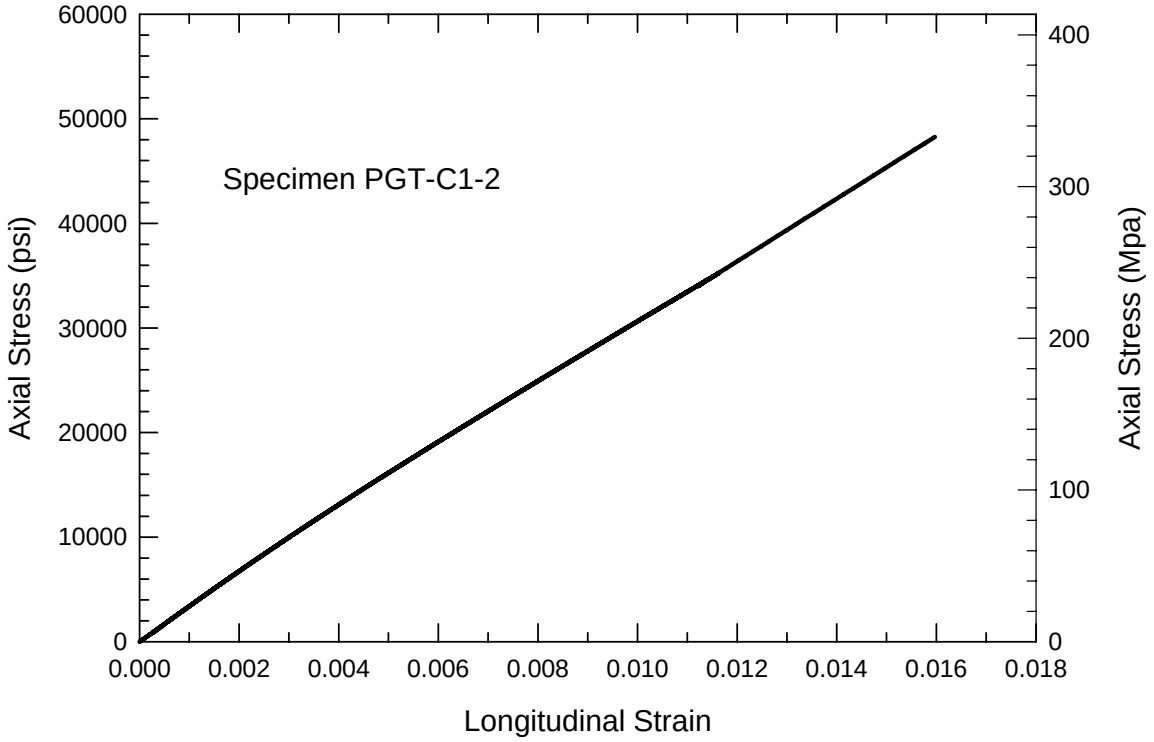
Specimen PGT-C1-2
Axial Stress (psi)
Axial Stress (Mpa)
Longitudinal Strain
60000
50000
40000
30000
20000
10000
0
400
300
200
100
0
0.000
0.002
0.004
0.006
0.008
0.010
0.012
0.014
0.016
0.018

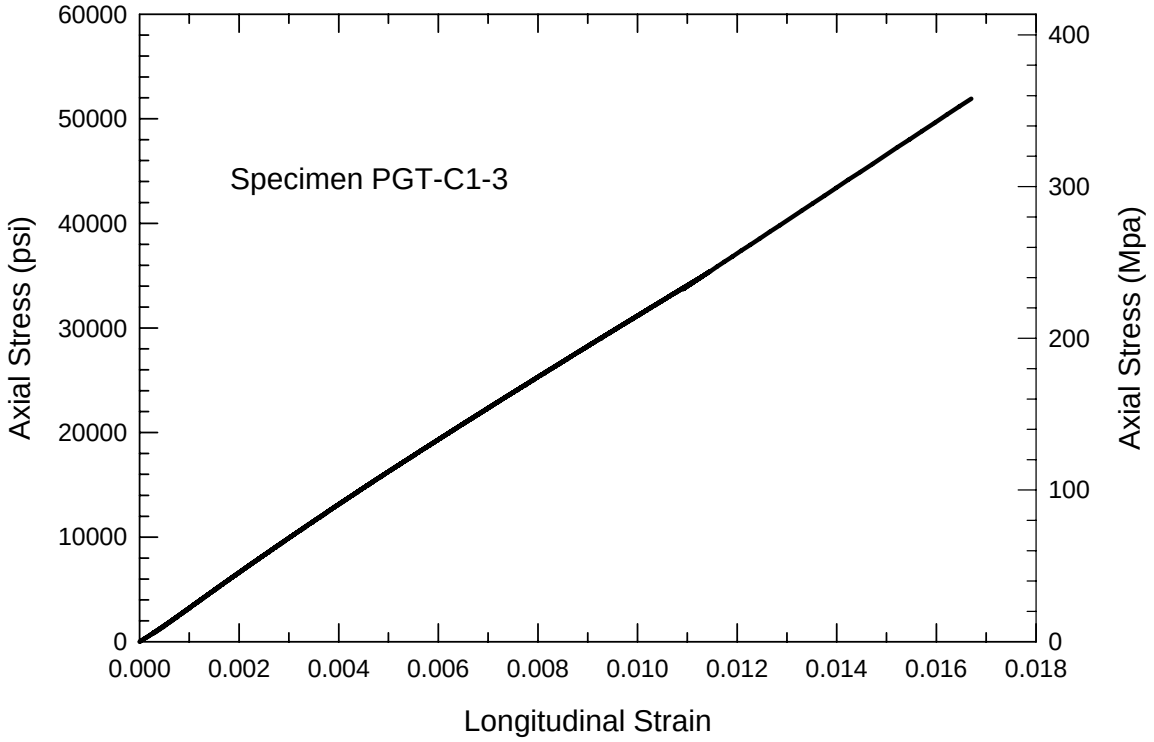
Specimen PGT-C1-3
Axial Stress (psi)
Axial Stress (Mpa)
Longitudinal Strain
60000
50000
40000
30000
20000
10000
0
400
300
200
100
0
0.000
0.002
0.004
0.006
0.008
0.010
0.012
0.014
0.016
0.018

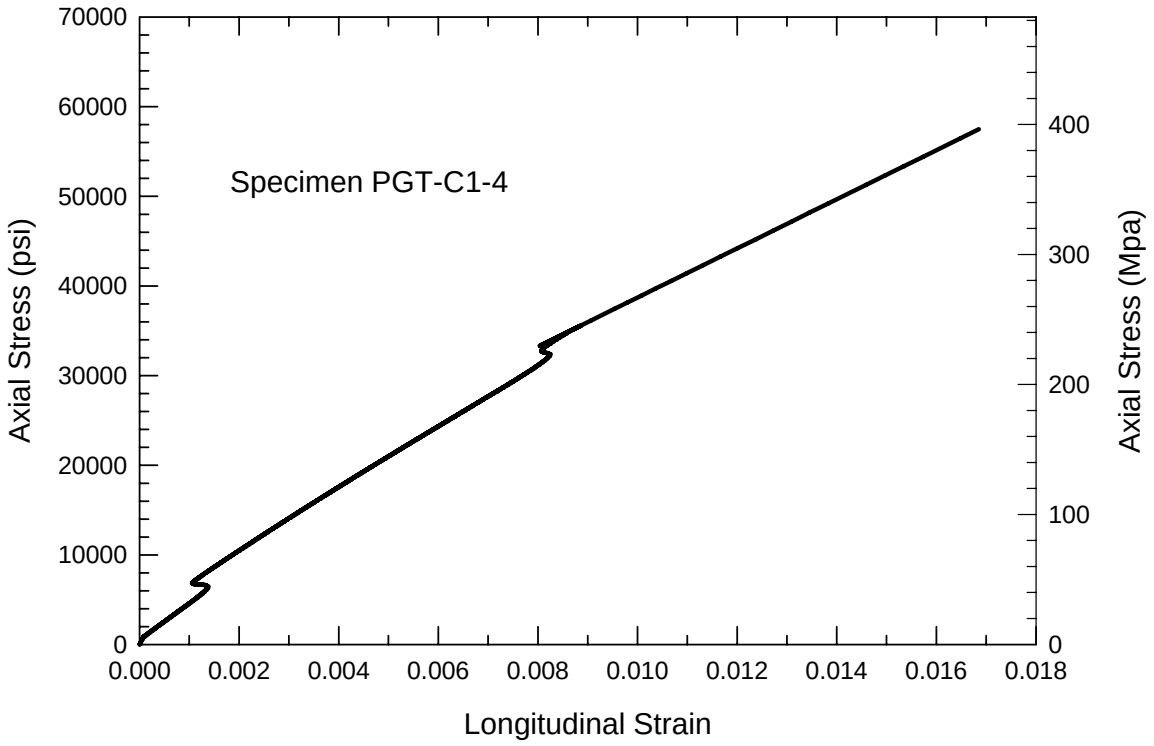
Specimen PGT-C1-4
Axial Stress (psi)
Axial Stress (Mpa)
Longitudinal Strain
70000
60000
50000
40000
30000
20000
10000
0
400
300
200
100
0
0.000
0.002
0.004
0.006
0.008
0.010
0.012
0.014
0.016
0.018

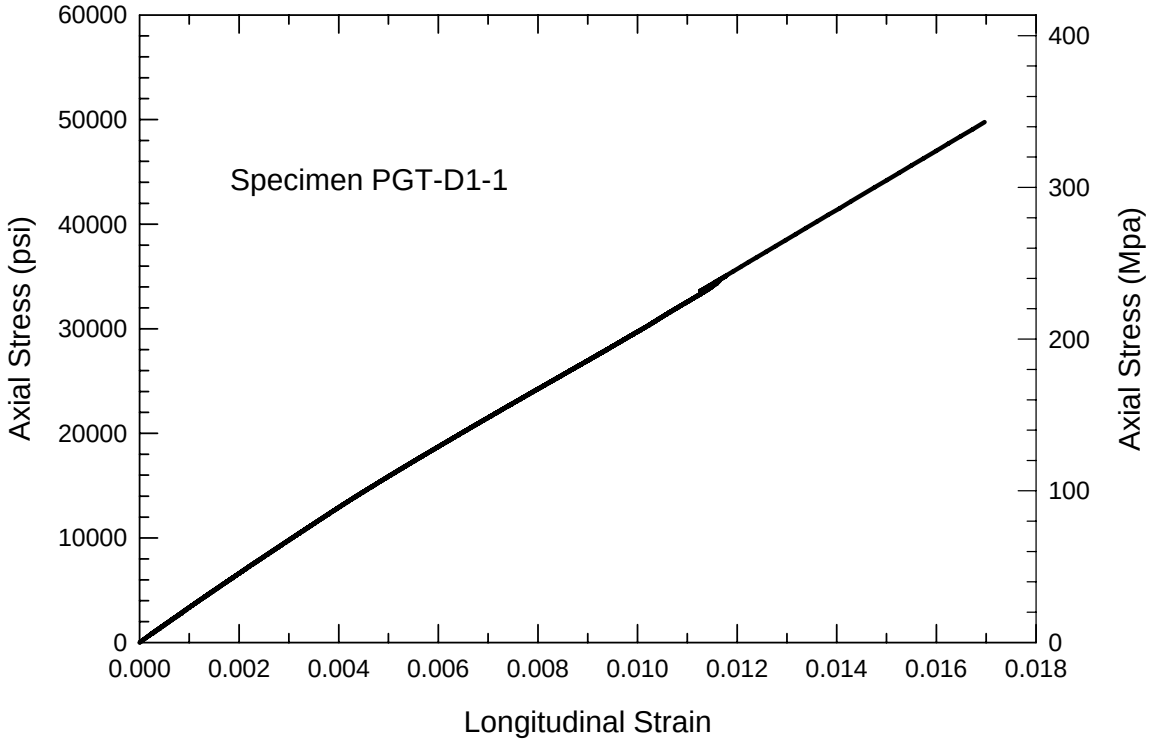
Specimen PGT-D1-1
Axial Stress (psi)
Axial Stress (Mpa)
Longitudinal Strain
60000
50000
40000
30000
20000
10000
0
400
300
200
100
0
0.000
0.002
0.004
0.006
0.008
0.010
0.012
0.014
0.016
0.018

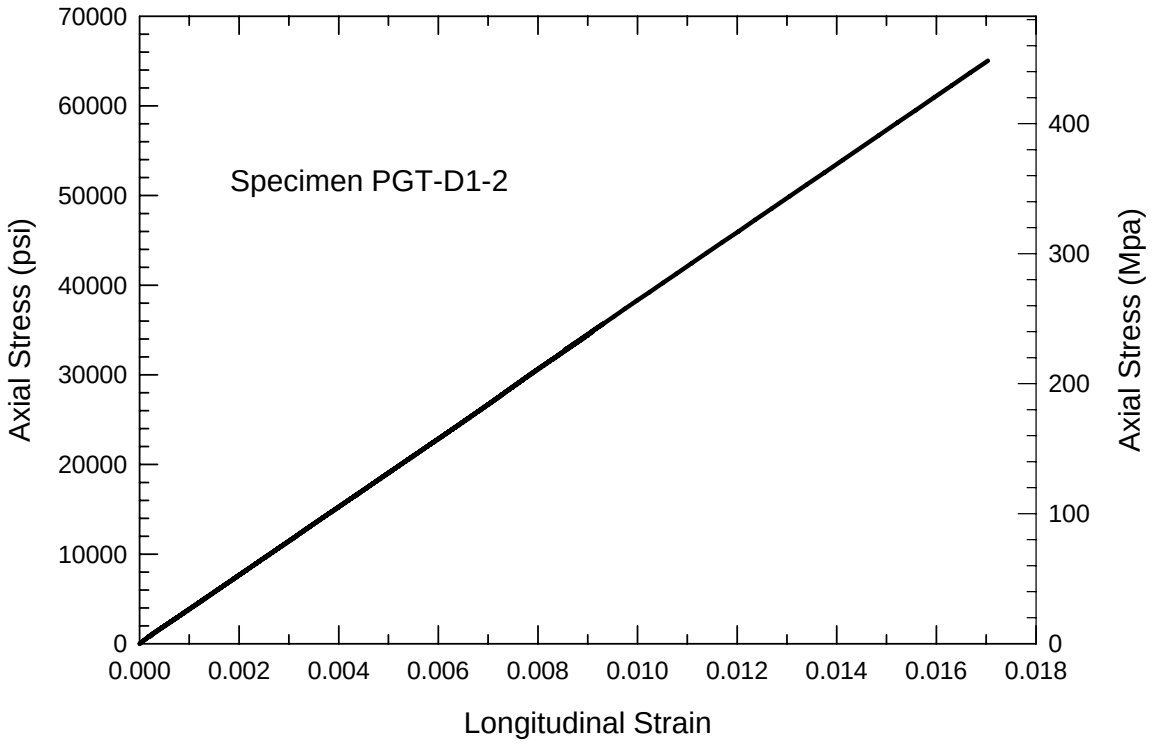
Specimen PGT-D1-2
Axial Stress (psi)
Axial Stress (Mpa)
Longitudinal Strain
70000
60000
50000
40000
30000
20000
10000
0
400
300
200
100
0
0.000
0.002
0.004
0.006
0.008
0.010
0.012
0.014
0.016
0.018

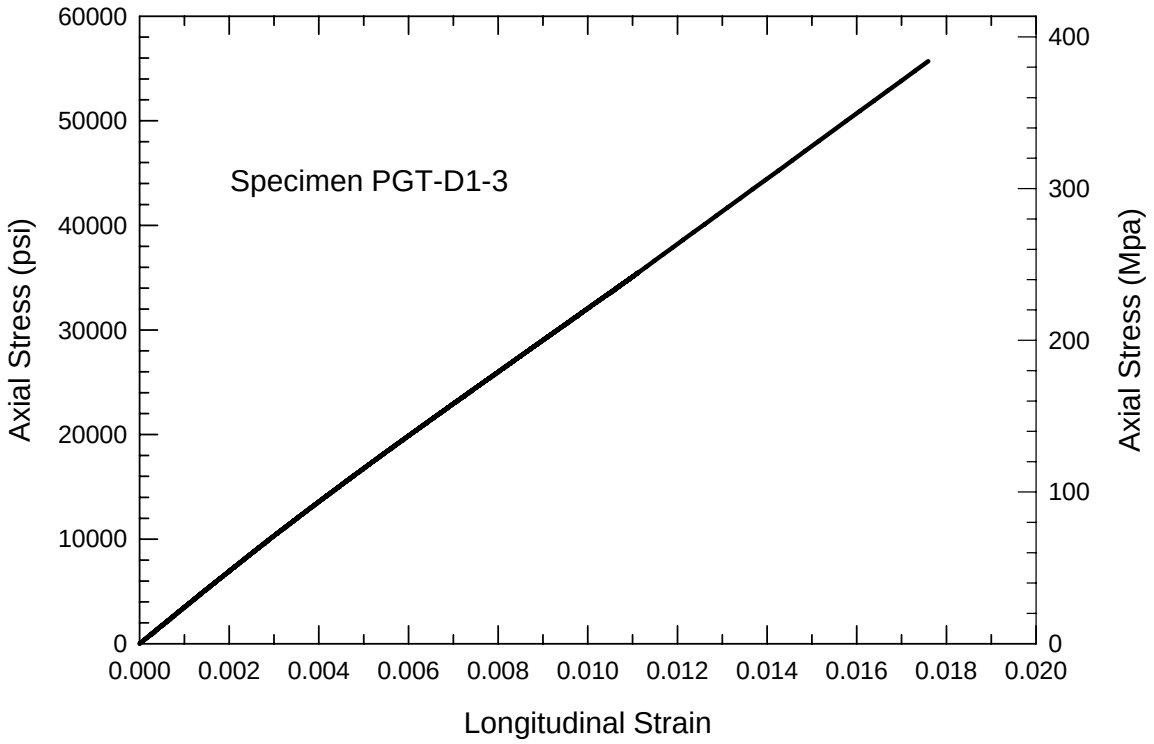
Specimen PGT-D1-3
Axial Stress (psi)
Axial Stress (Mpa)
Longitudinal Strain
60000
50000
40000
30000
20000
10000
0
400
300
200
100
0
0.000
0.002
0.004
0.006
0.008
0.010
0.012
0.014
0.016
0.018
0.020

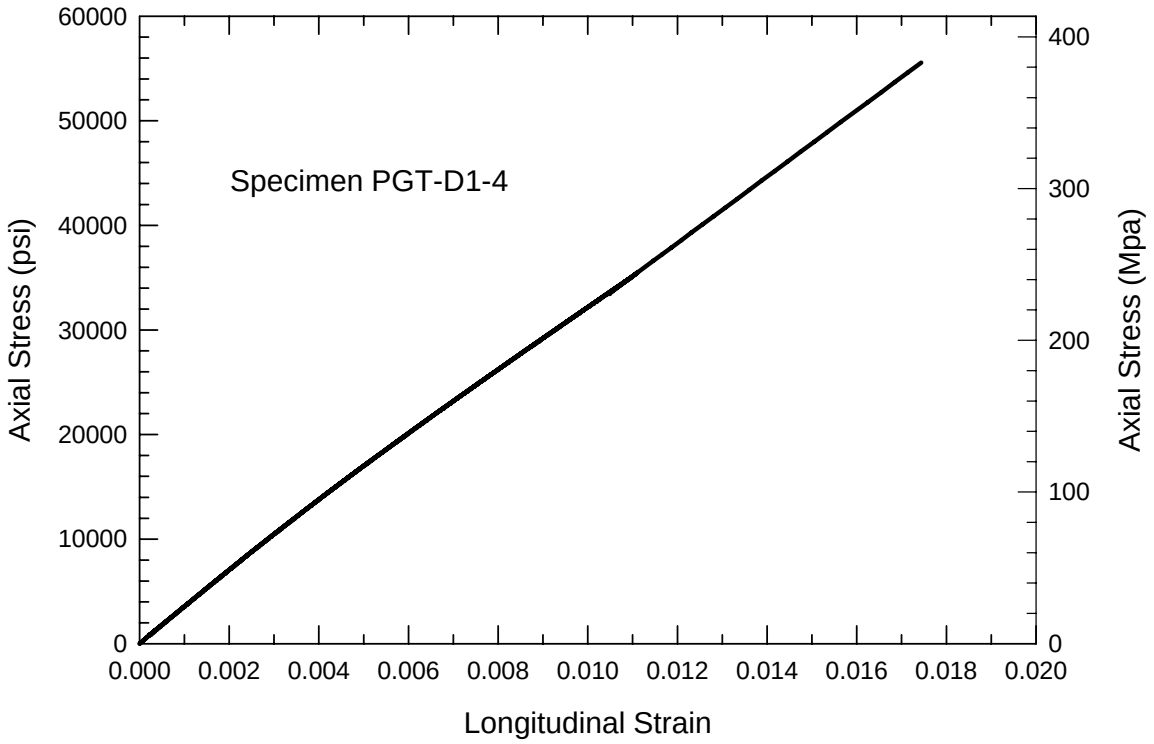
Specimen PGT-D1-4
Axial Stress (psi)
Axial Stress (Mpa)
Longitudinal Strain
60000
50000
40000
30000
20000
10000
0
400
300
200
100
0
0.000
0.002
0.004
0.006
0.008
0.010
0.012
0.014
0.016
0.018
0.020

SHORT-TERM COMPRESSION TESTS

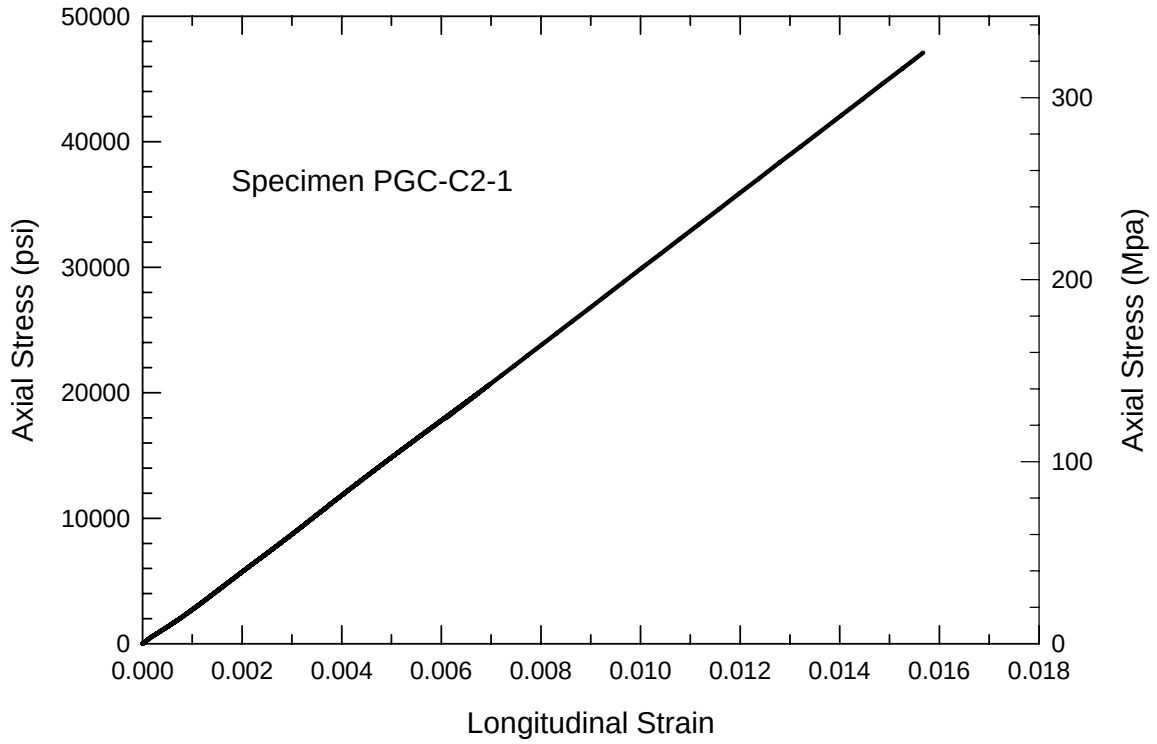

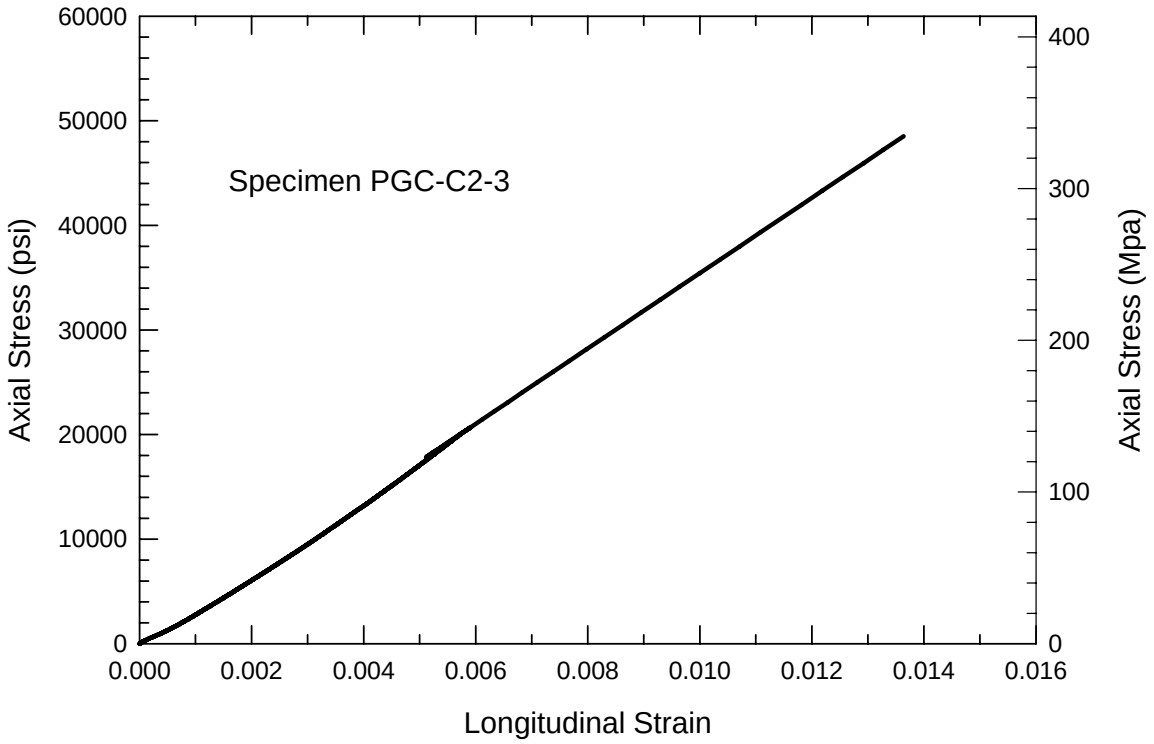
Specimen PGC-C2-3
Axial Stress (psi)
Axial Stress (Mpa)
Longitudinal Strain
60000
50000
40000
30000
20000
10000
0
400
300
200
100
0
0.000
0.002
0.004
0.006
0.008
0.010
0.012
0.014
0.016

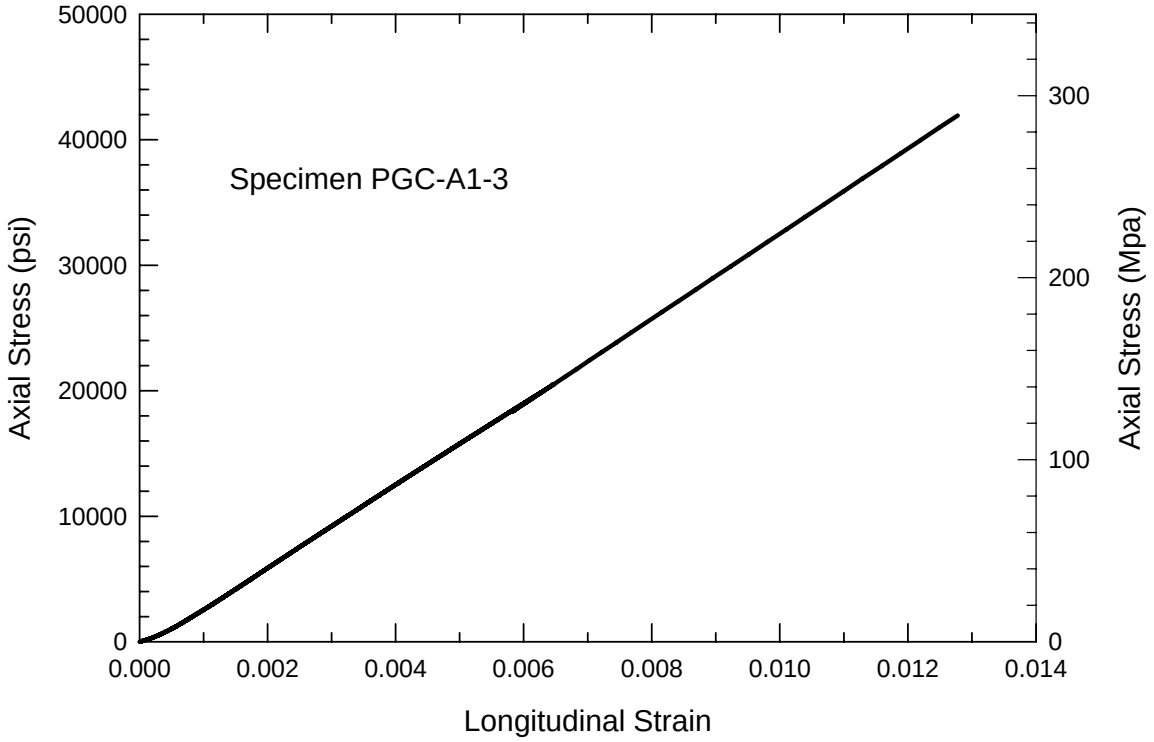
Specimen PGC-A1-3
Axial Stress (psi)
Axial Stress (Mpa)
Longitudinal Strain
50000
40000
30000
20000
10000
0
300
200
100
0
0.000
0.002
0.004
0.006
0.008
0.010
0.012
0.014

SHORT-TERM ELEVATED TEMPERATURE TESTS

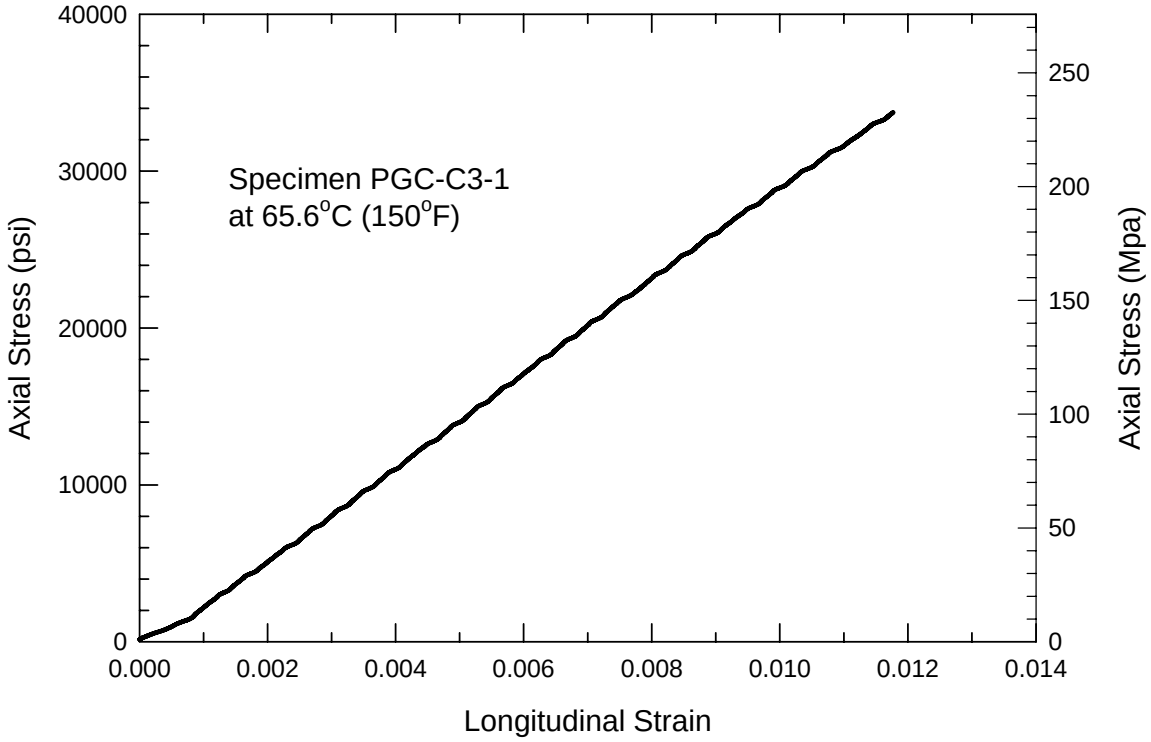

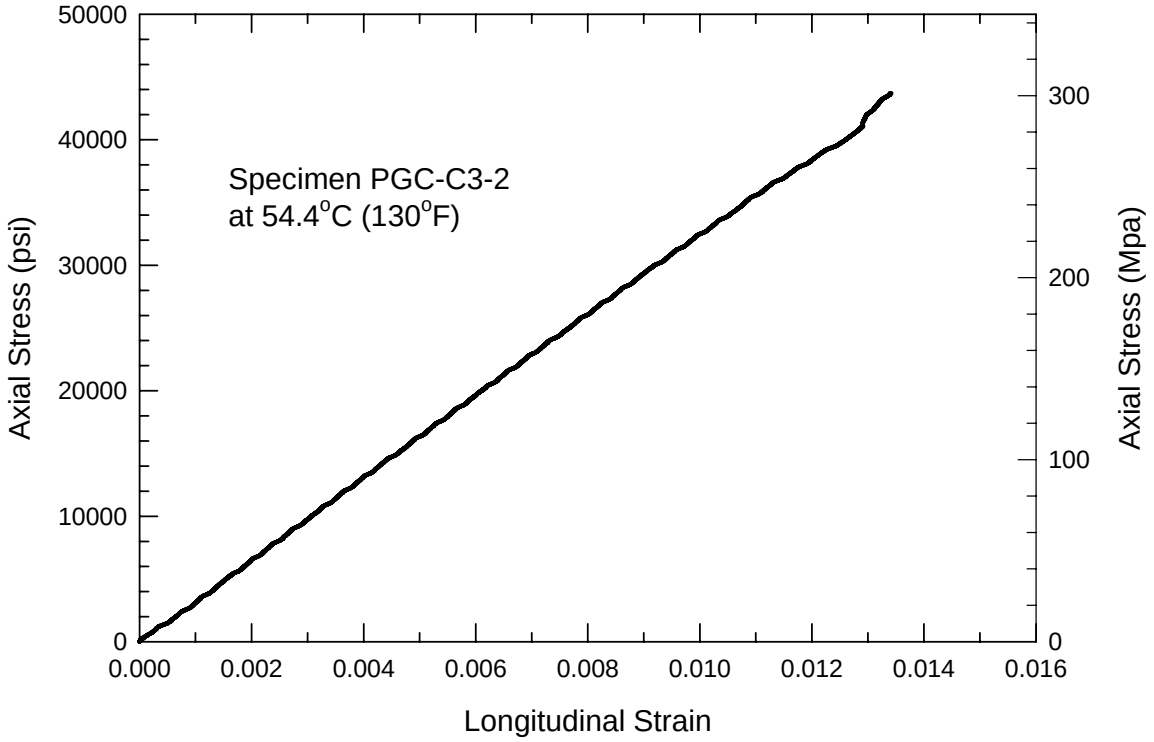
Specimen PGC-C3-2
at 54.4°C (130°F)
Axial Stress (psi)
Axial Stress (Mpa)
Longitudinal Strain
50000
40000
30000
20000
10000
0
300
200
100
0
0.000
0.002
0.004
0.006
0.008
0.010
0.012
0.014
0.016

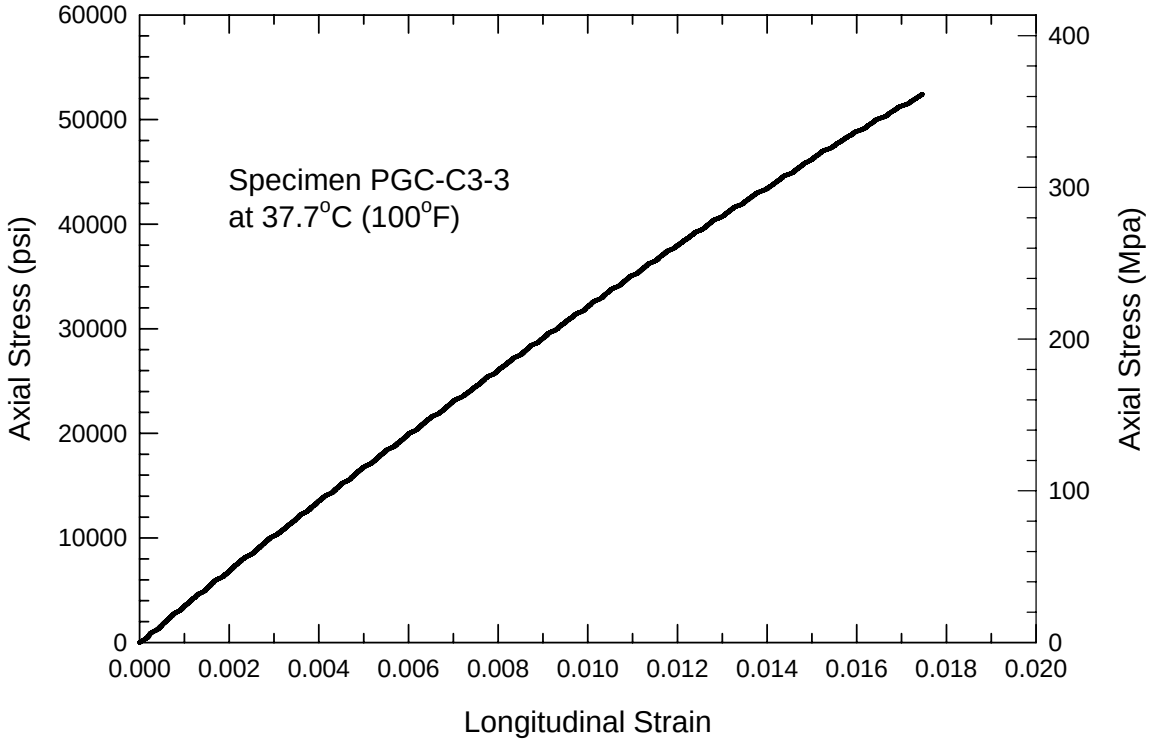
Specimen PGC-C3-3
at 37.7°C (100°F)
Axial Stress (psi)
Axial Stress (Mpa)
Longitudinal Strain
60000
50000
40000
30000
20000
10000
0
400
300
200
100
0
0.000
0.002
0.004
0.006
0.008
0.010
0.012
0.014
0.016
0.018
0.020

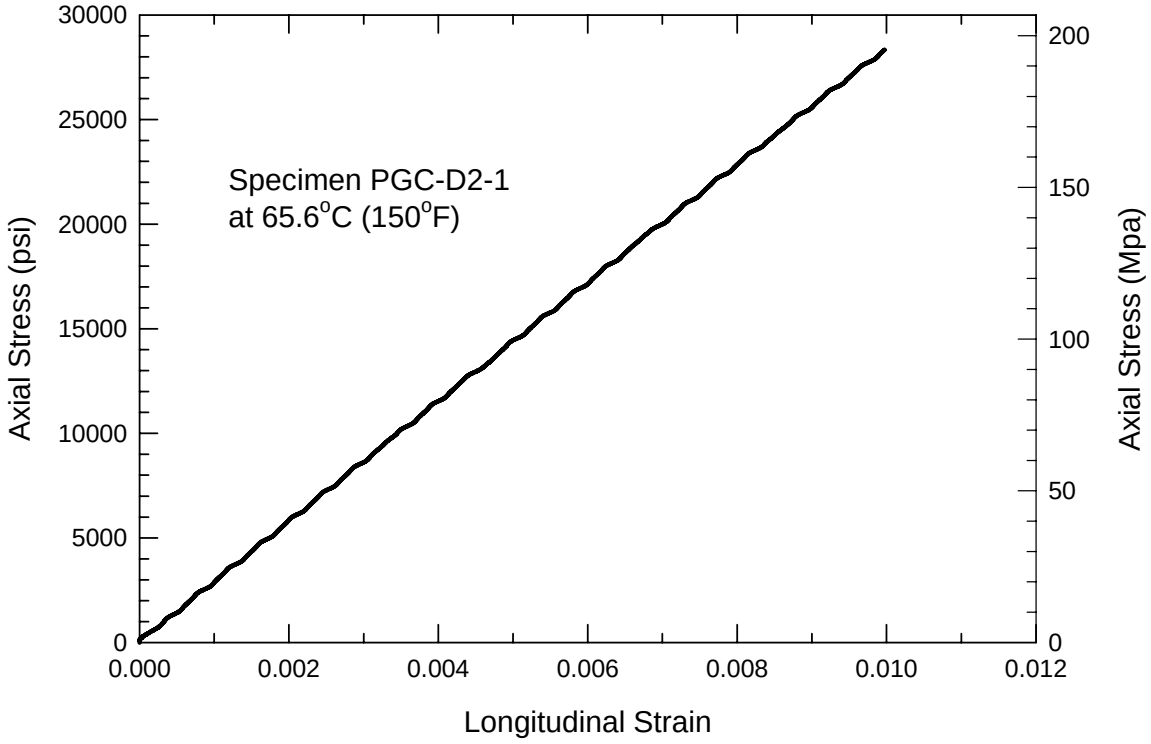
Specimen PGC-D2-1
at 65.6°C (150°F)
Axial Stress (psi)
Axial Stress (Mpa)
Longitudinal Strain
30000
25000
20000
15000
10000
5000
0
200
150
100
50
0
0.000
0.002
0.004
0.006
0.008
0.010
0.012

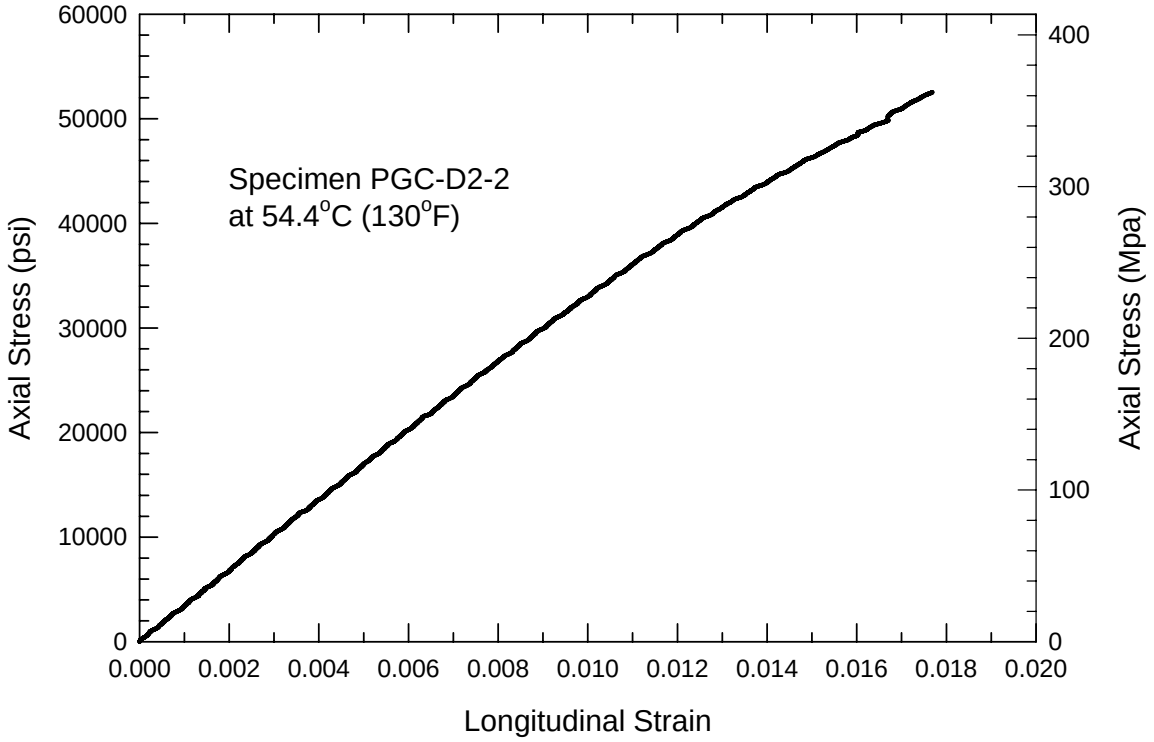
Specimen PGC-D2-2
at 54.4°C (130°F)
Axial Stress (psi)
Axial Stress (Mpa)
Longitudinal Strain
60000
50000
40000
30000
20000
10000
0
400
300
200
100
0
0.000
0.002
0.004
0.006
0.008
0.010
0.012
0.014
0.016
0.018
0.020

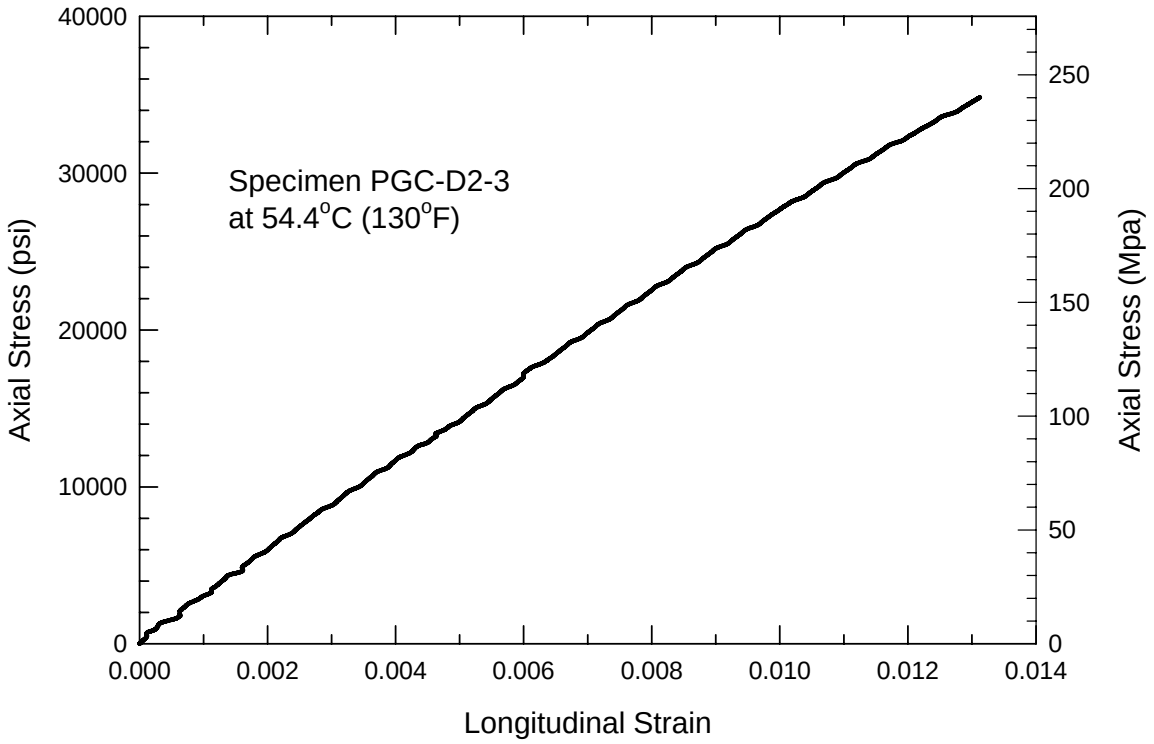
Specimen PGC-D2-3
at 54.4°C (130°F)
Axial Stress (psi)
Axial Stress (Mpa)
Longitudinal Strain
40000
30000
20000
10000
0
250
200
150
100
50
0
0.000
0.002
0.004
0.006
0.008
0.010
0.012
0.014

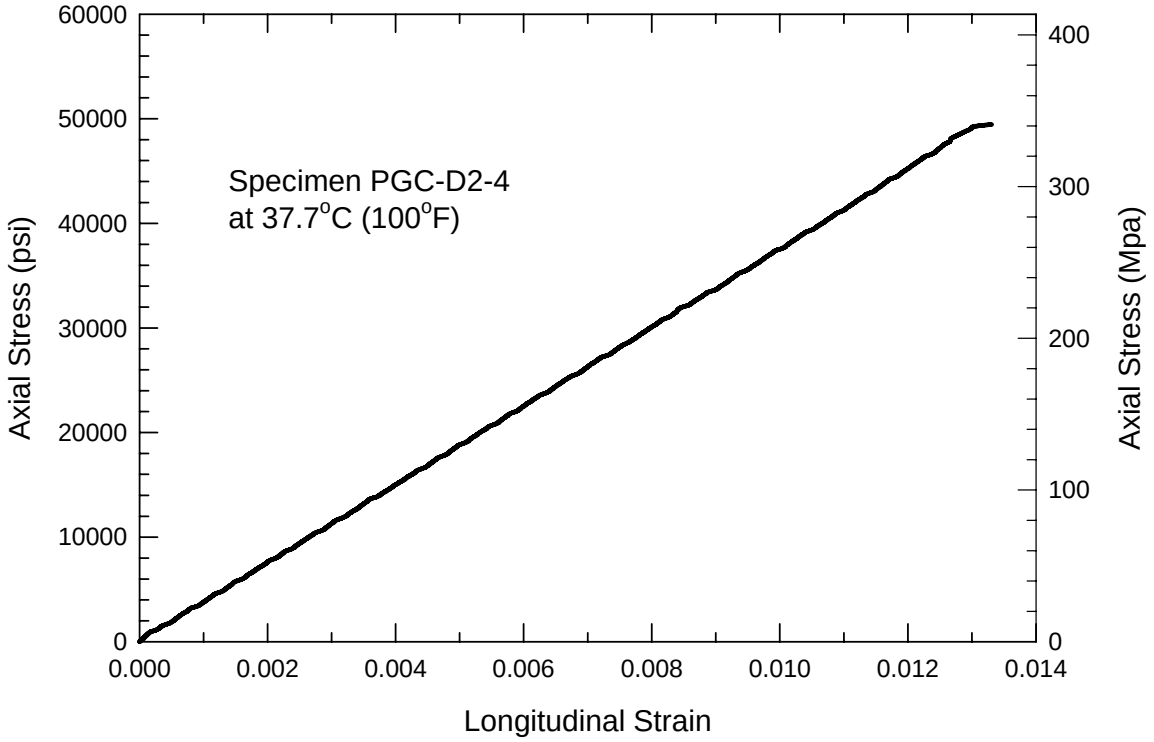
Specimen PGC-D2-4
at 37.7°C (100°F)
Axial Stress (psi)
Axial Stress (Mpa)
Longitudinal Strain
60000
50000
40000
30000
20000
10000
0
400
300
200
100
0
0.000
0.002
0.004
0.006
0.008
0.010
0.012
0.014

REFERENCES

ACI 440R-96 (1996), "State-of-the-Art Report of Fiber Reinforced Plastic (FRP) Reinforcement for Concrete Structures", American Concrete Institute, Farmington Hills, MI., 68 pp.

ASTM D3039/D3039M-93, Standard Test Methods for Tensile Properties of Polymer Matrix composite Materials, American Society for Testing and Materials

ASTM D3410/D3410M-95, Standard Test Method for Compressive Properties of Polymer Matrix Composite Materials with Unsupported Gage Section by Shear Loading, American Society for Testing and Materials

ASTM D638M (1996), "Standard Test Method for Tensile Properties of Plastics," American Society for Testing and Materials International

Bradley, S.W., Puckett, P.M., Baradley, W.L., and Sue, H.J. (1998), "Viscoelastic Creep Characteristics of Neat Thermosets and Thermosets Reinforced with E-glass", Journal of Composites, Technology, and Research, Vol. 20, No. 1, pp. 51-58.

Butz, T.M. (1997), *Tests on Pultruded Square Tubes Under Eccentric Axial Load*, M.S. Dissertation, Georgia Institute of Technology.

Dutta, P.K. and Hui, D. (2000), "Creep Rupture of a GFRP Composite at Elevated Temperatures", Computers and Structures, Vol. 76, No. 1-3, pp. 153-161

EUROCOMP (1996), *Structural Design of Polymer Composites*, Chapman and Hall, London, U.K., 751 pp.

Findley, W.N. (1944), "Creep Characteristics of Plastics", Symposium on Plastics, American Society for Testing and Materials, pp. 118-134.

Findley, W.N., Worley, W.J. (1951), "The Elevated Temperature Creep and Fatigue Properties of a Polyester Glass Fabric Laminate", Society of Plastic Engineers, Vol. V, No. 4, pp. 9-17.

Findley, W.N., Lai, J.S., Onaran, K. (1976), *Creep and Relaxation of Nonlinear Viscoelastic Materials*, Dover Publications Inc., New York, NY.

Findley, W.N. (1987), "26-Year Creep and Recovery of Poly(Vinyl Chloride) and Polyethylene", Polymer Engineering and Science, Vol. 27, No. 8, pp. 582-585.

Gates, T.S. (1993), "Effects of Elevated Temperature on the Viscoplastic Modeling of Graphite/Polymeric Composites", *High Temperature and Environmental Effects on Polymeric Composites, ASTM STP 1174*, pp. 201-221

Gibson, R.F., Hwang, S.J., Kathawate, G.R., Sheppard, C.H. (1991), "Measurement of Compressive Creep Behavior of Glass/PPS Composites Using the Frequency-Time Transformation Method", International SAMPE Technical Conference, Vol. 23, pp. 208-218.

Haj-Ali, Rami M., Muliana, Anastasia H. (2003), "A Micromechanical Constitutive Framework for the Nonlinear Viscoelastic Behavior of Pultruded Composite Materials", International Journal of Solids and Structures, Vol. 40, No. 5, pp. 1037-1057.

Kang, J.O. (2001), *Fiber Reinforced Polymeric Pultruded Members Subjected to Sustained Loads*, Ph. D. Dissertation, Georgia Institute of Technology.

Katouzian, M., Brueller, O.S., Horoschenkoff, A. (1995), "Effect of Temperature on the Creep Behavior of Neat and Carbon Fiber Reinforced PEEK and Epoxy Resin", Journal of Composite Materials, Vol. 29, No. 3, pp. 372-387.

McClure, G. and Mohammadi, Y. (1995), "Compression Creep of Pultruded E-glass Reinforced Plastic Angles", Journal of Materials in Civil Engineering, Vol. 7, No. 4 pp. 269-276.

Papanicolaou, G.C., Zaoutsos, S.P., Cardon, A.H. (1999), "Further Development of a Data Reduction Method for the Nonlinear Viscoelastic Characterization of FRPs", Composites- Part A: Applied Science and manufacturing, Vol. 30, No. 7, pp 839-848.

Raghavan, J., Meshii, M. (1997), "Creep of Polymer Composites", Composite Science and Technology, Vol. 57, No. 12, pp. 1673-1688.

Raghavan, J., Meshii, M. (1997), "Creep Rupture of Polymer Composites", Composite Science and Technology, Vol. 57, No. 4, pp. 375-388

Saadatmanesh, Hamid (1999), "Long-Term Behavior of Aramid Fiber Reinforced Plastic (AFRP) Tendons", ACI Materials Journal, Vol. 96, No. 3, pp. 297-305.

Scott, D.W., Zureick, A. (1998), "Creep behavior of Fiber-Reinforced Polymeric Composites: A Review of the Technical Literature", Journal of Reinforced Plastics and Composites, Vol. 14, pp. 588-617.

Scott, D.W., Zureick, A. (1998), "Compression Creep of a Pultruded E-glass/Vinylester Composite", Composites Science and Technology, Vol. 58, No. 8, pp. 1361-1369.

Spence, Brian R. (1990), “Compressive Viscoelastic Effects (Creep) of a Unidirectional Glass/Epoxy Composite Material”, National SAMPE Symposium and Exhibition (Proceedings), Vol. 35, No. 2, pp. 1490-1493.

STRONGWELL (2002), Extren Design Manual, Strongwell Corporation, Vristol, VA.

Tuttle, M.E., Brinson, H.F. (1986), “Prediction of the Long-Term Creep Compliance of General Composite Laminates”, Experimental Mechanics, Vol. 26, No. 1, pp. 89-102.

Wang, Youjiang and Zureick, A.H. (1994), “Characterization of the Longitudinal Tensile Behavior of Pultruded I-shape Structural Members Using Coupon Specimens”, Composite Structures, Vol. 29, No. 4, pp. 463-472.

Wen, V.F., Gibson, R.F., Sullivan, J.L. (1995), “Characterization of Creep Behavior of Polymer Composites by the use of Dynamic Test Methods”, American Society of Mechanical Engineers, Noise Control and Acoustics Division, Vol. 20, pp. 383-396.

Yen, Shing-Chung, Williamson, Fay L. (1990), “Accelerated Characterization of Creep Response of an Off-Axis Composite Material”, Composites Science and Technology, Vol. 38, No. 2, pp. 103-118.